



NIST  
PUBLICATIONS

**NIST** United States Department of Commerce  
Technology Administration  
National Institute of Standards and Technology

*NISTIR 5002*

**TEM/REVERBERATING CHAMBER  
ELECTROMAGNETIC RADIATION TEST  
FACILITY AT ROME LABORATORY**

---

---

Myron L. Crawford  
Bill F. Riddle  
Dennis G. Camell

QC  
100  
.U56  
NO. 5002  
1996



***NISTIR 5002***

# **TEM/REVERBERATING CHAMBER ELECTROMAGNETIC RADIATION TEST FACILITY AT ROME LABORATORY**

---

---

Myron L. Crawford  
Bill F. Riddle  
Dennis G. Camell

Electromagnetic Fields Division  
Electronics and Electrical Engineering Laboratory  
National Institute of Standards and Technology  
Boulder, Colorado 80303-3328

January 1996



---

U.S. DEPARTMENT OF COMMERCE, Ronald H. Brown, Secretary  
TECHNOLOGY ADMINISTRATION, Mary L. Good, Under Secretary for Technology  
NATIONAL INSTITUTE OF STANDARDS AND TECHNOLOGY, Arati Prabhakar, Director



## CONTENTS

	Page
List of Tables .....	iv
List of Figures .....	v
1. Introduction and Background .....	1
2. Anticipated Advantages and Limitations .....	2
3. Chamber Design and Theoretical Considerations .....	4
3.1 Theoretical Considerations for Design of Chamber .....	4
3.2 Description of RL TEM/Reverberating Chamber .....	7
4. CW Evaluation of the TEM/Reverberating Chamber .....	8
4.1 Measurement Approaches .....	8
4.1.1 TEM Mode .....	8
4.1.2 Reverberating Mode .....	8
4.2 NIST CW Evaluation System .....	9
4.3 CW Evaluation and Calibration Results .....	9
4.3.1 TEM Line and Antenna VSWR and Chamber Coupling Efficiency .	9
4.3.2 Chamber Quality Factor .....	11
4.3.3 Tuner Effectiveness .....	11
4.3.4 E-Field Amplitude Calibration .....	12
4.3.5 Test Zone E-Field Uniformity .....	14
4.3.6 Summary of CW Calibration and Evaluation Results .....	15
5. Pulsed RF/Time-Domain Evaluation of the TEM/Reverberating Chamber .....	16
5.1 Background .....	16
5.2 NIST Pulsed RF Evaluation System .....	16
5.3 Pulsed RF Evaluation Results .....	17
5.4 Comments on Pulsed RF Measurements Results .....	18
6. Performing EMC/V Measurements Using the TEM/Reverberating Chamber ..	18
6.1 Performing EMC/V Measurements with Manual Operations .....	18
6.2 Automated EMC/V Measurements .....	21
6.2.1 TEM Mode Measurement Procedures .....	21
6.2.2 Reverberating Mode-Tuned Measurement Procedure .....	22
6.2.3 Reverberating Mode-Stirred Measurement Procedure .....	23
6.2.4 Comparison of TEM/Reverberating Chamber Measurements with Anechoic Chamber Tests - Some Examples .....	24
7. Summary and Conclusions .....	24
8. References .....	26

## LIST OF TABLES

		Page
Table 3.1	Ratio of test field strengths generated in the RL TEM/reverberating chamber (zinc finish steel reverberating chamber, 3.7 m x 5.2 m x 9.8 m) to that generated in an anechoic chamber at 3 m separation distance for same transmitted power. Test volume definition in anechoic chamber is ( $\pm 3$ dB). . . . .	28
Table 3.2	Ratio of test fields strengths generated in the RL TEM/reverberating chamber to that generated in an anechoic chamber for same transmitted power. Separation distances in anechoic chamber are 1 and 3 m. . .	28
Table 3.3	Test volume for radiated fields in anechoic chamber at 1 m and 3 m separation distances with selected transmitting antenna gain. Test volume definition is based on half-power points of the radiation pattern. . . . .	29
Table 3.4	Theoretical mode frequencies and gaps between adjoining modes for RL TEM/reverberating chamber, $a = 3.69$ m, $b = 5.18$ m, and $d = 9.78$ m. . . . .	30
Table 4.1	Spatial variations in E-fields measured inside the RL TEM/reverberating chamber over test volume defined by probes shown in figure 4.14. . . . .	31
Table 4.2	Summary of cw operation characteristics of RL TEM/reverberating chamber. . . . .	32
Table 5.1	Comparison of measured and calculated charge/decay time of the RL TEM/reverberating chambers determined from chamber average loss measurements (figure 4.4) and from data shown in figure 5.3. . . . .	33

## LIST OF FIGURES

		Page
Figure 3.1	Theoretical mode distribution for the RL TEM/reverberating chamber (3.69 m x 5.18 m x 9.78 m). . . . .	34
Figure 3.2	Cross-sectional sketches of the RL TEM/reverberating chamber. . . . .	34
Figure 3.3(a)	Photographs of the RL TEM/reverberating chamber showing tuner and top plate installation with plastic rods. . . . .	35
Figure 3.3(b)	Photographs of the RL TEM/reverberating chamber showing side plate installation, the side plate end transition to coaxial connector and the access panels. . . . .	36
Figure 4.1	Block diagram of the instrumentation used in the cw evaluation of the RL TEM/reverberating chamber. . . . .	37
Figure 4.2	Measured composite VSWR of the top plate and side plate TEM lines (0.001 to 1.0 GHz) and the broadband ridged horn antenna (1.0 to 18 GHz) transmitting into the RL TEM/reverberating chamber. . . . .	38
Figure 4.3	Measured coupling efficiency (loss) between the top and side plates (transmitting) and log periodic antenna (receiving, 0.1 to 1.0 GHz) and the broadband horn antennas (transmitting and receiving, 1.0 to 18 GHz) in the RL TEM/reverberating chamber. . . . .	39
Figure 4.4	Measured average and minimum coupling efficiency (loss) between the top and side plates (transmitting, 0.1 to 1.0 GHz) and log periodic antenna (receiving, 0.1 to 1.0 GHz) and the broadband horn antennas (transmitting and receiving, 1.0 to 18 GHz) in the RL TEM/reverberating chamber. . . . .	40
Figure 4.5	(a) Theoretical and experimental Q of the RL TEM/reverberating chamber and (b) ratio of theoretical to experimental Q (K-factor), 0.01 to 18 GHz. . . . .	41
Figure 4.6	Vertical polarized component of E-field versus tuner position. Measurements made at selected frequencies at the center of RL TEM/reverberating chamber test zone with 1 W RF applied at the input of the top plate. . . . .	42
Figure 4.7	Horizontal polarized component of E-field versus tuner position. Measurements made at selected frequencies at the center of RL TEM/reverberating chamber test zone with 1 W RF applied at the input of the side plate. . . . .	43

Figure 4.8	Measured tuner effectiveness in the RL TEM/reverberating chamber using receiving antenna power measurements. (Same receiving antennas as figure 4.4.) . . . . .	44
Figure 4.9	E-field components measured at the center of the RL TEM/reverberating chamber using a NIST isotropic (5 cm dipole) probe (position #2 in figure 4.14) with chamber excited by top plate: (a) average, (b) maximum. Net input power is 1 W. . . . .	45
Figure 4.10	E-field components measured at the center of the RL TEM/reverberating chamber using NIST isotropic (5 cm dipole) probe (position #2 in figure 4.14) with chamber excited b side plate: (a) average, (b) maximum. Net input power is 1 W. . . . .	46
Figure 4.11	Maximum and average vertical component of E-field measured at (a) center and (b) position 6 (figure 4.14) in RL TEM/reverberating chamber using NIST 5 cm and 0.8 cm dipole probes and log periodic (0.1 - 1.0 GHz) and broadband horn (1.0 - 18 GHz) antennas. Chamber excited by 1 W input to top plate (0.001 - 1 GHz) and broadband horn (1 - 18 GHz). . . . .	47
Figure 4.12	Maximum and average horizontal component of E-field measured at (a) center and (b) position 6 (figure 4.14) in RL TEM/reverberating chamber using NIST 5 cm and 0.8 cm dipole probes, and log periodic (0.1 - 1 GHz) and broadband horn (1.0 - 18 GHz) antennas. Chamber excited by 1 W input to side plate (0.001 - 1 GHz) and broadband horn (1 - 18 GHz). . . . .	48
Figure 4.13	Input power required to generate a 200 V/m maximum E-field at the center of the RL TEM/reverberating chamber using: (a) top plate (Vert. Pol.) and (b) side plate (Hor. Pol.). (0.001 - 1 GHz) and broadband horn antenna (1 - 18 GHz). . . . .	49
Figure 4.14	Cross-sectional sketch of the RL TEM/reverberating chamber showing placement of calibrated isotropic probes for measuring spatial E-field uniformity. . . . .	50
Figure 4.15	Photographs of interior of RL TEM/reverberating chamber showing placement of NIST isotropic probes for evaluation of spatial distribution of E-field. . . . .	51
Figure 4.16(a)	Spatial distribution of the E-field components in the RL TEM/reverberating chamber measured with nine NIST isotropic probes (5 cm dipoles) for 1 W net input power to the top plate and horn transmitting antenna: average and maximum values. Average of the average components shown as solid curve. Average values of components, top plate, and ridged horn antenna.	52

Figure 4.16(b)	Spatial distribution of the E-field components in the RL TEM/reverberating chamber measured with nine NIST isotropic probes (5 cm dipoles) for 1 W net input power to the top plate and horn transmitting antenna: average and maximum values. Average of the maximum components shown as solid curve. Maximum values of components, top plate, and ridged horn antenna. . . . .	53
Figure 4.17(a)	Spatial distribution of the E-field components in the RL TEM/reverberating chamber measured with nine NIST isotropic probes (5 cm dipoles) for 1 W net input power to the side plate and horn transmitting antenna: average and maximum values. Average of the average components shown as solid curve. Average values of components, side plate, and ridged horn antenna. . . . .	54
Figure 4.17(b)	Spatial distribution of the E-field components in the RL TEM/reverberating chamber measured with nine NIST isotropic probes (5 cm dipoles) for 1 W net input power to the side plate and horn transmitting antenna: average and maximum values. Average of the maximum components shown as solid curve. Maximum values of components, side plate, and ridged horn antenna. . . . .	55
Figure 5.1	Block diagram of instrumentation used in pulsed rf evaluation of the RL TEM/reverberating chamber . . . . .	56
Figure 5.2(a)	Maximum and average values of received rf pulse waveforms inside the RL TEM/reverberating chamber determined by mode-tuned approach. Chamber empty (no absorber). Measurements were taken at nine selected frequencies and three pulse widths. . . . .	57
Figure 5.2(b)	Maximum and average values of received rf pulse waveforms inside the RL TEM/reverberating chamber determined by mode-tuned approach. Chamber empty (no absorber). Measurements were taken at nine selected frequencies and three pulse widths. . . . .	58
Figure 5.2(c)	Maximum and average values of received rf pulse waveforms inside the RL TEM/reverberating chamber determined by mode-tuned approach. Chamber empty (no absorber). Measurements were taken at nine selected frequencies and three pulse widths. . . . .	59
Figure 5.3	Time required for rf signal transmitted into the RL TEM/reverberating chamber to rise 63% and 90% of steady-state amplitude . . . . .	60
Figure 5.4	Estimated correction factors for amplitude response of rf test pulses in the RL TEM/reverberating chamber at selected frequencies as a function of input pulse width . . . . .	61

Figure 5.5	Estimated correction factors for amplitude response of rf test pulses in the RL TEM/reverberating chamber at selected input pulse widths as a function of frequencies. . . . .	62
Figure 6.1	Block diagram of swept frequency EM radiated immunity and shielding effectiveness measurement system using TEM/reverberating chamber.	63
Figure 6.2	Block diagram of swept frequency EM radiated emissions and shielding effectiveness system using TEM/reverberating chamber. . . . .	64
Figure 6.3	Measured SE data of 3 cm x 6 cm TEM cell with 15 mm diameter circular aperture using TEM/reverberating chamber and swept frequency measurement system. (a) reference antenna (no shielding), (b) TEM cell with aperture. . . . .	65
Figure 6.4	Block diagram of automated susceptibility measurement system using the TEM/reverberating chamber in the TEM mode of operation. . . . .	66

TEM/Reverberating Chamber  
Electromagnetic Radiation Test Facility  
at Rome Laboratory

Myron L. Crawford  
Bill F. Riddle  
Dennis G. Camell

Electromagnetic Fields Division  
National Institute of Standards and Technology  
Boulder, CO 80303-3328

This report summarizes the measurement and evaluation of a TEM/reverberating chamber. This chamber was developed as a single, integrated facility for testing radiated electromagnetic compatibility/vulnerability (EMC/V) of large systems of a large shielded enclosure configured as a transverse electromagnetic (TEM) transmission line-driven reverberating chamber. TEM mode test fields are generated at frequencies below multimode cutoff, and mode-stirred test fields are generated at frequencies above multimode cutoff. The report discusses the basis for such a development including the theoretical concepts, the advantages and limitations, the experimental approach for evaluating the operational parameters, and the procedures for using the chamber to perform EMC/V measurements. Both the chamber's cw and pulsed rf characteristics are measured and analyzed.

**Key Words:** cw and pulsed rf testing; radiated EM compatibility and vulnerability measurements; reverberating chamber; TEM cell

## 1. Introduction and Background

The ability to simulate an operating environment for accurately measuring the performance of electronic equipment is fundamental to ensuring the electromagnetic compatibility (EMC) of the equipment. In recent years, the Fields and Interference Metrology Group of the National Institute of Standards and Technology (NIST) in Boulder, Colorado, has been developing improved methods and facilities for EMC testing. Two such facilities are the transverse electromagnetic (TEM) cell and the reverberating (mode-stirred) chamber. Each has its advantages and limitations.

The TEM cell [1,2] is an expanded  $50 \Omega$  rectangular coaxial transmission line, with tapered sections at both ends, that operates ideally with only the TEM mode to generate the equivalent of a planar fields. The cell's use is limited to frequencies below a few hundred megahertz, depending upon the size of the equipment under test (EUT) and hence the size of the cell. This limitation is due to the requirement that only the fundamental TEM mode exist in the cell at frequencies for which tests are to be made.

The reverberating chamber [3,4,5,6] is a shielded room with one or more rotating stirrers to mix the fields transmitted from an antenna placed inside the chamber. The test field is determined statistically (maximum and average values) from the multimoded, complex fields. This technique has significant advantages for testing large EUTs efficiently and cost effectively. However, the method is restricted to frequencies above a few hundred megahertz, again depending upon the size of the test chamber. This limitation is a consequence of requiring the chamber to be electrically large enough so that sufficient numbers of modes exist inside the chamber. This is needed for adequate mode mixing and spatial averaging to ensure that relatively uniform fields will be generated for testing.

Combining these two measurement techniques into a single facility will allow EMC testing over the combined frequency range of the TEM cell and the mode-stirred chamber [7]. This should result in significant cost and time savings with a possible improvement in measurement accuracy in performing essential EMC tests. A combined TEM/reverberating chamber will have three distinct regions of operation: (a) TEM, (b) transition, and © reverberating. The TEM region will cover the low-frequency range near dc to the first multimode cutoff frequency. The transition region covers the range above this cutoff frequency, up through the frequencies for which the first few higher modes are excited in the chamber, but insufficient in number to provide adequate spatial averaging. The test field will be a combination of the TEM mode and a limited number of higher order modes that yield a complex field that is rather difficult to define both in polarization and amplitude. Techniques such as absorber loading to suppress the quality factors of the higher order modes, and/or field averaging over the volume using a matrix of isotropic E-field probes must be used to define the test field parameters. The reverberating region of operation will cover the higher frequency range for which sufficient modes exist to ensure adequate mode mixing and spatial averaging. This test field simulates a complex, real-world field environment.

This report summarizes the measurement and evaluation results of a particular "hybrid" TEM/reverberating chamber located at Rome Laboratory (RL), Griffiss AFB, NY. The chamber has dimensions of 3.69 m x 5.18 m x 9.78 m. Both the continuous wave (cw) and pulsed rf characteristics of the chamber were evaluated. Anticipated advantages and limitations of this combined chamber are outlined in Section 2. A description of the chamber itself is given in Section 3. Section 4 describes the system used for performing the cw evaluation/calibration of the chamber and presents the results obtained. Section 5 describes the pulsed rf, time-domain evaluation systems and the associated measurement results. Section 6 outlines the measurement procedures for performing EM susceptibility and shielding effectiveness tests with the chamber by both manual and automated operations. Finally, Section 7 gives a summary and some conclusions derived from this effort and from previous work in developing the TEM cell and reverberating chamber measurement techniques.

## 2. Anticipated Advantages and Limitations

Motivation for developing a TEM/reverberating chamber arises from its potential for realizing a number of significant advantages. These include the following:

- a. The chamber is electrically isolated from the environment.
- b. It is an indoor facility making it readily accessible.
- c. High test fields can be generated over a large volume efficiently. For example, 1 W of rf power applied to the transmitting antenna inside this chamber, operating in the reverberating mode at 1 GHz, generates a maximum test field of approximately 50 V/m.
- d. Tests can be performed over a broad range of frequencies covering from 10 kHz to 18 GHz with possible extension up to 40 GHz.
- e. Testing is cost effective. The cost of a TEM/reverberating chamber is estimated to be less than half of an equivalent anechoic chamber. This is due primarily to the cost of rf absorbers and fire protection systems associated with an anechoic chamber. Also, rf source power requirements are significantly less for a TEM/reverberating chamber than for an anechoic chamber as indicated in section 4. Test time for using the hybrid chamber is anticipated to be approximately one-fifth of that required when using an anechoic chamber to characterize the maximum response of an EUT.
- f. The TEM/reverberating chamber is a reciprocal facility. That is, it can be used for both radiated immunity and emission testing.
- g. Minimal or no rotation of the EUT is required. This results from the two separate orthogonal plates designed for TEM mode operation (see section 4) and the inherent test field characteristics of the chamber operating in the reverberating mode.
- h. Physical security can be maintained because the chamber is an enclosed facility.
- i. The chamber can be used for both cw and pulsed rf testing.

There are also disadvantages or limitations when using such a hybrid chamber. Some of these are:

- a. Directional or polarization characteristics of the EUT, placed inside the chamber, are lost when operating in the reverberating mode.
- b. The test field is limited to simulating, planar fields at lower frequencies (TEM mode of operation), and complex multimode fields at higher frequencies (reverberating mode of operation).
- c. Only the total power radiated from the EUT or its immunity to a complex field exposure can be measured in the reverberating region of operation. However, the total power radiated, the directional characteristics of the emissions, and polarization sensitivity (angle of entry information for immunity testing) can be determined in the TEM mode region of operation.
- d. The maximum response of an EUT measured in the reverberating region is less than when measured in an open field or in an anechoic chamber, for exposure to the same test field amplitude. The correlation factor is the EUT's free-space directivity. Hence, the susceptibility criteria determined for an EUT measured in the reverberating region of operation must include an additional factor equal to the EUT's estimated free-space conditions are to be obtained.
- e. Relatively large measurement uncertainty (as great as  $\pm 15$  dB) can exist for establishing the test field in the frequency range of the transition region between TEM mode of operation and reverberating mode of operation of the chamber. It may be possible to

reduce this uncertainty by using absorber loading and multi-probe field mapping as referred to in the introduction.

### 3. Chamber Design and Theoretical Considerations

#### 3.1 Theoretical Considerations for Design of Chamber

Factors which influence the chamber's electrical and operational characteristics include: (a) the size of the chamber and materials used in the chamber's construction, (b) the characteristic impedance of the transmission lines used for TEM mode operation of the chamber, and © the EUT's mechanical and electrical operational requirements.

The size, shape, and materials used in the chamber determine the test volume, quality factor, and shielding effectiveness of the chamber. The size and shape also influence the frequency distribution, number of modes, and density of the modes that are excited inside the chamber. At low frequencies, only the fundamental or TEM mode can exist in the chamber. As the frequency increases, higher order modes may begin to propagate. The resonant frequencies of these modes can be determined by

$$f_{l np} = 150 \sqrt{(\ell/a)^2 + (n/b)^2 + (p/d)^2} , \quad (1)$$

where  $\ell$ ,  $n$ , and  $p$  are integers, and  $f_{l np}$  is in megahertz when the rectangular chamber's internal dimensions  $a$ ,  $b$ , and  $d$  are expressed in meters. By carefully selecting the chamber dimensions, we can minimize redundant modes (modes occurring at the same frequency), thus obtaining a more uniform mode distribution.

The quality factor of the resonant modes in the chamber determines the input power requirements or establishing test fields when the chamber is operated in the reverberating mode. The theoretical composite quality factor of a reverberating chamber is approximately [8, 9]

$$\tilde{Q} = \frac{3}{2} \frac{V}{S \delta_s \mu_r} \frac{1}{1 + \frac{3\lambda}{16} \left( \frac{1}{a} + \frac{1}{b} + \frac{1}{d} \right)} \approx \frac{3}{2} \frac{V}{S \delta_s \mu_r} , \quad (2)$$

where  $V$  is the chamber's volume in cubic meters,  $S$  is the internal surface area in square meters,  $\delta_s = \sqrt{2/(\omega \mu \sigma)}$  is the skin depth of the chamber wall in meters,  $\sigma$  is the wall conductivity in S/m,  $\mu = \mu_0 \mu_r$  is the wall permeability in H/m,  $\mu_0 = 4\pi(10)^{-7}$  H/m is the free-space permeability,  $\mu_r$  is the relative permeability, and  $\lambda$  is the wavelength in meters. This composite  $\tilde{Q}$  is determined by averaging the  $Q$  values of all possible modes within a small frequency interval around the frequency of interest [8]. The composite  $\tilde{Q}$  estimated from eq (2) is considered an upper bound because it does not take into account losses other than that due to wall conductivity. In reality, other losses will also occur during the measurement, for example, due to leakage from the chamber, antenna support structures and rf loading, and the chamber's wall coatings. The loading

effect in the cavity due to the transmitting antenna(s) is accounted for in the Q calculations by measuring the net input power (incident minus reflected). However, the receiving antenna(s) must still be accounted for. The Q of a cavity with perfectly conducting walls but loaded with a receiving antenna is [10]

$$Q_a = 2 \left( \frac{\omega}{c} \right)^3 \frac{V}{\pi} . \quad (3)$$

The use of probes to measure fields inside the cavity also loads the cavity's Q. However, typical probes are high-impedance devices and have little impact on the net Q of the chamber; therefore, their effect is ignored for this analysis. The theoretical "net" Q is then [10]

$$\tilde{Q}_{net} = \frac{1}{\frac{1}{\tilde{Q}} + N_a \frac{1}{Q_a}} , \quad (4)$$

where  $N_a$  is the number of receiving antenna in the chamber.

At high frequencies the theoretical Q of the chamber is determined by the lossy cavity walls. At low frequencies the loading effect of the receiving antenna dominates the cavity Q. This effect is clearly shown later in Section 4.

An alternative means of determining the chamber's Q is also available by measuring the chamber's loss [11]. Chamber loss is determined experimentally by measuring the difference between the net input power  $P_t$  delivered to the chamber's transmitting antenna or transmission lines and the power,  $P_r$ , available at a reference antenna or an EUT. Both  $P_t$  and  $P_r$  are measured in the same units (watts or milliwatts). If the energy were uniformly distributed over the volume of the chamber, an empirical value of the chamber's quality factor ( $Q'$ ) could be obtained using the equation [11]

$$Q' \approx 16 \pi^2 \frac{V}{\lambda^3} \frac{P_r}{P_t} , \quad (5)$$

where  $V$  and  $\lambda$  are as previously defined.

The "equivalent" power density,  $P_d'$ , in a reverberating chamber may be determined by [5]

$$P_d' = \frac{4\pi P_r}{\lambda^2} \quad W/m^2 . \quad (6)$$

If a chamber factor  $K = \tilde{Q}_{net} / Q'$  is determined, assuming high-frequency mode-stirred operation, we can relate  $P_d'$  to the net input power  $P_t$  with the aid of eqs (2), (5), and (6) by

$$P_d' \approx \frac{3\lambda P_t}{8\pi K S \delta_s \mu_r} W/m^2. \quad (7)$$

As can be seen from eq (7), the material used in constructing the chamber as well as the chamber's dimensions influence the input power requirements for establishing a specified test field in the chamber. Typical K factors for reverberating chambers are in the range of 2 to 5.

Obviously, the electrical properties of the materials also influence the shielding characteristics of the chamber. Since the chamber is anticipated for use at frequencies as low as 10 kHz, steel with a relatively high permeability is required to obtain adequate shielding from magnetic fields. The chamber described in this report is constructed from galvanized steel, so it has a surface metal (zinc) with high conductivity. This contributes to a high cavity Q while retaining the magnetic shielding of steel.

It is of interest to compare the power densities of test fields anticipated inside a reverberating chamber with that anticipated inside an anechoic chamber assuming the same available input power. The power density,  $P_d'$  generated inside an anechoic chamber, assuming far-field conditions, can be determined by

$$P_d = \frac{P_t G}{4\pi r^2} W/m^2, \quad (8)$$

where G is the free-space, far-field gain of the transmitting antenna and r is the separation distance between the antenna and the test location in m. A comparison of the test fields given as the ratio,  $P_d' / P_d$ , obtained from eqs (7) and (8) for the RL zinc-finish, reverberating chamber with a large anechoic chamber is given in table 3.1 at frequencies from 100 MHz to 500 MHz. Tuned dipoles were used for these comparisons. The table also gives the size of the test volume that falls within  $\pm 3$  dB region in the anechoic chamber at  $r = 3$  m. The ratios,  $P_d' / P_d$ , for  $r = 1$  m and 3 m obtained using open-ended waveguide and horn transmitting antennas in the anechoic chamber, at frequencies from 0.2 to 18 GHz, are given in table 3.2. The test volume definitions for the radiated fields in the anechoic chamber as a function of antenna gain at 1 m and 3 m separation distances are given in table 3.3. These tables demonstrate that significantly less power should be required to generate the same maximum amplitude test fields in the reverberating chamber over large volumes than in an anechoic chamber over comparable volumes.

Calculated resonant-mode frequencies for the chamber using eq (1) are given in table 3.4. The theoretical mode distribution obtained from these data is shown in figure 3.1 in terms of the percentage frequency interval (gap) between adjoining modes as a function of frequency.

### 3.2 Description of RL TEM/Reverberating Chamber

The RL TEM/reverberating chamber is made from a large modular shielded enclosure 3.69 m x 5.18 m x 9.78 m that was previously in operation as a reverberating chamber [12]. The enclosure is constructed from galvanized steel panels with an integrated panel and joiner system. The interior finish of the chamber is of galvanized zinc. The chamber was modified into a TEM/reverberating chamber by installing two orthogonal plates as shown in the cross-sectional drawing of figure 3.2. The top plate and side plates are designed to operate as 50  $\Omega$  and 65  $\Omega$  characteristic impedance transverse electromagnetic (TEM) transmission lines respectively. Equations and graphs needed to design the plates can be found in reference [13]. Photographs showing different views are shown in figure 3.3. Figure 3.3(a) shows the tuner before installation of the top plate, the top plate installation, and the tuner protruding through the top plate after its installation. Plastic rods and click studs were used to mount the plate to the ceiling of the chamber. Figure 3.3(b) shows the side plate installation, one of its end transitions to a coaxial connector and the chamber's access panels. Again plastic rods with click studs were used to mount the plate to the side wall. The click studs consisted of short threaded rods mounted on 8 cm diameter thin metal bases that were epoxied to the ceiling and wall of the chamber. Their use allowed mounting of the plates without penetrating the chamber's shield (inner surfaces).

The test volume in the chamber is the region centered beneath the top plate and the floor, and between the side plate and its opposite parallel wall. The size of the usable test volume is determined by the mode of operation of the chamber. For TEM mode of operation (approximately from 10 kHz to 30 MHz), the maximum recommended test volume is from one-half to one-third the region between the plates and opposite walls. For reverberating mode of operation (from 100 MHz up), the test volume is the total region between the plates and opposite walls minus approximately 30 cm separation distance from the plates, walls and tuner (or  $\geq 1/6$  wavelength at frequencies above 100 MHz). For reverberating mode of operation, this corresponds to approximately 1.6 m x 3.8 m x 9.0 m for the RL TEM/reverberating chamber.

A single large tuner is used for stirring or redistributing the reflected energy associated with modes excited inside the chamber for the reverberating mode of operation. The tuner consists of 4 rectangular blades, 0.91 m x 1.2 m in cross section, made from plastic foam covered with heavy ( $\geq 0.25$  mm) aluminum foil. The blades are mounted at offset angles (30 to 45°) with respect to the steel drive shaft that is connected to a precision control, so that the tuner revolution rates and positions can be controlled manually or automatically.

The chamber is equipped with two bulkhead access panels shown in a photo on figure 3.3(b), located on the opposite side wall of the side plate providing access to the chamber operation and amplifier equipment rooms. There are also personnel and equipment access doors located on the chamber's end wall and between the operation room and chamber as shown in reference [12].

## 4. CW Evaluation of the TEM/Reverberating Chamber

### 4.1 Measurement Approaches

#### 4.1.1. TEM Mode

For TEM mode of operation in the frequency range from 10 kHz to 30 MHz, two techniques are employed in determining and monitoring the E-fields inside the chamber. The first technique uses measurements of the incident and reflected powers on the sidearms of a bidirectional coupler, the impedance of the TEM transmission lines, the separation distance between the plates and ground plane, and the location between the plates (anticipated placement of the EUT). The second technique is to place a calibrated isotropic E-field probe in the area where the field is to be measured. Using these two techniques gives a double check to help assure consistency and validity of measured data while providing a real-time display of the field strength as measurements are being made.

#### 4.1.2 Reverberating Mode

For reverberating mode of operation at 100 MHz or higher frequencies, the chamber was evaluated using two different operational approaches called mode-tuned and mode-stirred [5].

For the mode-tuned tests, the tuner is stepped at selected, uniform increments. The net input power supplied to the transmitting antenna, the power received by a reference antenna, the field-measuring probe responses, and the EUT response at each tuner position are measured and recorded. Corrections are then made for the changes in the transmitting antenna's input impedance as a function of tuner position and frequency. The measurement results are then normalized to a constant net input power value. The number of tuner steps used per revolution was 200 (increments of  $1.8^\circ$ ).

For the mode-stirred tests, the tuner is continuously rotated while sampling the power received by the reference antenna, the field probe response, and the EUT response. Sampling rates much faster than the tuner revolution rate are used. These measurements are made using a spectrum analyzer and "smart" voltmeters with diode detectors. The smart voltmeters are capable of data storage and calculation of various arithmetic functions. Large data samples (up to 9999) are obtained for a single tuner revolution. Tuner revolution rates are adjusted to meet the EUT output monitor, the diode probe response time, and the sampling rate requirements of the instrumentation. Typical rates used are approximately 2 to 4 min per revolution. The input power is measured only at the beginning of each measurement cycle. For the cw tests, a calibrated bidirectional coupler is used to measure the net input power to the transmitting antenna.

The field inside the chamber is determined using two techniques similar to TEM mode of operation. One technique uses a reference antenna to measure the power density of the field inside the chamber by use of eq (6) given in section 3.1. The other technique uses one or more calibrated probes to measure the E-field. These measurements are described in more detail later.

## 4.2 NIST CW Evaluation System

The block diagram of the system used in the w evaluation is shown in figure 4.1. The test field is established inside the chamber by means of an rf source connected to the appropriate transmitting antenna or plate. Placement of an EUT should fall within the test volume as defined in section 3.2 except, possibly, relative to the floor. The separation distance between the EUT and the floor may be less than 30 cm depending upon the EUT intended use configuration relative to the ground plane. (For some applications, the EUT is mounted close to or directly on a ground plane. In these cases the EUT should be mounted the same in the chamber for test purposes.) Test leads and cables are routed to appropriate monitors, for example, outside the chamber through shielded feed-through connectors. Coaxial cables are used for rf signals, and high-resistance lines are used for dc signals. This is done to prevent leakage of the EM energy to the outside environment or into the instrumentation room. A 10 dB attenuator is used whenever possible between the receiving antenna and the 50  $\Omega$  power sensor or spectrum analyzer. This is done to minimize impedance mismatch with the receiving antenna and to prevent measurement system overload.

The transmitting and reference receiving antennas used for the cw tests are the top and side plate transmission lines (1MHZ to 1GHZ transmitting), a log periodic antenna (0.1 to 1 GHz receiving), and broadband horn antennas (1 to 18 GHz transmitting and receiving). A reference receiving antenna is not used at frequencies below 100 MHZ. For these frequencies the field was determined using calibrated probes.

## 4.3 CW Evaluation and Calibration Results

### 4.3.1 TEM Line and Antenna VSWR and Chamber Coupling Efficiency

The efficiency with which energy can be injected into or coupled out of the chamber by the transmitting transmission lines or antennas and the receiving antennas is determined by: (a) the VSWR of the lines or antennas [that is, the impedance match between the rf source and the transmitting line or antenna (load) or between the receiving antenna (acting as the source) and its output detector (load)], and (b) the ability of the lines or antennas to couple energy into or out of the particular modes (TEM or higher order modes) that exist at the test frequencies of interest. For the reverberating mode of operation, rotating the tuner changes the characteristics of the field inside the chamber. This in turn influences the effective in-situ VSWR of the antennas. Hence, the net input power to the chamber and the received power detected by the reference antenna vary as a function of tuner position. That is, the impedance matches between the rf source and transmitting antenna, and between the receiving antenna and its termination, affect the power transfer between the two antennas. This can result in errors in determining the amplitude of the field inside the chamber if no correction is made. The equation for calculating the magnitude of the error caused by the impedance mismatch is

$$P_f = \frac{\text{fraction of maximum available power absorbed by the load}}{|-\Gamma_S \Gamma_L|^2} = \frac{(1 - |\Gamma_S|^2)(1 - |\Gamma_L|^2)}{|-\Gamma_S \Gamma_L|^2}, \quad (9)$$

where  $\Gamma_S$  and  $\Gamma_L$  denote the complex reflection coefficients for the sources and loads respectively as defined above. Their magnitudes,  $|\Gamma_S|$  and  $|\Gamma_L|$ , can be obtained from the appropriate VSWR by the expression,

$$\Gamma_i = (\text{VSWR}_i - 1) / (\text{VSWR}_i + 1), \quad I = S \text{ or } L.$$

The VSWRs of the transmission lines (plates) and the broadband ridged horn antennas used to excite the chamber are shown in figure 4.2. Figure 4.2 gives the composite VSWRs of the top plate and side plate (1 MHz to 1 GHz) and the broadband ridged horn antenna (1 to 18 GHz) in the transmission mode. The receiving antenna's (log periodic, 0.2 to 1 GHz, and broadband ridged horn, 1 to 18 GHz) VSWRs are similar to figure 4.2. The figures show the maximum, average, and minimum VSWR obtained by rotating tuner through a complete revolution (360°). Large variations and high values of VSWR exist, especially at frequencies between approximately 16 MHz and 1 GHz. At higher frequencies (> 1 GHz) the VSWRs' variations become less and their values are lower, approaching the free-space VSWR of the antennas. At frequencies below approximately 16 MHz, the VSWR of the lines is unaffected by the tuner rotation. At frequencies above approximately 16 MHz the high VSWR results from moding effects in the chamber and lines impedance mismatch. The high VSWR at 16 MHz measured for the top plate was not expected since the first cavity mode resonance for the chamber was theoretically predicted to occur at 32.76 MHz. It is presumed this large VSWR is due to a resonance effect associated with the large hole in the middle of the plate needed to accommodate the tuner. This high VSWR spike is not present in the measurements of the side plate VSWR.

The coupling efficiency of the chamber is defined as the ratio of the net input power delivered to the transmitting plate or antenna to the power available at the 50  $\Omega$  impedance matched terminals of the receiving antenna. These ratios, called the chamber loss, are given in figure 4.3. The curves show the minimum composite loss for the top and side plates transmitting with the log periodic antenna receiving (0.1 to 1 GHz) and the ridged horns transmitting and receiving (1 to 18 GHz). The average and minimum losses measured by the mode-turned approach, using the same plates and antenna combinations over the same frequency ranges are shown in figure 4.4. Impedance mismatch between the receiving antenna and power detector used to measure the received power is not accounted for in these measurements. The magnitude of the error (uncertainty) resulting from this is discussed in [2, 5, 12] and is included in table 4.2.

### 4.3.2 Chamber Quality Factor

The chamber's quality factor,  $Q$ , influences the reverberating region of operation of the chamber in a number of ways. Examples are tuner effectiveness, rf input power requirements and the accuracy with which test field levels can be established inside the chamber. The chamber's  $Q$  also influences the time required for the chamber to charge up to a steady state condition after the input signal is applied. This affects the chamber's response for pulsed rf testing, as is discussed later.

Results obtained by using eq (4) to calculate  $\tilde{Q}_{net}$  and using the chamber's minimum loss data shown in figure 4.4 together with eq (5) to determine  $Q'$  are shown in figure 4.5. The relative permeability used in expression (4) for the galvanized steel is assumed to be equal to 1. Figure 4.5 (a) gives the theoretical and experimental  $Q$  for the chamber, and figure 4.5 (b) gives the ratio (K-factor) of theoretical to experimental  $Q$ . At the higher frequencies the ratio approaches about 5. This compares to a K-factor of approximately 1.6 determined for the chamber before installation of the plates [12]. This suggests that at these frequencies, the plastic rods used to mount the top and side plates are contributing significantly to the additional losses in the chamber (approximately  $5/1.6$  or up to 5 dB additional loss in the chamber).

### 4.3.3 Tuner Effectiveness

Proper operation of the chamber in the reverberating mode depends upon the effectiveness of the tuner to obtain randomness in the distribution of the test field inside the chamber. To achieve this the tuners must be electrically large and shaped or oriented to distribute energy as equally as possible into all chamber resonant modes. A test to determine how well the tuners are functioning is to measure the ratio of the maximum to minimum E-field in the test volume in the chamber as a function of tuner position. This is done by either measuring the maximum to minimum ratio of the received power at the terminals of the receiving antenna, or by measuring the maximum to minimum electric field in the chamber using a calibrated probe. The measurements are corrected for a constant net input power to the transmitting antenna.

Measurement results for the RL chamber are given in figures 4.6 through 4.8. Figure 4.6 gives the E-field measured at selected frequencies using a calibrated 5 cm dipole aligned with the vertically polarized component of the field. The probe is centered between the top plate and floor. Figure 4.7 gives the E-field measured at the same frequencies with the probe aligned with the horizontally polarized component and centered between the side plate and opposite wall. A constant net input power of 1 W was applied to the top or side plate. At 30 MHz there is almost no variation in the field as a function of tuner position. As the frequency increases, both the amplitude and number of variations increases significantly. This is summarized in figure 4.8 at frequencies above 0.1 GHz. This figure shows the ratio of the maximum to minimum receiving antenna power measurements for a complete revolution of the tuner as a function of frequency. This ratio, determined in decibel, is the same measure of tuner effectiveness as would be determined from figures 4.6 and 4.7. The measurements were obtained by using the same transmitting and receiving antennas as noted in figure 4.4. This ratio is also influenced, in addition to the tuner size and shape, by the chamber  $Q$ . For example, placing rf absorber and/or

an EUT inside the chamber will lower the chamber's Q. A minimum ratio of 20 dB is recommended to assure proper operation of the chamber [5]. As seen in figure 4.8, a tuner effectiveness greater than 20 dB is achieved at frequencies above 100 MHz for the RL chamber.

#### 4.3.4 E-Field Amplitude Calibration

The E-field amplitude in the chamber can be determined either from measurements of the input power to the transmission lines (TEM operation) or from the power received at the terminal of the receiving antennas (reverberating operation). It can also be determined by measuring the E-field with calibrated probes.

For low frequencies (TEM region of operation), the electric field can be calculated by using the expression,

$$E \approx \frac{\sqrt{P_n R}}{b} \text{ V/m}, \quad (10)$$

where b is the separation distance between the plate and the opposite wall or floor in m,  $P_n$  is the net input power to the line in W, and R is the transmission line's impedance ( $\approx 50$  or  $65 \Omega$ ).

For high frequencies (reverberating region of operation), an equivalent electric field in the chamber may be calculated using the expression,

$$\bar{E}_a = \sqrt{\eta P'_d} \approx \frac{4\pi}{\lambda} \sqrt{30 \bar{P}_r} \text{ V/m}, \quad (11)$$

where  $\eta$  is the average wave impedance of the chamber ( $377 \Omega$ ),  $\bar{P}_d$  is the equivalent power density in  $\text{W/m}^2$ ,  $\lambda$  is the wavelength in m, and  $\bar{P}_r$  is the measured average received power in watts. The validity of eq (11) has been verified and discussed in [5].

Results of the measured electric fields in the chamber for 1 W net input power are shown in figures 4.9 through 4.12. Figures 4.9 and 4.10 give the average and maximum electric field components, obtained with a calibrated probe made of three orthogonal dipoles, placed at the center of the chamber. The x, y, and z components are the transverse (side to side), the longitudinal (end to end) and the vertical (top to bottom). In addition, the total magnitude (Root Sum Square (RSS) value of the three components) is also included and labeled by T. Figures 4.11 and 4.12 give the maximum and average electric fields determined from received power measurements and eq (11) and from measurements using calibrated 5 cm and 8 mm dipole probes. The probes were aligned to give the tem polarization matched component of the electric fields associated with the specified plate excited. Receiving antennas used included a log periodic, 0.1 to 1 GHz and a broadband ridged horn, 1 to 18 GHz. The chamber was excited using the top plate, figure 4.11, or side plate, figure 4.12, at frequencies from 0.001 to 1 GHz. Fields were generated in the chamber, at frequencies from 1 to 18 GHz, using a broadband ridged horn

antenna oriented toward a corner of the chamber. Measurements were made with the probes placed at two locations, (a) at the center of the test zone, and (b) offset along the length of the plate 1.5 cm toward the end (position 6 of figure 4.14) of the chamber. The tuner was rotated through one complete cycle ( $360^\circ$ ) for all four figures, 4.9 through 4.12.

Two locations for the probes were chosen because of the anticipated effect of the hole in the top plate on the test field characteristics at the center of the chamber (directly below the tuner). The field is significantly lower at the center, directly below the tuner, than at position 6. Based on these results, we recommended that equipment to be tested at frequencies below 100 MHz, for vertical polarization, be placed offset along the chamber's length so as to fall under a solid portion of the top plate.

These data clearly indicate three distinct regions of operation for this chamber. At frequencies below approximately 16 MHz for the top plate and approximately 30 MHz for the side plate, the field is characteristic of the TEM mode and the tuner rotation has little or no effect upon the field's amplitude. Hence, the maximum and average E-field are the same. The amplitude of the component corresponds to the calculated value determined from measuring the net input power and applying eq (10). At frequencies between approximately 16 MHz (top plate) or 30 MHz (side plate) and 100 MHz, the chamber operates in the transition region where higher order modes exist in addition to the TEM mode but in insufficient numbers for the chamber to reverberate properly. Large variations in the field strength exist in this region. At frequencies above approximately 100 MHz, enough modes are generated so that the chamber is reverberating effectively. In this region the effective Q of the resonant modes is evident and the tuner is effective in redistributing the fields within the chamber. Thus the maximum amplitude of the field is substantially higher than that for the TEM mode of operation (as great as 30 dB) for the same net input power (1 W). Also, the polarization properties of the components are lost. Note that the amplitudes of the three components in figures 4.9 and 4.10 in this frequency region are approximately the same, and that the total magnitude (RSS value) of the components for the average values is a ratio of 3 or about 4.8 dB higher than each individual component. This indicates that the measured value of the average of each component is independent of polarization of the dipole probe. The total magnitude, however, of the E-field components' maxima is less than 4.8 dB (approximately 3 dB). This indicates that the maximum measured values for each component are not independent (that is,  $E_{X(\text{total})}$  is a function of  $E_{Y(\text{total})}$ , etc.). This is similar to the results obtained for other reverberating chambers and appears to be inherent in the reverberating chamber measurement method. The implication is that if multiple receptors are used (for example an isotropic probe whose output is a function of all three orthogonal dipoles) in establishing the test field amplitude inside a reverberating chamber, the results will be biased by either 3 dB for maximum response data or 4.8 dB for average response data.

The three-orthogonal-dipole probes used to measure the fields in figures 4.9 to 4.12 were calibrated in a planar far-field. A TEM cell [14] was used at frequencies up to 500 MHz and an anechoic chamber was used at frequencies from 500 MHz to 18 GHz [15]. The assumption is made that the average field over the aperture of the probe inside the reverberating chamber will approximate the planar field used to calibrate the probe. This is reasonable, at least at frequencies

for which the probe is electrically small. Also, the open-space far-field gain of an electrically small dipole is small (1.76 dB). Thus, the probe-measured fields should be equivalent, within approximately 1.76 dB, to the E-fields determined using a receiving antenna. This is true if the polarization properties of the probe and receiving antenna are effectively eliminated in the chamber. The variations in the fields determined by using received power measurements and by using the probes (figures 4.11 and 4.12) are typical of the random variations in the data used to determine the field strength inside reverberating chambers. The agreement between the two methods is considered reasonable.

Using the results of figures 4.11 and 4.12, we can calculate the input power requirements for establishing a given field level in the chamber. An example is shown in figure 4.13. This figure gives the net input power required to generate a 200 V/m field in the RL chamber using the top and side plates (0.001 to 1 GHz) and a ridged horn antenna (1 to 18 GHz).

#### 4.3.5 Test Zone E-Field Uniformity

Tests were made to determine the E-field uniformity in the chamber as a function of spatial position and frequency. Nine small NIST isotropic probes [16, 17, 18] designed to operate at frequencies up to 2 GHz were placed at various locations inside the chamber (positions 1, 2, 3, 4, 6, 7, 8, 9, and 10) as shown in figure 4.14. No position 5 was designated. Photographs of the interior of the chamber showing the placement of the probes are given in figure 4.15. Each probe has three orthogonally oriented dipoles which are aligned with the three axes of the chamber as shown on figure 4.14. Measurements were made of the field strength of each orthogonal component at the nine locations for each tuner position (200 steps of  $1.8^\circ$ ) for frequencies from 1 to 2000 MHz. Again these data were normalized for a net input power of 1 W applied at the input terminals of the transmission lines or transmitting antenna. The maximum and average values for each component and the RSS value were then determined from the complete data sets. The results of these measurements obtained when driving the chamber top and side plates are shown in figures 4.16 and 4.17. The figures give the individual data obtained for all nine probes as well as the average values calculated for each set of probe measurements. Again, the three regions of operation are apparent. The spread in the data shows spatial field variations inside the chamber at the indicated frequencies. Note that the dominant components match with the TEM mode E-field polarization for each driven plate in the TEM mode region (below 30 MHz). For example, the  $E_z$  component is dominant for the top plate, and the  $E_x$  is dominant for the side plate. These results are in agreement with figures 4.9 and 4.10. Gradients in the E-fields between the plates, however, are significant. This is due to the placement of the plates close to the top and side walls as necessary for a clear test volume. The vertical E-field difference for the top plate, figure 4.16, over one-half the vertical separation distance (positions 1 to 2 and 2 to 3), is relatively small, approximately 4 dB ( $\pm 2$  dB) at frequencies below a few megahertz. However, the amplitude of the field is about 10 dB lower than anticipated if there were no hole in the plate and as measured at positions 6 and 9 or 7 and 10. This is why we recommend placing the EUT between positions 6 and 7 or positions 9 and 10 when performing low frequency vertically polarized tests. At these positions, variations in the field along the vertical axis for one-half the separation distance are greater than at the center, approximately 8 dB ( $\pm 4$  dB), but are more

consistent with the TEM mode field and hence more theoretically predicible as a function of frequency. Also, the  $E_z$  values at positions 6 and 7 or 9 and 10 are approximately the same, so the field is relatively uniform along the length of the plate, away from the hole in the center.

The polarization matched component,  $E_x$ , generated when the side plate is driven (figure 4.17) varies about 20 dB between positions 4 and 8. Again, this is due to the placement of the plate close to the side wall as required to maximize the chamber's test volume.  $E_x$  along the length of the plate, positions 6 and 7 or 9 and 10, however, are about the same and the  $E_x$  values at positions 1 and 3 toward the plate edges are within a few decibels of position 2.

At frequencies above about 100 MHz (reverberating region) the amplitudes of the field components in figures 4.16 and 4.17 are approximately the same. The total magnitude or RSS value of the average field is approximately 4.8 dB greater than the individual components. This is similar to that shown in figures 4.9 and 4.10. Also, the differences between the maximum and average amplitudes, (a) and (b) of figures 4.16 and 4.17, at frequencies above 100 MHz, approach about 8 dB. This is another indication that the chamber is operating properly, at these frequencies, in the reverberating mode.

A summary of the spatial field distribution obtained from figures 4.16 and 4.17 is given in table 4.1. As mentioned earlier, the E-field amplitude in the chamber is influenced by the chamber's Q. Inserting the nine probes into the chamber with their lossy transmission lines lowers the chamber's Q and hence the field strength in the chamber compared to what is present without the loading effect of the multi-probe system.

#### 4.3.6 Summary of CW Calibration and Evaluation Results

Results of the CW calibration and evaluation of the RL TEM/reverberating chamber indicate three distinct frequency regions of operation as summarized in table 4.2. The TEM mode region extends from 10 kHz to approximately 16 MHz (top plate) or 30 MHz (side plate). This is slightly lower in frequency than where the first higher order mode becomes resonant. Test fields established in this region simulate planar fields with the E-field normal to the driven plate and the magnetic field tangential around the plate. The large differences in the fields that exist in the test volume between the plates and their opposite ground planes are due to the close proximity of the plates to the chamber's top or side wall. The accuracy with which the E-field, at the center of this unperturbed volume, can be established is estimated to be approximately  $\pm 3$  dB. This assumes, for vertical polarization (top plate excitation), offsetting the test volume either half way between positions 6 and 7 or positions 9 and 10, along the center of the chamber. Input power requirements to establish the required test field are determined by the plate driven (see figure 4.13).

The second frequency region, referred to as the transition region, extends from approximately 16 (or 30) MHz to 100 MHz. The test fields are a combination of TEM plus an increasing number of higher order modes, as a function of increasing frequency. Thus, the field is no longer a simple equivalent plane-wave simulation, but now includes higher order modes. For this reason,

the amplitude of the test field has errors that can be as large as  $\pm 15$  dB. The input power required to generate test fields decreases with increasing frequency. The polarization of the test field changes from vertical or horizontal at 16 or 30 MHz to undefined or complex (reverberating field) at 100 MHz.

The third (reverberating) region extends from approximately 100 MHz to 18 GHz or possibly 40 GHz or higher. The test fields are complex multimoded fields simulating a near-field environment. The uncertainty of determining the maximum or average amplitude of the test field varies from an estimated  $\pm 8$  dB at 100 MHz down to  $\pm 4$  dB at frequencies above 2 GHz [12]. The input power required to generate a maximum test field of 200 V/m varies from about 40 W at 100 MHz decreasing to about 15 W at 2 GHz, then increasing again to about 60 W at 18 GHz. (See figure 4.13 for reference.)

## 5. Pulsed RF/Time-Domain Evaluation of the RL TEM/Reverberating Chamber

### 5.1 Background

Parameters of EMI signals that can contribute to upset in electronic equipment include: (a) total energy, (b) peak amplitude, and (c) transient characteristics. All these parameters are different inside a reverberating chamber than in free space. Their characterization inside a reverberating chamber, particularly for pulsed rf fields, provides information required for making necessary analysis to determine correction factors as a function of the input pulse parameters. The term "pulsed rf" refers to pulse-modulated cw with characteristics similar to a pulsed radar signal. Their characterization also provides insight into the inherent limitations associated with using this complex environment for pulsed rf EMS/V testing. Obviously, these parameters are influenced by the chamber's Q factor. This is because the time required for a pulsed wave's amplitude to rise to its steady-state value inside the chamber and to decay to zero after the input signal is removed, is a function of the chamber's Q. These charge and decay times can be reduced by artificially lowering the chamber's Q, for example, by inserting small amounts of rf absorber. However, this reduces the accuracy of determining the test field amplitude. Results of work to evaluate the response characteristics of the chamber when excited by pulsed rf of various pulse widths and frequencies are discussed in this section.

### 5.2 NIST Pulsed RF Evaluation System

A block diagram of the system used for the pulsed rf evaluation measurements of the chamber is given in figure 5.1. A test field is established inside the chamber by means of a pulsed rf source connected to a broadband ridged horn antenna. The input signal is monitored by a calibrated diode detector connected to the side arm of a calibrated directional coupler. The output of this detector is connected to one channel of the transient digitizing oscilloscope. The field established inside the chamber is monitored by a broadband ridged-horn receiving antenna and calibrated diode detector connected to the second channel of the same oscilloscope. The receiving antenna is similar to the antenna used for transmitting the signal. As in the cw tests, the tuner is rotated to redistribute the rf energy inside the chamber.

The mode-tuned approach was used to optimize the measurement accuracy and to obtain complete statistical information for evaluating the time-domain response characteristics of the signal detected at the terminals of the receiving antenna. The digitizing oscilloscope used is capable of measuring signals with rise times of approximately 30 ps, at a sampling rate of 50 kHz, with sample sizes up to 1024 per scan.

The measurements were made by digitizing each pulse using 512 samples in time, at each of the 200 angular positions of the tuner for one complete revolution. Corrections were made to each measurement for cable loss, coupling ratio of the directional coupler, attenuator calibrations, and diode detector readings.

### 5.3 Pulsed RF Evaluation Results

Measurements were made to determine: (a) the ratio of the received pulse amplitude versus input pulse amplitude as a function of time after the input pulse is turned on, and (b) the time required for the chamber to charge up to its steady-state amplitude and then to decay to zero after the pulse is turned off. These measurements were made with the chamber empty (no absorber). Results of these measurements are given in figure 5.2 for three input pulse widths, 1  $\mu$ s, 3  $\mu$ s, and 10  $\mu$ s, at nine frequencies. Each graph shows two curves, one for the maximum and one for the average received signals. By examining these data at the selected frequencies, we can determine the approximate charge-decay times as a function of frequency. These results are shown in figure 5.3. The results show the time required for the received signal to rise to 63% (1 to 1/e), and 90% of the maximum amplitude. The implication of figure 5.3 is that the input pulse width, at the frequencies of interest, should be equal to or longer than the values shown by the curves for the pulsed rf test field amplitude to reach 63 or 90% of the maximum steady-state amplitude. The steady-state amplitude is achieved if the input pulse width is sufficient for the chamber to charge up to 100%, or to its maximum output for a given input pulse amplitude.

If the transmitted input pulse width is shorter than the charge time of the chamber, an error will result in terms of establishing a known peak amplitude of the test signal in the chamber. An estimate of a correction factor to apply for this condition can be found by calculating the ratio of the received signal amplitude to the steady-state transmitted signal amplitude as a function of time after turning on the transmitted pulse. Figure 5.4 gives these results, determined from the data of figures 5.2 and 5.3. The data are projected down to input pulse widths of 0.3  $\mu$ s. Figure 5.5 shows another way to display the data given in figure 5.4. The correction factors are given, for discrete input pulse widths, as a function of frequency rather than for discrete frequencies as a function of input pulse width. The symbols, #, +, \*, and •, indicate the actual data extracted from figure 5.4, and the solid curves are the smoothed approximations for these data.

It is interesting to compare the chamber's response time calculated from the experimentally determined, average Q values, with the measured response time. The response time is approximately  $20/\omega$  for the signal to rise or decay to 63% of the steady-state amplitude. These results are shown in table 5.1. The table gives the measured average chamber losses, the associated calculated Q factors, the calculated charge-decay times, and the measured charge-decay

times at the selected frequencies. The measured response times are somewhat lower than the calculated response times, but are still within the margin of error expected for this type of measurements.

#### 5.4 Comments on Pulsed RF Measurements Results

For part of the data, the maximum amplitude of the pulsed rf field strength, when measured immediately after the pulse is turned on, appears to be slightly greater than the steady-state value. This overshoot is thought to be due to the imperfect leading edge of the pulse produced by the pin diode switch in the pulse source. The overall trend, however, is for the shorter pulses to have a smaller value of peak detected voltage. This is because the on-time is not sufficient for the EM energy in the reverberating chamber to reach its steady-state value. Thus, data were taken for a range of pulse widths to determine the correction factor to be applied when using the chamber to take EMS/V data for very short radar pulses.

### 6. Performing EMC/V Measurements Using the TEM/Reverberating Chamber

#### 6.1 Performing EMC/V Measurements with Manual Operations

An especially useful application of the TEM/reverberating chamber is to perform shielding effectiveness (SE) measurements. Block diagrams of two simple, manually operated systems are shown in figures 6.1 and 6.2. These systems do not require the use of a computer controller. Figure 6.1 employs the radiated immunity measurement approach and figure 6.2 uses the radiated emissions approach. The systems use a sweep oscillator and spectrum analyzer to cover approximately octave bandwidths in the frequency range of interest. Two measurement approaches are required depending upon the region of operation (TEM or reverberating mode).

The example used for explaining the application of figures 6.1 and 6.2 is for cable/connector SE measurements. In the TEM mode region of operation, a reference cable is placed in the chamber oriented to maximize coupling either to the electric field or to the magnetic field of the TEM mode. This cable typically consists of a section of bare (unshielded) center conductor of a cable similar to and of equal length to the cable under test (CUT). Reference measurements are made by either (a) establishing the test field in the chamber at the frequencies of interest and recording the power coupled to the output of the reference cable (immunity, figure 6.1), or (b) by driving the reference cable and measuring its radiated emissions (figure 6.2). The CUT is then placed in the chamber in the same location as the reference cable and with the same orientation and the measurements are repeated. The SE is then determined using the expression

$$SE_i = 10 \log \frac{P_{CUT} P_{i(ref)}}{P_{ref} P_{i(CUT)}}, \quad (12)$$

where  $I = n$  or  $r$  for immunity or emission testing. For immunity testing,  $P_{CUT}$  is the power coupled to the CUT,  $P_{n(CUT)}$  is the net input power applied to the chamber when measuring  $P_{CUT}$ ,

$P_{ref}$  is the power coupled to the reference cable and  $P_{n(ref)}$  is the net input power applied to the chamber when measuring  $P_{ref}$ . Impedance mismatch errors are corrected by using eq (9) as described in section 4.3.1.

For radiated emission testing,  $P_{r(CUT)}$  is the power coupled to the output of the chamber's appropriate TEM plate with the net power,  $P_{CUT}$ , applied to the CUT.  $P_{r(ref)}$  is the power coupled to the output of the chamber's appropriate TEM plate with the net power,  $P_{ref}$  applied to the reference cable. Both  $P_{CUT}$  and  $P_{ref}$  must be determined as net (incident minus reflected) power.

A unique feature of the TEM/reverberating chamber, operating in the TEM mode, is the ability to determine equivalent free-space radiated power from the CUT. This is based upon measurements of the power radiated from the CUT or, in general from the equipment under test (EUT), that are coupled by the chamber's TEM mode to the appropriate TEM plates output port. The following equation is then used [2]:

$$P_r \approx \frac{2 P_m \eta_o}{3 \pi Z_o} \left( \frac{k b}{\tilde{E} \cos \theta} \right), \quad (13)$$

where  $P_r$  is the equivalent free-space power radiated from the CUT or EUT in W,  $P_m$  is the power measured at the output port of the cell (with the opposite port terminated into  $50 \Omega$ ) in W,  $\eta_o$  is the intrinsic wave impedance ( $\approx 120 \pi \Omega$ ) in the chamber,  $Z_o$  is the chamber's TEM plate characteristic impedance ( $\approx 50$  or  $65 \Omega$ ),  $E$  is the normalized electric field inside the chamber relative to the field strength at the center of the chamber's test region (midway between the plate and opposite wall),  $\cos \theta$  corresponds to the polarization match between the radiated fields from the CUT or EUT and the TEM mode field characteristics in the chamber,  $k$  is equal to  $2 \pi / \lambda$  where  $\lambda$  is the wavelength of the radiated signal in m, and  $b$  is the separation distance between the chamber's plate and the opposite wall in m. Maximum coupling occurs when  $\cos \theta = 1$  or if the CUT or EUT is oriented for polarization match to the chamber's TEM field. This equation is valid only as  $\cos \theta$  approaches 1.

Measurements are made in the reverberating region of operation in much the same manner as for TEM mode of operation. The exceptions are that now the tuner(s) are rotated at revolution rates fast (for example, 0.5/s) compared with the sweep oscillator sweep speed (for example, 100 s/sweep). The spectrum analyzer is set up to measure in its maximum hold mode and to scan the same frequency band as the oscillator. The analyzer's scan rates used are as fast as possible (for example, 20 to 30 ms/scan). Resolution and video bandwidths selected must be compatible with the scan rate and dynamic range requirements to ensure that the analyzer is operating within calibration. If the SE of the CUT is high ( $> 40$  dB), a calibrated attenuator is used between the output of the reference antenna (or cell when driving the reference cable) and the analyzer. Typically a reference antenna is used in place of the reference cable at frequencies in the reverberating mode region of operation.

The steps for performing immunity sweep frequency testing proceed as follows: First, connect the reference cable or antenna to the analyzer and the sweep oscillator output to one of the

chamber's TEM plates or to its transmitting antenna. Take a sweep and store the analyzer measurement results in decibel milliwatts in one of its channels, for example channel A, while also recording the net input power to the chamber using a calibrated dual-directional coupler with detectors and an XY recorder. Next, replace the reference cable or antenna with the CUT, connect the output from the CUT up to the analyzer, and repeat the measurement. Measure the net input power to the chamber to be sure it is either the same as for the first set of measurements with the reference cable or antenna, or that correction can be made to normalize the analyzer data as if the net input power were the same for the two measurements. Store the results in decibel milliwatts in the analyzer's channel B. Then subtract channel B from A and add the calibrated attenuator factor in decibels, if used, to get the SE in decibels. The cable lengths for connecting the reference antenna and the CUT to the analyzer should be the same or differences must also be corrected for. If a single or limited number of sweeps is made, use the envelope of the CUT data to subtract from the reference cable or antenna data so that the minimum SE values are obtained. Using this procedure will ensure adequate accuracy without requiring excessively long sweep times or a large number of repeated sweeps. The results obtained using this procedure give nearly continuous frequency coverage measurements of SE.

Measurements of an EUT's response to determine its susceptibility or to determine the shielding effectiveness of enclosures proceed in much the same manner as above.

For some applications, it may be advisable to determine the shielding factor (SF) of the EUT. This is defined as the ratio of the EUT's response, expressed in power, to the test field's power density, or

$$SF = 10 \log \left( P_d' / P_{EUT} \right) \text{ dB/m}^2, \quad (14)$$

where  $P_{EUT}$  is the power coupled to the EUT in W, and  $P_d'$  is the power density inside the chamber in watts per square meter. The SF is similar in concept to the well known antenna factor used in antenna calibrations.

The steps for using the radiated emissions measurements approach for cable/connector sweep-frequency SE testing in the reverberating region of operation are as follows: First, connect up the system as shown in fig. 6.2 with the reference cable or antenna connected to the sweep oscillator via a calibrated dual-directional coupler. The output from the chamber's selected TEM plate or receiving antenna is connected to the spectrum analyzer. The measurements then proceed in much the same fashion as for the immunity measurement approach. That is, the sweep oscillator is turned on and the output from the chamber recorded on channel A of the analyzer while the net input power to the reference cable or antenna is monitored (or recorded on an XY recorder). The reference cable or antenna is then replaced by the CUT; the output from the oscillator is then connected to the CUT and the measurement repeated with the analyzer results recorded in chamber B. Again the net input power to the CUT is monitored to be sure it is the same as for the reference cable or antenna (or the results are normalized as if it had remained the same.) The SE is then determined by subtracting channel B from channel A. Comments on the need for multiple sweeps and how to minimize measurement time are the same as for immunity

testing. For cable/connector assembly SE measurements, mismatch errors caused by large VSWRs of the CUT are minimized by using the radiated emissions approach. This is because use of a bidirectional coupler to measure the net input power to the reference cable or CUT gives the equivalent of an impedance match sources for the measurements.

For radiated emission measurements in general, the EUT is not connected to the rf source, but rather, is the source itself. For this case, power radiated from the EUT excites the chamber and hence couples to the chamber's receiving antenna. This coupled power is measured on one channel of the analyzer. The EUT is then turned off and power is applied to the chamber's transmitting antenna or one of its plates. The output power from the oscillator is adjusted to give approximately the same coupled power to the reference antenna. This may require the use of a calibrated attenuator between the reference antenna and analyzer to keep from reducing the oscillator output power too low. These measurements are recorded on another channel of the analyzer. The radiated power from the EUT is then determined by

$$P_{rad(EUT)} = P_{n(t)} \frac{P_{rec(EUT)}}{P_{rec(t)}}, \quad (15)$$

where  $P_{ref(EUT)}$  is the power received by the reference antenna when the EUT radiates,  $P_{n(t)}$  is the net input power applied to the chamber's transmitting antenna or plate, and  $P_{rec(t)}$  is the power received by the reference antenna when the chamber's transmitting antenna or plate is excited. All the powers are expressed in the same unit, watts or milliwatts.

An example of SE data obtained using the block diagram of figure 6.1 is given in figure 6.3. The EUT is a TEM cell having a cross section area of 3 cm x 6 cm with a 15 mm circular aperture. This EUT is a control standard device developed at NIST for SE measurement standardization. Two traces are shown in figure 6.3. The top trace is the measurement of the reference antenna received power recorded, in decibel milliwatts, on channel A of the analyzer. The bottom trace is the received power coupled to the EUT recorded, in decibel milliwatts, on channel B of the analyzer. A 10 decibel attenuator was used between the reference antenna and analyzer in performing this measurement. This 10 decibel must be added to the difference,  $P_{ref} - P_{EUT}$ , in calculating the SE of the EUT.

## 6.2 Automated EMC/V Measurements

### 6.2.1 TEM Mode Measurement Procedures

Detailed step-by-step procedures for using TEM cells for performing radiated immunity measurements are given in reference [2]. Measurements using the TEM/reverberating chamber in the TEM mode region of operation follow the same steps. These steps consist of the following:

- (a) Determine the EUT test parameter requirements in terms of test field amplitude, wave-shape, modulation, frequency range and interval, exposure polarization, exposure time

requirements, and EUT performance degradation criteria.

(b) Place the EUT inside the cell in one of two locations for testing. The first location is close to the ground plane to minimize exposure of the EUT's input/output, power, and monitor leads to the field generated inside the cell. The second position is midway between the plate and ground plane. This position provides greater field exposure to the EUT's leads and hence gives an indication of how energy is coupled to the EUT.

(c) Access the EUT as required for operation and performance monitoring. The EUT input/output and ac power leads should be as nearly the same as in its intended use. Leads should be the same length, if possible, and be terminated into their equivalent operational impedances so as to simulate the EUT in its operational configuration. Take care in routing the leads including monitor leads (if not transparent to the rf field) inside the chamber to obtain the most meaningful, repeatable results. Placement of the leads, wiring harness, etc. should be recorded for future reference so that if repeat measurements are required, the leads can be placed as nearly identical to the original tests as possible. Fiber optics or high-resistance lines should be used for monitoring the operation of the EUT if possible. Such leads minimize coupling to and distortion of the test fields.

(d) Connect up the measurement system as shown in figure 6.4

(e) Apply power to the chambers TEM lines as needed to establish the desired test field and, with the EUT in operation, record the EUT's monitor responses as a function of the test field level, modulation parameters, polarization, and frequency to determine immunity.

### 6.2.2 Reverberating Mode-Tuned Measurement Procedure

A detailed step-by-step measurement procedure and flow diagram for performing automated radiated immunity tests using a reverberating chamber is contained in reference [5]. The procedure is the same for the TEM/reverberating chamber used in the reverberating region of operation. It is summarized briefly as follows:

(a) Determine the testing requirements for the EUT as referred to in section 6.2.1 item (a) above.

(b) Place the EUT inside the chamber and access it for operation and monitoring.

(c) Connect up the measurement system as shown in figure 6.4 with switches  $S_1$  and  $S_2$  and connected as appropriate for the frequency range of interest (that is,  $S_1$  to the plates for frequencies below 1 GHz and to the ridged-horn antenna at frequencies above 1 GHz, and  $S_2$  either to the EUT or to an appropriate receiving antenna.) An alternative is to have both the EUT and receiving antenna connected to their own detectors/monitors simultaneously and the measurement results sent to the computer as needed.

(d) Input the measurement and calibration parameters into the computer. These include frequency ranges and increments for the tests, number of tuner steps to be used, signal generator output levels to generate the required test field amplitudes, maximum EUT output level allowed (to prevent damage to the EUT), EUT response time, and cables, directional couplers, and sensors calibration factors.

(e) Perform the measurements in automated sequence starting at the lowest frequency and test field amplitude. Increase the frequency in increments at the initial test field amplitude and then increase the field amplitude while scanning the frequencies until the maximum test field amplitude is achieved or the EUT maximum allowable response is reached. Correct the measurement data using the appropriate calibration factors preciously put into the computer. (This can occur simultaneously with making and recording the measurements.) The optimum technique for obtaining mode-tuned data is to step or increment the frequencies at each tuner position before stepping the tuner to its next position. When the tuner is stepped, it should be allowed to stabilize while power meters, voltmeter, monitors, etc. are being zeroed and residual offsets measured. Be sure the rf is turned off while this is done. The rf power is then turned on, the test field is established, the measurements are made at each frequency, and the data are corrected (with respect to a desired net input power) and stored. The corrected data are then reconfigured by frequency at the end of the run, after the tuner has been stepped through all positions to complete one revolution ( $360^\circ$ ). Calculations of statistical quantities are then made and the data are presented in the final form.

### 6.2.3 Reverberating Mode-Stirred Measurement Procedure

Although the mode-stirred measurements begin in a similar manner to the mode-tuned described above, the automated measurement sequence of events is different. Hence, some parameters necessary for performing the measurements differ from the mode-tuned approach. The procedure is summarized briefly as follows. After determining the EUT test parameters:

(a) Place the EUT inside the chamber and access it for operation and monitoring.

(b) Connect up the measurement system as shown in figure 6.4 with  $S_1$  and  $S_2$  connected as appropriate.

(c) Input the measurement and calibration parameters into the computer. These include the frequency ranges and increments, the signal generator output range and increments, the EUT output minimum and maximum response limits, the EUT response time, the cables, directional couplers, and sensors calibration factors, and the tuners rotation rates.

(d) Perform the measurements using the automated sequence which includes setting the generator to its first frequency, starting the tuners in motion, and monitoring the EUT response (s) while slowly increasing the test fields. When the EUT minimum response is exceeded or the maximum test field is reached, the tuners are stopped, the system is initialized with the monitor voltmeters and spectrum analyzer set up to start taking data when triggered. The rf power is

turned on, the net input power is measured and the tuners are placed into motion as the voltmeters and spectrum analyzer are triggered into performing their measurements.

(e) Make calculations of corrections for calibration factor while the measurement proceeds. The results are then compiled at the end of each frequency run after one complete revolution of the tuner and stored in memory for presentation at the conclusion of the measurements. If the maximum allowable EUT response is reached during the measurement, the generator output is reduced by an interval of 1 dB and the measurement is repeated starting with a complete new initialization and a full 360° revolution of the tuners. This ensures accurate results without damaging the EUT.

#### 6.2.4 Comparison of TEM/Reverberating Chamber Measurement Results with Anechoic Chamber Tests - Some Examples

Comparisons of the EUT response obtained using a reverberating chamber and an anechoic chamber are typically made in terms of maximum or peak data values. The main reason for this is that the EUT's worst case performance or susceptibility is normally what is desired. An additional practical consideration is that it is very difficult to obtain a true average EUT response from anechoic chamber data. Even determining the EUT's peak response in an anechoic chamber may require considerable effort involving complete pattern measurements.

The benefit of making this type of comparison is to obtain a correlation factor between results obtained in the TEM/reverberating chamber and those obtained in an anechoic chamber. This has been done for three reference EUTs. These are: (a) a 1 cm dipole probe, (b) a small broadband horn antenna similar to what is used at frequencies from 0.8 to 18 GHz in the RL chamber, and © a small TEM cell with 3 cm x 6 cm cross section and a 15 mm diameter circular aperture in the outer conductor. The measurements were performed in a combination of facilities including the RL's small 1.41 m x 1.57 m aluminum reverberating chamber located at Griffiss AFB, NY, the NIST 2.74 m x 3.05 m x 4.57 m steel reverberating chamber located in Boulder, CO, the USAEPG 1/10 scaled 1.31 m x 2.41 m x 3.87 m TEM/reverberating chamber located at Ft. Huachuca, AZ, and the NIST 4.9 m x 6.7 m x 8.5 m anechoic chamber located in Boulder, CO. The results of these measurements are contained in reference [7].

### 7. Summary and Conclusions

As noted earlier, the RL TEM/reverberating chamber has three distinct regions of operation as outlined in table 4.2. Test fields are excited in the chamber at frequencies up to approximately 1 GHz by using the transmission lines. At frequencies above approximately 1 GHz, ridged-horn antennas are used. When the plate lines are not in use, they should be unterminated (open circuit) with the bulkhead feed-through connectors capped to prevent rf leakage to outside the chamber. Other important characteristics are summarized as follows together with some recommendations:

(a) Spatial variations of the maximum and average electric fields in the test volume of the chamber are given in table 4.1 at a few selected discrete frequencies. These data were obtained

using the NIST multi-probe system and the mode-tuned approach with 200 tuner increments per revolution at frequencies from 0.002 to 2 GHz. The limitation for determining the spatial E-field variation depends on the mode density and hence field complexity in the chamber as a function of frequency. The spatial E-field variations should decrease as frequency increases above 2 GHz to less than the result of  $\pm 2$  dB shown in the table for 2 GHz.

(b) Expected fields generated in the three frequency regions of operation are given in figure 4.13. Estimated uncertainties are given in table 4.2.

(c) The maximum E-field established inside the chamber at frequencies above 100 MHz is about 7 to 8 dB greater than the average E-field. This is consistent with the previous results obtained for other reverberating chamber such as this chamber before its modification into a TEM/reverberating chamber, the Naval Surface Weapons Center (NSWC) chamber, and the NIST reverberating chamber.

(d) The directional characteristics of an antenna or EUT placed inside this hybrid chamber operated in the reverberating region of frequencies are lost, resulting in an equivalent directivity of 0 dB in the highly complex field environment.

(e) The correlation factor between free-space (anechoic chamber) and TEM/reverberating chamber measurement results obtained when operating in the reverberating mode for the same EUT is approximately the free-space (far-field) gain of the EUT. This implies that susceptibility criteria determined for an EUT when using the chamber in the reverberating mode should include an additional factor proportional to the EUT's open-field estimated gain as a function of frequency.

(f) If the chamber is used for pulsed rf EMS/V testing, and the input pulse widths are shorter than the chamber's charge time, an error will result in establishing a known maximum amplitude of the test signal. An estimate of the correction factors to apply for shorter pulses is given in figures 5.4 and 5.5.

(g) If the chamber is to be used for immunity testing, and EUT responses to absolute levels of the test fields are required, the mode-tuned approach is recommended for use at frequencies from 30 MHz to 1 GHz. The number of tuner positions recommended is 100 from 30 to 200 MHz and 200 from 200 to 1000 MHz. The mode-stirred approach is recommended for use at frequencies above 1 GHz for absolute measurements (with more than 3000 samples per revolution for frequencies between 1 to 4 GHz, and more than 5000 samples per revolution for frequencies above 4 GHz). The mode-stirred approach is also recommended for all frequencies above 100 MHz if only relative measurements are made.

(h) Antennas for transmitting rf energy into the chamber and for measuring the test E-field should not be used outside their specified frequency range. For example, the 0.8 to 18 GHz ridged-horn antennas should not be used outside their specified band.

(i) Additional work is needed to verify experimentally the correction factors shown in figures 5.4 and 5.5. This could be accomplished by comparing the measured responses of a well characterized EUT to cw and pulsed rf fields as a function of frequency and pulse widths using both an anechoic chamber and the TEM/reverberating chamber.

(j) If corrections are not made for mismatches of the transmitting and receiving antenna, absolute amplitude measurements of the rest field inside the chamber will be lower than the actual values. Experiences in performing this type of measurements indicate that these errors may be as great as 5 dB when VSWRs exceed 15 to 1.

(k) The average wave impedance in the reverberating region of operation, when the maximum response of an EUT is measured, may be higher than  $377 \Omega$ . This is especially true for frequencies lower than 1 GHz. This means that if a wave impedance of  $377 \Omega$  is assumed when determining the maximum amplitude of an exposure field, there will be a systematic error resulting in too low a calculated E-field, and thus also in too high an EUT response. It probably is more accurate to determine the field strength by using calibrated E-field probes at these frequencies.

Work described in this report was sponsored by the Rome Laboratory, Griffiss AFB, NY, with Charles Blank as project officer. The authors acknowledge his assistance in making this project possible. In addition, the authors express their appreciation to Motohisa Kanda for his support and helpful comments.

## 8. References

- [1] Crawford, M.L. Generation of standard EM fields using TEM transmission cells. IEEE Trans. Electromag. Compat. EMC-16 (4):189-195; 1974, November.
- [2] Crawford, M.L.; Workman, J.L. Using a TEM cell for EMC measurements of electronic equipment. Nat.Bur.Stand. (U.S.) Tech. Note 1013; Revised 1981 July.
- [3] Corona, P.; Latmiral, G.; Paolini, E.; Piccioli, L. Performance of a reverberation enclosure for power measurements in the microwave range. 2<sup>nd</sup> Symp. Tech Exhibition on EMC; 1977; Montreux, Switzerland.
- [4] Bean, J.L.; Hall, R.A. Electromagnetic susceptibility measurements using a mode-stirred chamber. IEEE Intl. Symp. on EMC; 1978 June; Atlanta, GA.
- [5] Crawford, M.L.; Koepke, G.H. Design, evaluation and use of a reverberation chamber for performing electromagnetic susceptibility/vulnerability measurements. Nat. Bur. Stand. (U.S.) Tech. Note 1092; 1986 April.
- [6] Ma, M.T.; Kanda, M.; Crawford, M.L.; Larson, E.B. A review of electromagnetic compatibility/interference measurement methodologies. Proc., IEEE; Vol. 73, No. 3; 1985 March.
- [7] Crawford, M.L.; Ma, M.T.; Ladbury, J.M.; Riddle, B.F. Measurement and evaluation of a TEM/reverberating chamber. Nat. Bur. Stand. (U.S.) Tech Note 1342; 1990 July.

- [8] Liu, B.H.; Chang, D.C.; Ma, M.T. Eigenmodes and the composite quality factor of a reverberating chamber. Nat. Bur. Stand. (U.S.) Tech Note 1066; 1983 August.
- [9] Dunn, J.M. Local, high-frequency analysis of the fields in a mode-stirred chamber. IEEE Trans. Electromag. Compat. EMC-32 (1): 53-58, 1990 February.
- [10] Loughry, T.A. Frequency stirring; an alternate approach to mechanical mode-stirring for the conduct of electromagnetic susceptibility testing. PL-TR-91-1036; 1991 November.
- [11] Corona, P.; Latmiral, G.; Paolini, E. Performance and analysis of reverberating enclosures with variable geometry. IEEE Trans. Electromag. Compat. EMC-22 (1): 2-5; 1980 February.
- [12] Crawford, M.L.; Koepke, G.H.; Ladbury, J.M. EMR test facilities - Evaluation of reverberating chamber located at RADC, Griffiss AFB, Rome, NY. Nat. Bur. Stand. (U.S.) NBSIR 87-3080; 1987 December.
- [13] Tippet, J.C. Characteristic impedance of a rectangular coaxial line with offset inner conductor. IEEE Trans. Microwave Theory Tech. MTT-26 (11); 1978 November.
- [14] Crawford, M.L. Generation of standard EM fields for calibration of power density meters: 20 kHz to 1000 MHz. Nat. Bur. Stand. (U.S.) NBSIR 75-804; 1975 January.
- [15] Bowman, R.R. Calibration techniques for electromagnetic hazard meters: 500 MHz to 20 GHz. Nat. Bur. Stand. (U.S.) NBSIR 75-805; 1976 April.
- [16] Larsen, E.B.; Ries, F.X. Design and calibration of the NBS isotropic electric-field monitor [EFM-5], 02. to 1000 MHz. Nat. Bur. Stand. (U.S.) Tech. Note 1033; 1981 March.
- [17] Kanda, M.; Driver, L.D. An isotropic electric-field probe with tapered resistive dipoles for broad-band use, 100 kHz to 18 GHz. IEEE Trans. Microwave Theory Tech. MTT-35 (2); 1987 February.
- [18] Bensema, W.D.; Reeve, G.R.; Koepke, G.H. A multi-sensor automated EM field measurement system. Proc. IEEE IMTC; 1985; Tampa, FL.

Table 3.1. Ratio of test field strengths generated in the RL TEM/reverberating chamber (zinc finish steel reverberating chamber, 3.7 m x 5.2 m x 9.8 m) to that generated in an anechoic chamber at 3 m separation distance for same transmitted power. Test volume definition in anechoic chamber is  $\pm 3$  dB.

Frequency (MHz)	P'd/Pd (dB)	Dimensions (m)
100	20.0	X = $\pm 3.08$ Y = $\pm 1.49$ Z = 2.06 - 4.33
200	24.3	X = $\pm 3.01$ Y = $\pm 1.44$ Z = 2.11 - 4.25
300	25.9	X = $\pm 3.00$ Y = $\pm 1.43$ Z = 2.12 - 4.24
500	27.5	X = $\pm 3.00$ Y = $\pm 1.42$ Z = 2.12 - 4.24

Table 3.2. Ratio of test field strengths generated in the RL TEM/reverberating chamber to that generated in an anechoic chamber for same transmitted power. Separation distances in anechoic chamber are 1 and 3 m.

Frequency (GHz)	Gain (dB)	r = 1 m Pd'/Pd (dB)	r = 3 m Pd'/Pd (dB)
0.20	7.0	12.2	21.8
0.50	9.0	10.3	19.8
1.0	12.0	7.2	16.8
2.0	15.0	3.2	12.8
4.0	15.0	2.2	11.8
8.0	15.0	1.2	10.8
12.0	15.0	0.2	9.8
18.0	15.0	-0.8	8.8

Table 3.3. Test volume for radiated fields in anechoic chamber at 1 m and 3 m separation distances with selected transmitting antenna gain. Test volume definition is based on half-power points of the radiation pattern.

Frequency (GHz)	Nominal Gain (dB)	Test Volume Definition					
		3 dB Beamwidths E-Plane H-Plane Deg. Deg.		r = 1 Meter		r = 3 Meter	
				Max. D of EUT (m) $2D^2/\lambda$	Volume (m) within 3 dB	Max. D of EUT (m) $2D^2/\lambda$	Volume (m) within 3 dB
0.2	7.0	102	64	0.87	1.23 X = + 0.62 Y = + 1.23 Z = 1 +/- 0.41/0.29	1.50	2.12 X = + 1.87 Y = + 3.70 Z = 3 +/- 1.24/0.88
0.5	13.0	30	27	0.55	0.78 X = + 0.24 Y = + 0.27 Z = 1 +/- 0.41/0.29	0.95	1.34 X = + 0.72 Y = + 0.80 Z = 3 +/- 1.24/0.88
1.0	15.0	30	27	0.39	0.55 Same as at 0.5 GHz	0.67	0.95 Same as at 0.5 GHz
4.0	18.0	23	22	0.19	0.27 X = + 0.19 Y = + 0.20 Z = 1 +/- 0.41/0.29	0.34	0.47 X = + 0.58 Y = + 0.61 Z = 3 +/- 1.24/0.88
12.0	21.0	12	13	0.11	0.16 X = + 0.11 Y = + 0.11 Z = 1 +/- 0.41/0.29	0.19	0.27 X = + 0.34 Y = + 0.32 Z = 3 +/- 1.24/0.88

Table 3.4. Theoretical mode frequencies and gaps between adjoining modes for RL TEM/reverberating chamber,  $a = 3.69$  m,  $b = 5.18$  m, and  $d = 9.78$  m.

<u>Mode #</u>	<u>Indices</u>	<u>Frequency MHz</u>	<u>Gap Size MHz</u>
1	011	32.76	32.76
2	012	42.17	9.41
3	101	43.44	1.27
4	110	49.91	6.47
5	102	50.92	1.01
6	111	52.51	1.30
7	013	54.35	2.14
8	112	58.57	4.23
9	021	59.91	1.33
10	103	61.38	1.47
11	022	65.53	4.15
12	014	67.81	2.28
13	113	67.87	0.06
14	120	70.76	2.89
15	121	72.40	1.64
16	104	73.57	1.17
17	023	73.95	0.38
18	122	77.11	3.16
19	114	79.06	1.95
20	015	81.94	2.87
21	201	82.73	0.80
22	024	84.35	1.61
23	123	84.39	0.04
24	210	86.30	1.91
25	105	86.76	0.46
26	202	86.89	0.13
27	211	87.65	0.77
28	031	88.21	0.56
29	115	91.47	3.25
30	212	91.59	0.12
31	032	92.12	0.54
32	203	93.41	1.28
33	124	93.63	0.22
34	130	95.91	2.28
35	025	96.07	0.16
36	016	96.43	0.36
37	131	97.13	0.70
38	213	97.79	0.66
39	033	98.29	0.50
40	220	99.82	1.53

Table 4.1. Spatial variations in E-fields measured inside the RL TEM/reverberating chamber over test volume defined by probes shown in figure 4.14.

<b>Top plate</b>	
Frequency (MHz)	E-field variation (dB)
0.002-16	$\pm 8$
16-100	$\pm 15$
100	$\pm 8$
300	$\pm 5$
500	$\pm 3$
1000	$\pm 2.5$
2000	$\pm 2$
<b>Side plate</b>	
Frequency (MHz)	E-field variation (dB)
0.002-30	$\pm 10$
30-100	$\pm 12$
100	$\pm 8$
300	$\pm 5$
500	$\pm 3$
1000	$\pm 2.5$
2000	$\pm 2$

Table 4.2. Summary of cw operation characteristics of RL TEM/reverberating chamber.

<b>1. TEM region (planar field simulation, TEM mode operation)</b>	
Top plate driven	Side plate driven
Freq. $\approx$ 10 kHz to 16 MHz	Freq. $\approx$ 10 kHz to 30 MHz
Vertical polarization	Horizontal polarization
1 W input power yields	1 W input power yields
Approximately 2.5 V/m maximum	Approximately 1.6 V/m maximum
Midway between plate and floor (shifted under plate)	Midway between plate and wall
E-field uniformity over 1/2	E-field uniformity over 1/2
Volume $\geq \pm 8$ dB	Volume $\leq \pm 10$ dB
Uncertainty of $E_v$ -field at center of volume (under plate) $\geq \pm 3$ dB	Uncertainty of $E_H$ -field at center of volume $\leq \pm 3$ dB
<b>2. Transition region (TEM field plus limited higher-order modes)</b>	
Freq. $\approx$ 16 MHz to 100 MHz	Freq. $\approx$ 30 MHz to 100 MHz
Polarization shifting from vertical to variable	Polarization shifting from horizontal to variable
1 W input yields approximately 2.5 V/m to 32 V/m	1 W input yields approximately 1.6 V/m to 32 V/m
Uncertainty in E-field $\leq \pm 15$ dB	Uncertainty in E-field $\leq \pm 12$ dB
<b>3. Reverberating region (complex field simulation)</b>	
Freq. $\approx$ 100 MHz to 18 GHz or higher	
1 W input yields approximately 32 to 50 V/m	
Uncertainty in E-field $\leq \pm 8$ to 4 dB [15]	

Table 5.1. Comparison of measured and calculated charge/decay time of the RL TEM/reverberating chambers determined from chamber average loss measurements (figure 4.4) and from data shown in figure 5.3.

Frequency (GHz)	Average loss (dB)	Average quality factor ( $10^4$ )	Calculated charge/delay *time ( $\mu$ s)	Measured charge/delay time ( $\mu$ s)
0.9	18.8	1.05	3.7	3.2
1.3	22.5	1.35	3.3	2.9
2.0	26.7	1.87	3.0	2.5
2.9	30.6	2.32	2.6	2.2
4.2	34.8	2.69	2.0	1.8
5.65	38	3.13	1.8	1.5
8.9	43	3.87	1.4	1.1
12.0	46	4.75	1.26	0.8
16.0	49	5.64	1.12	0.6
18.0	50.5	5.69	1.01	—

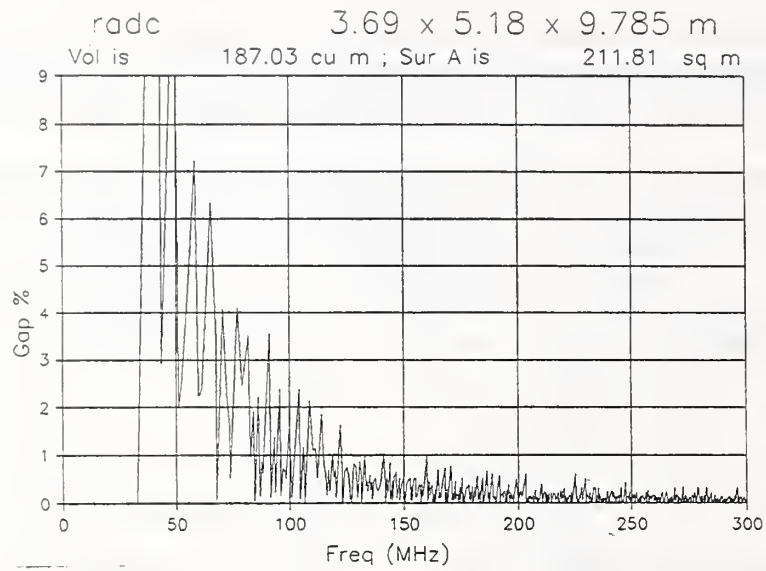


Figure 3.1 Theoretical mode distribution for the RL TEM/reverberating chamber (3.69 m x 5.18 m x 9.78 m).

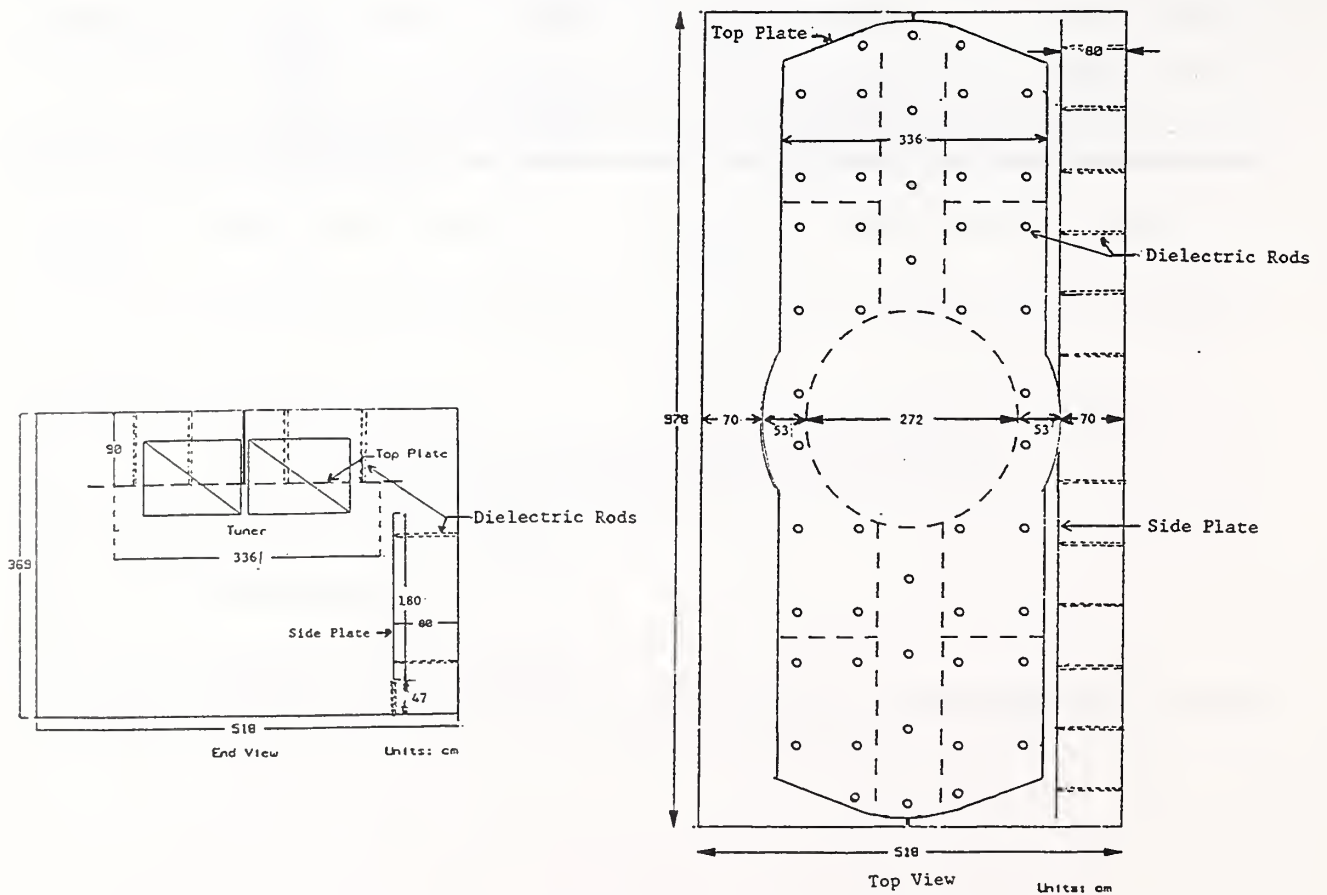


Figure 3.2 Cross-sectional sketches of the RL TEM/reverberating chamber.

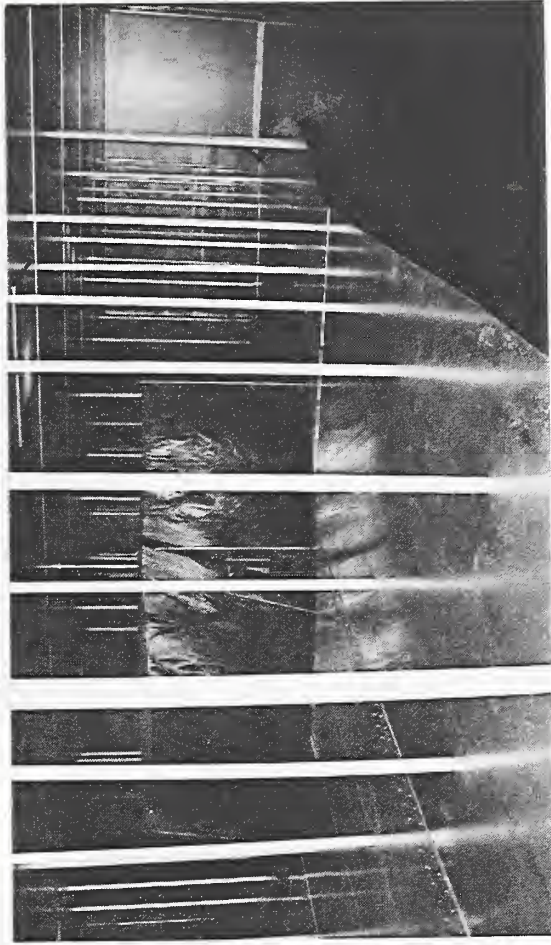
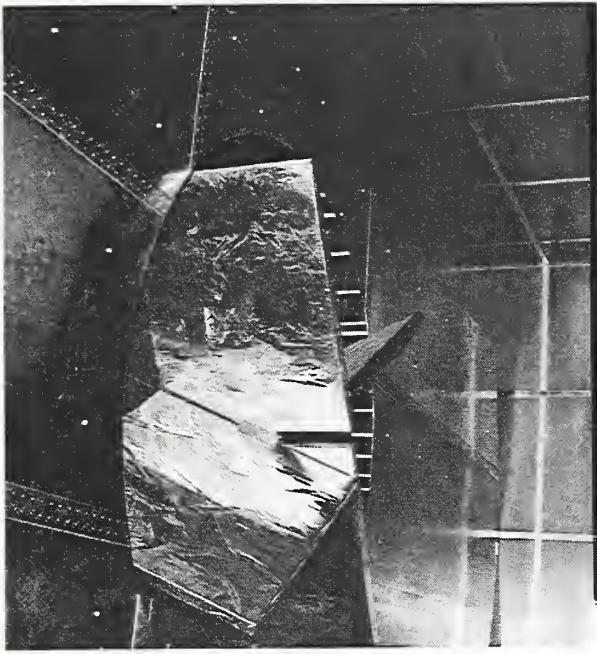


Figure 3.3(a) Photographs of the RL TEM/reverberating chamber showing tuner and top plate installation with plastic rods.

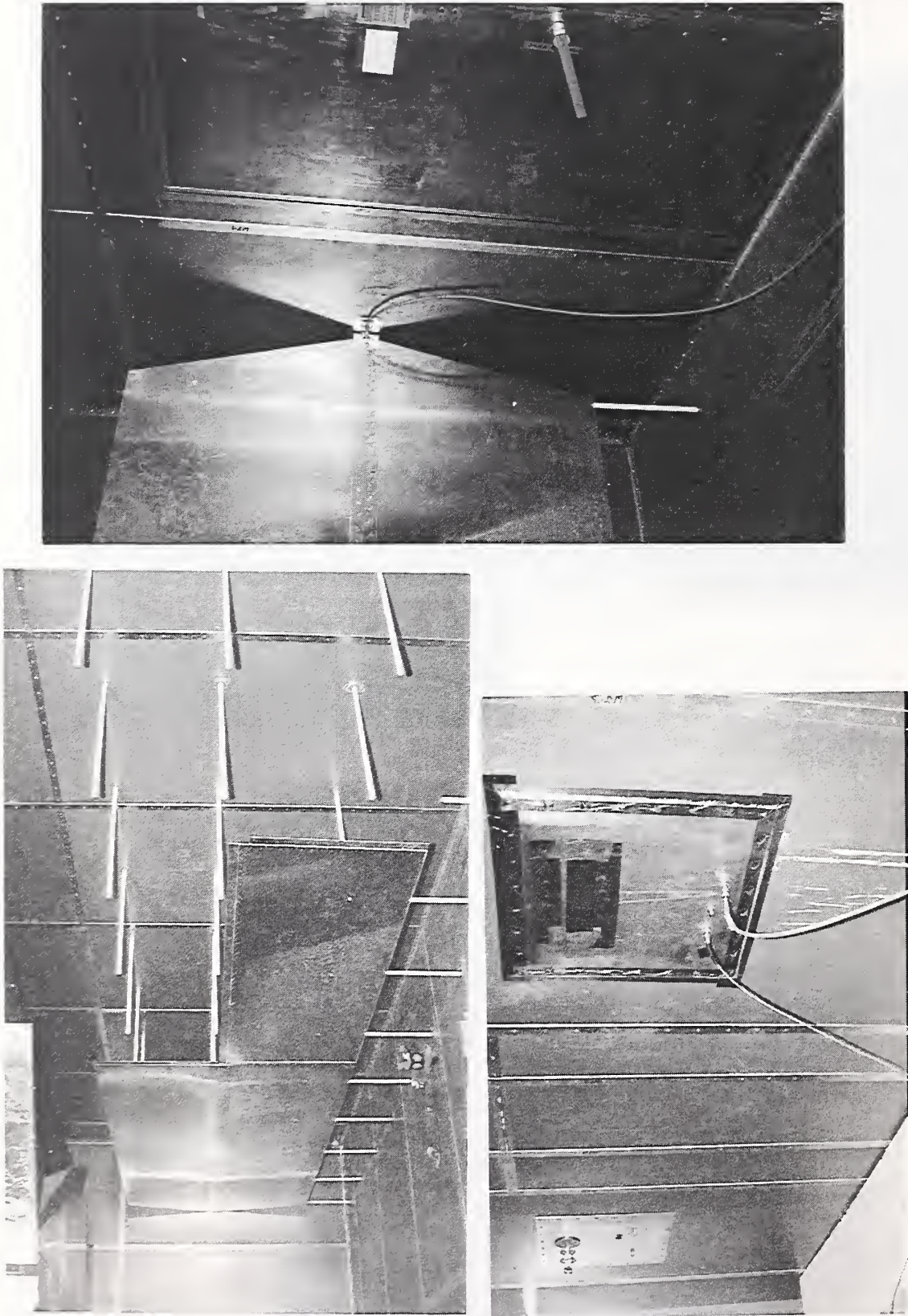


Figure 3.3(b) Photographs of the RL TEN/reverberating chamber showing side plate installation, the side plate end transition to coaxial connector and the access panels.

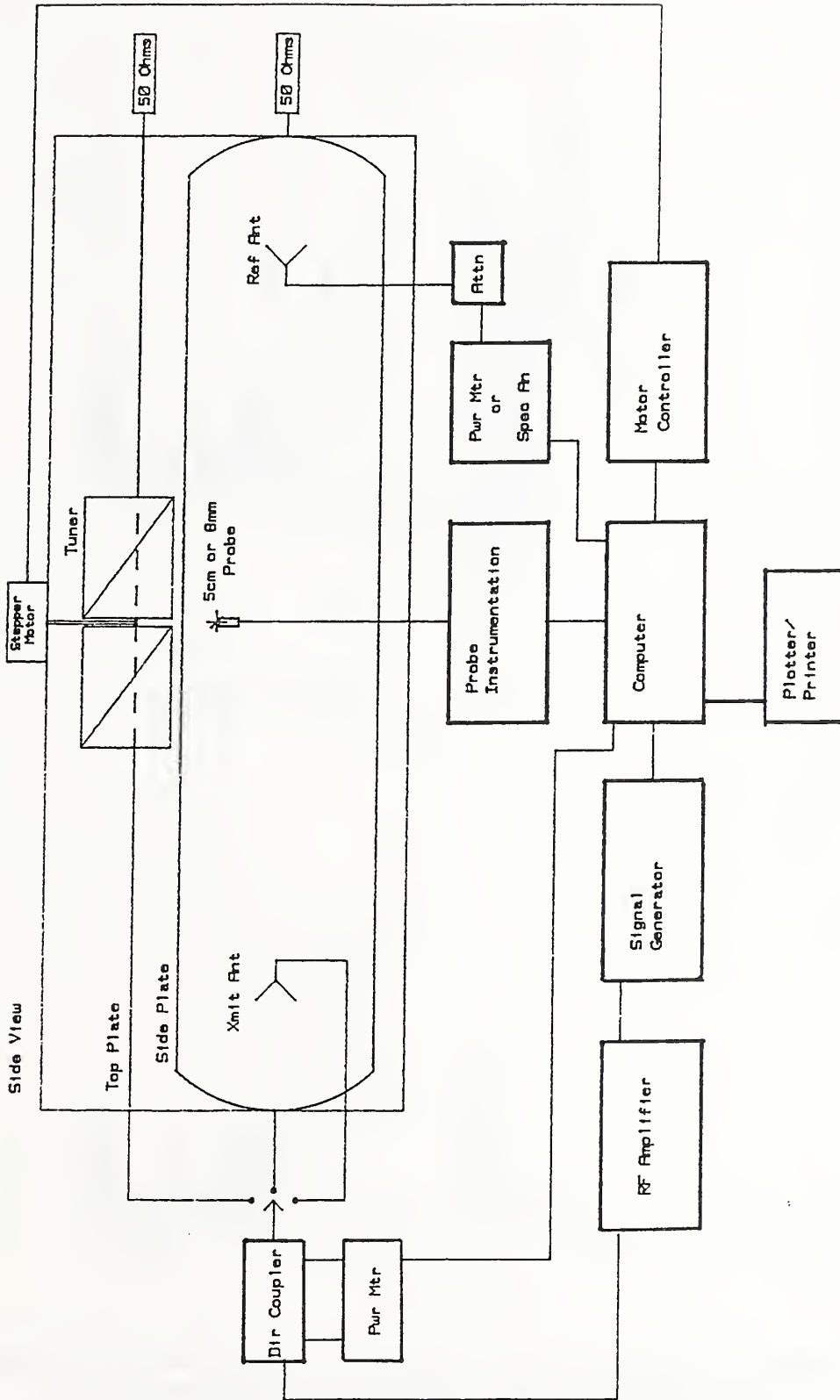


Figure 4.1 Block diagram of the instrumentation used in the cw evaluation of the RL TEM/reverberating chamber.

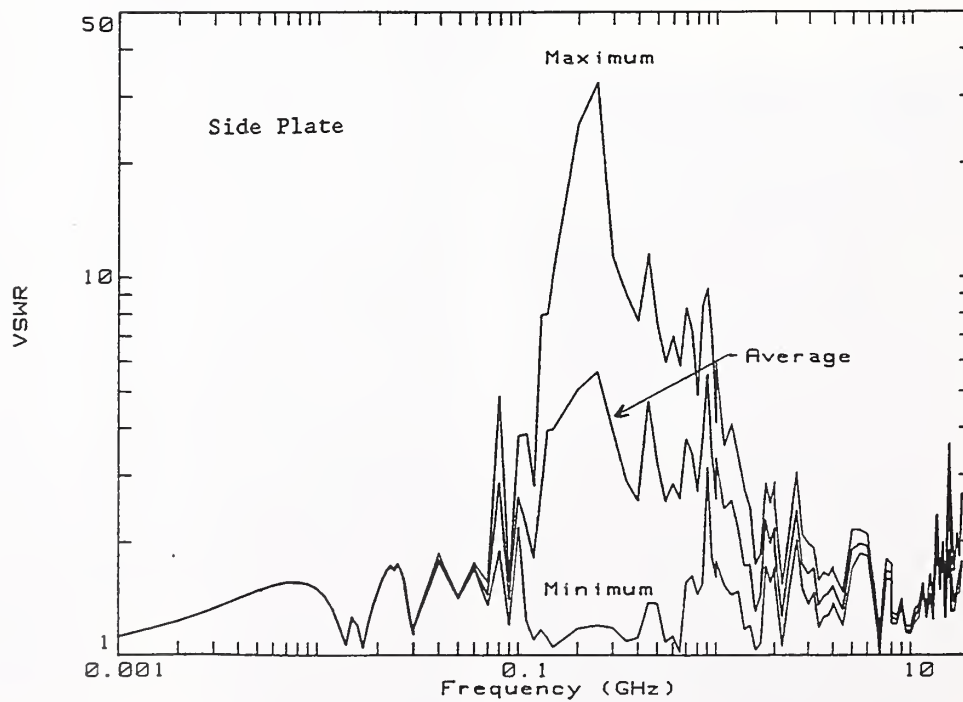
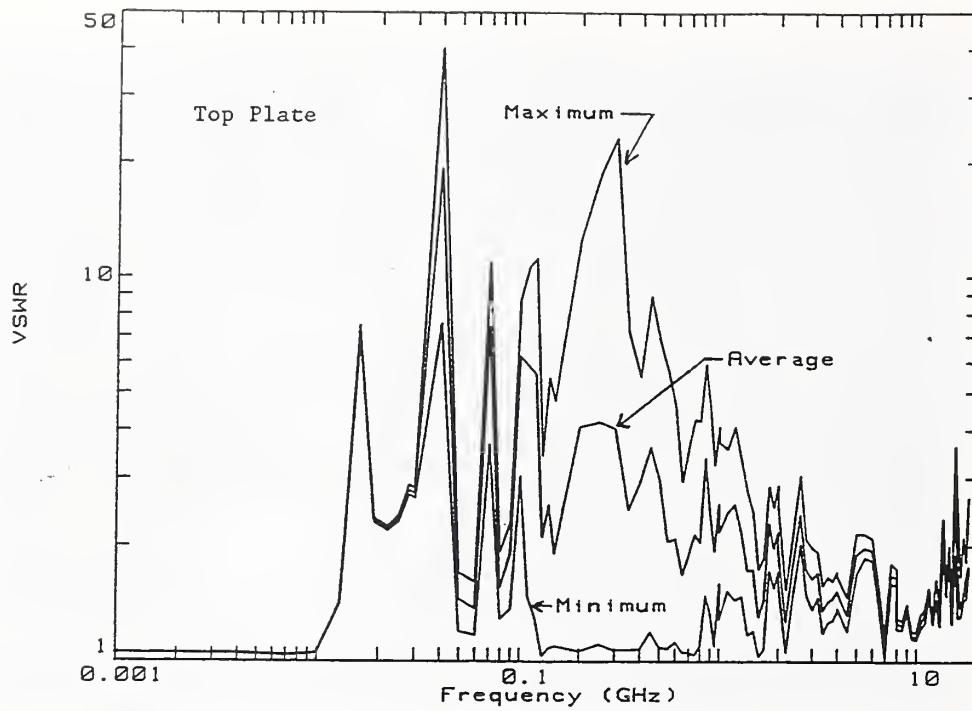


Figure 4.2 Measured composite VSWR of the top plate and side plate TEM lines(0.001 to 1.0 GHz) and the broadband ridged horn antenna (1.0 to 18 GHz) transmitting into the RL TEM/reverberating chamber.

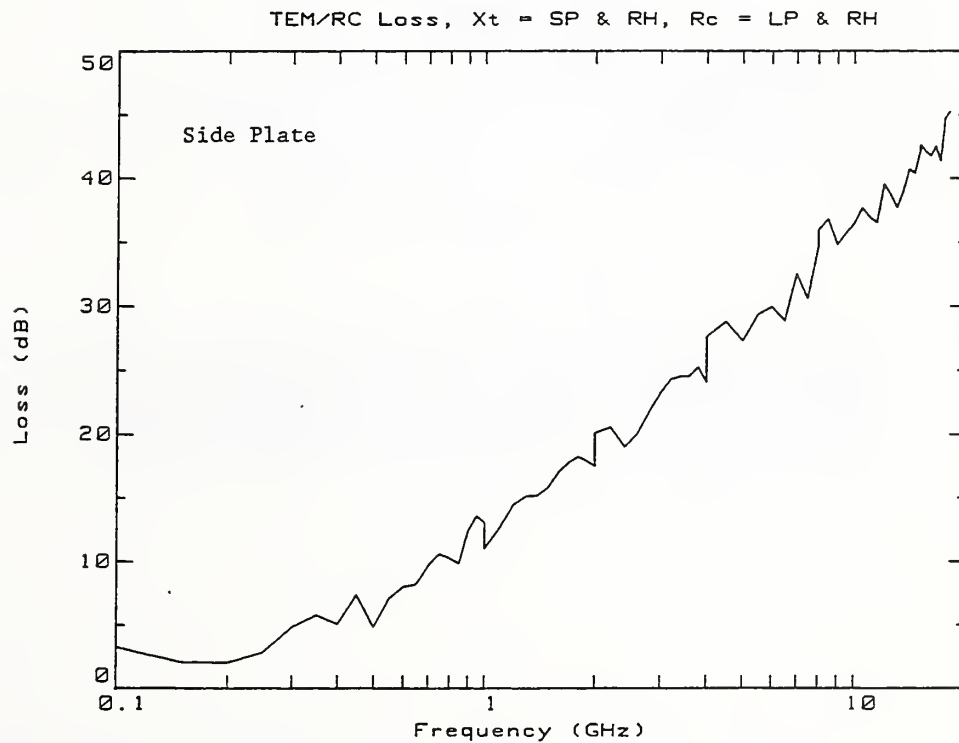
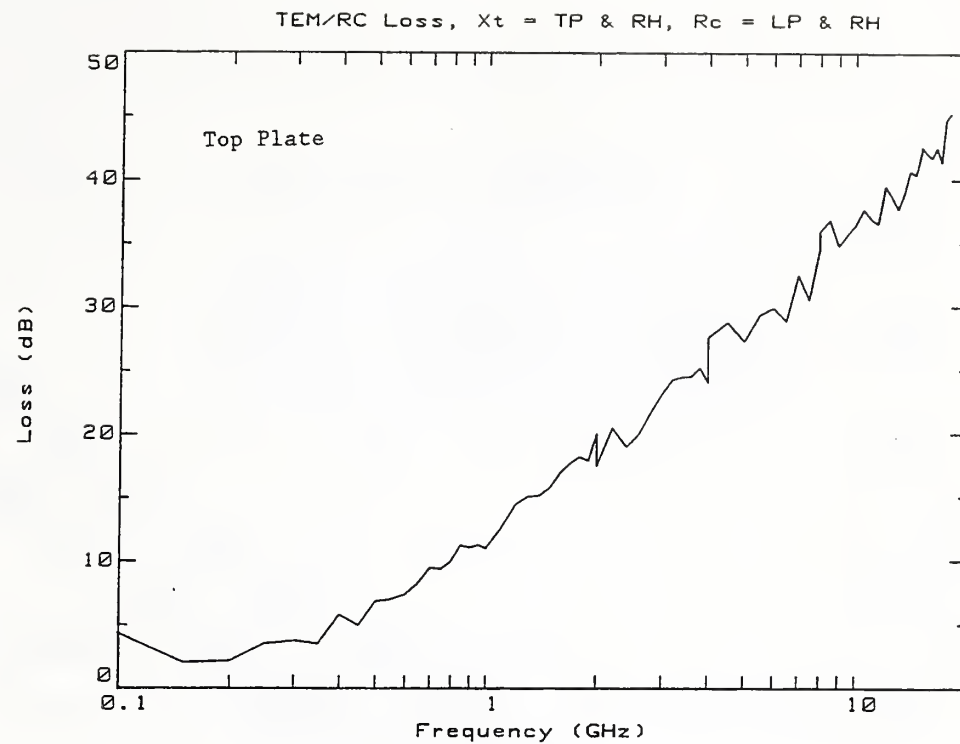


Figure 4.3 Measured coupling efficiency (loss) between the top and side plates (transmitting) and log periodic antenna (receiving, 0.1 to 1.0 GHz) and the broadband horn antennas (transmitting and receiving, 1.0 to 18 GHz) in the RL TEM/reverberating chamber.

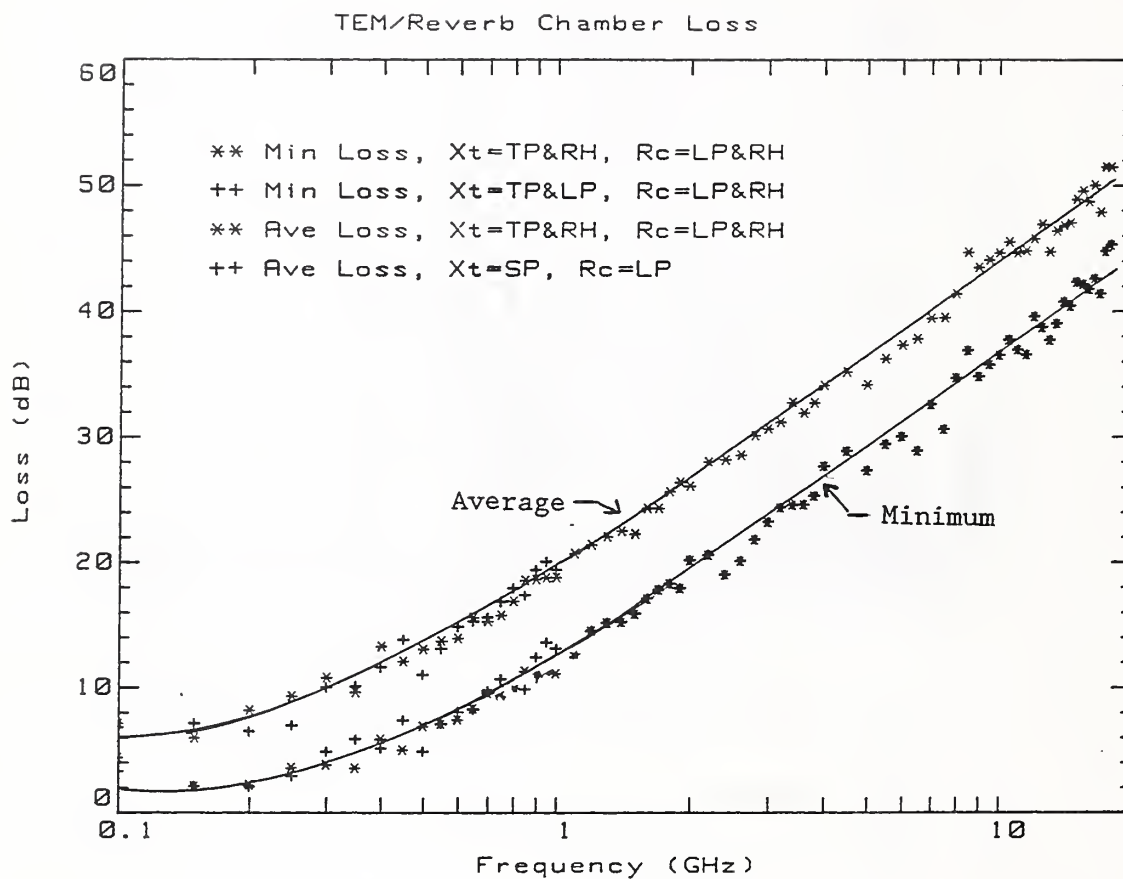


Figure 4.4 Measured average and minimum coupling efficiency (loss) between the top and side plates (transmitting, 0.1 to 1.0 GHz) and log periodic antenna (receiving, 0.1 to 1.0 GHz) and the broadband horn antennas (transmitting and receiving, 1.0 to 18 GHz) in the RL TEM/reverberating chamber.

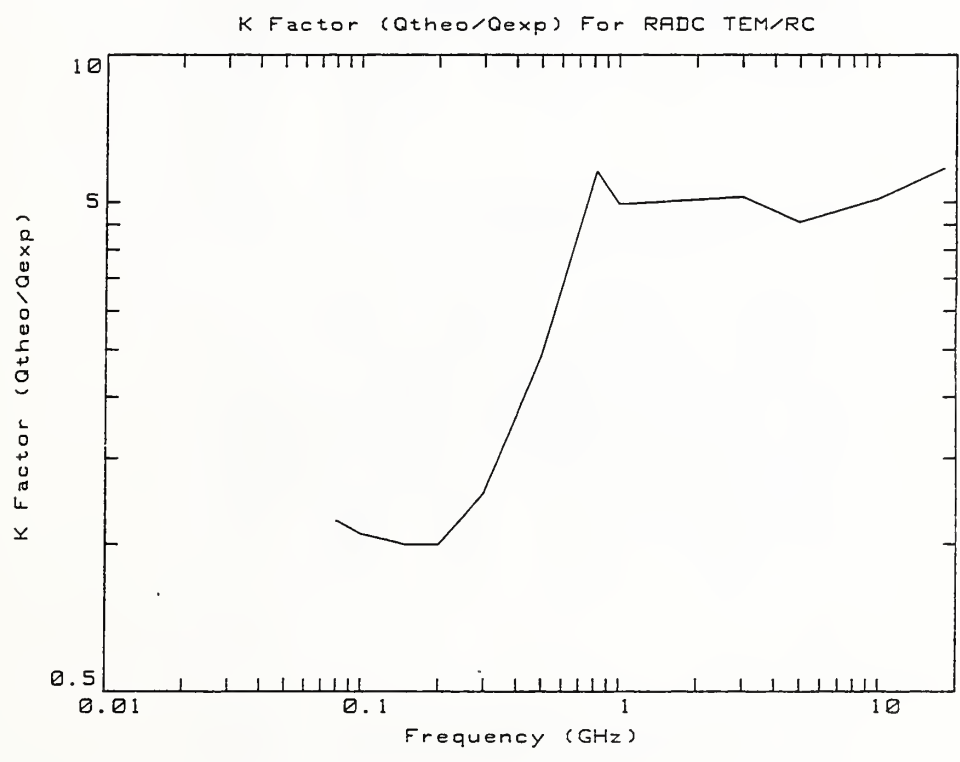
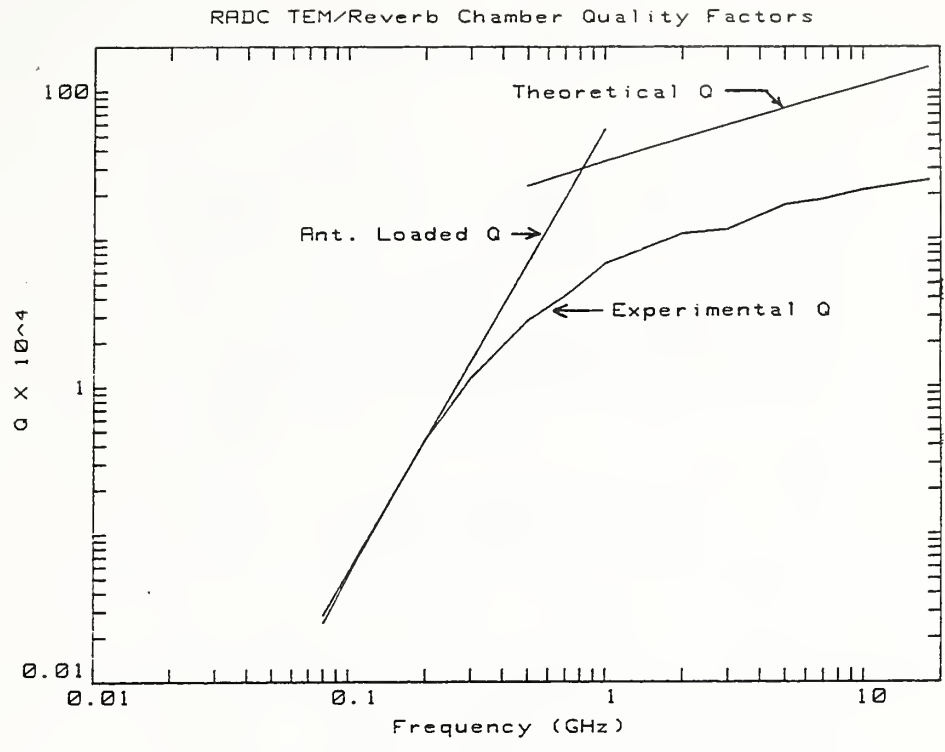


Figure 4.5 (a) Theoretical and experimental Q of the RL TEM/reverberating chamber and (b) ratio of theoretical to experimental Q (K-factor), 0.01 to 18 GHz.

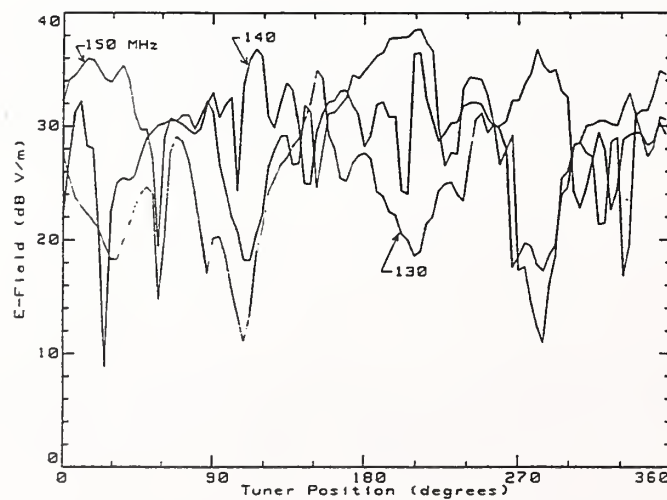
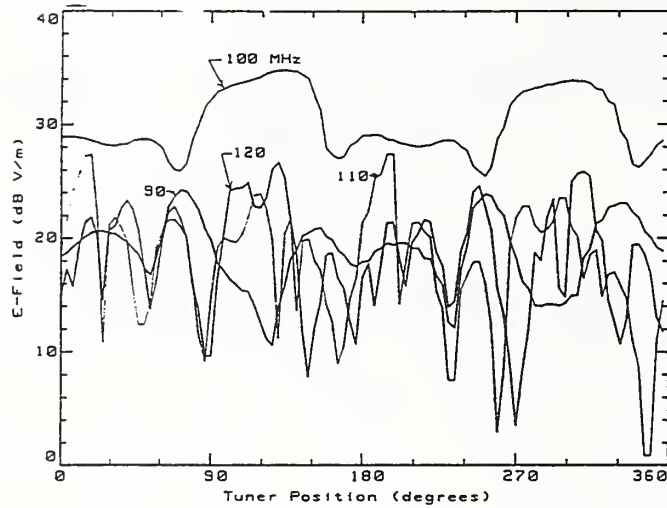
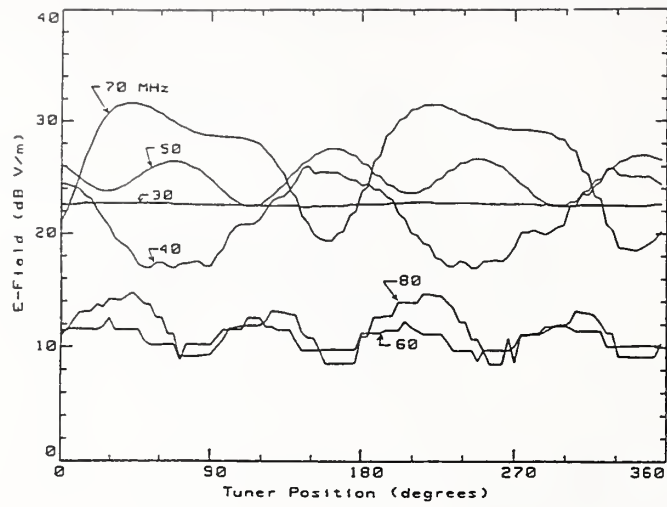


Figure 4.6 Vertical polarized component of E-field versus tuner position. Measurements made at selected frequencies at the center of RL TEM/reverberating chamber test zone with 1 W RF applied at the input of the top plate.

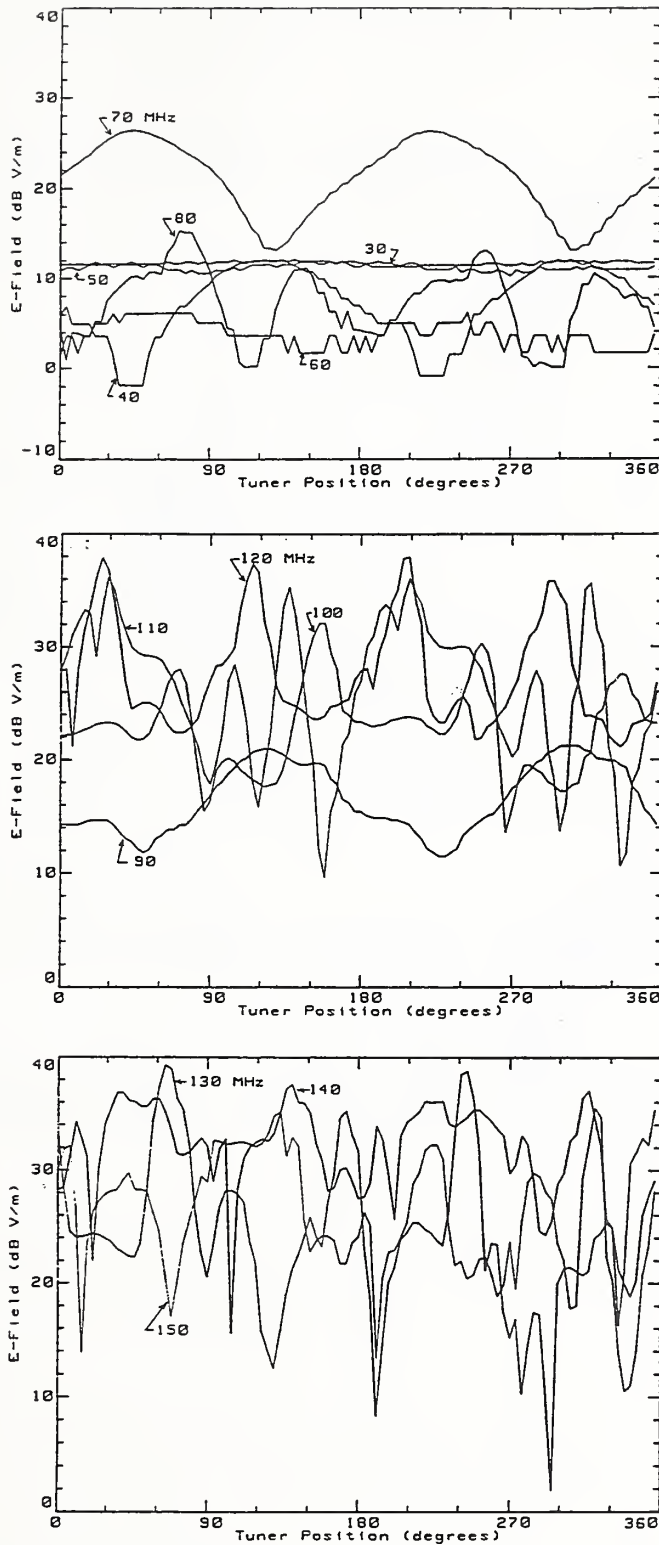


Figure 4.7 Horizontal polarized component of E-field versus tuner position. Measurements made at selected frequencies at the center of RL TEM/reverberating chamber test zone with 1 W RF applied at the input of the side plate.

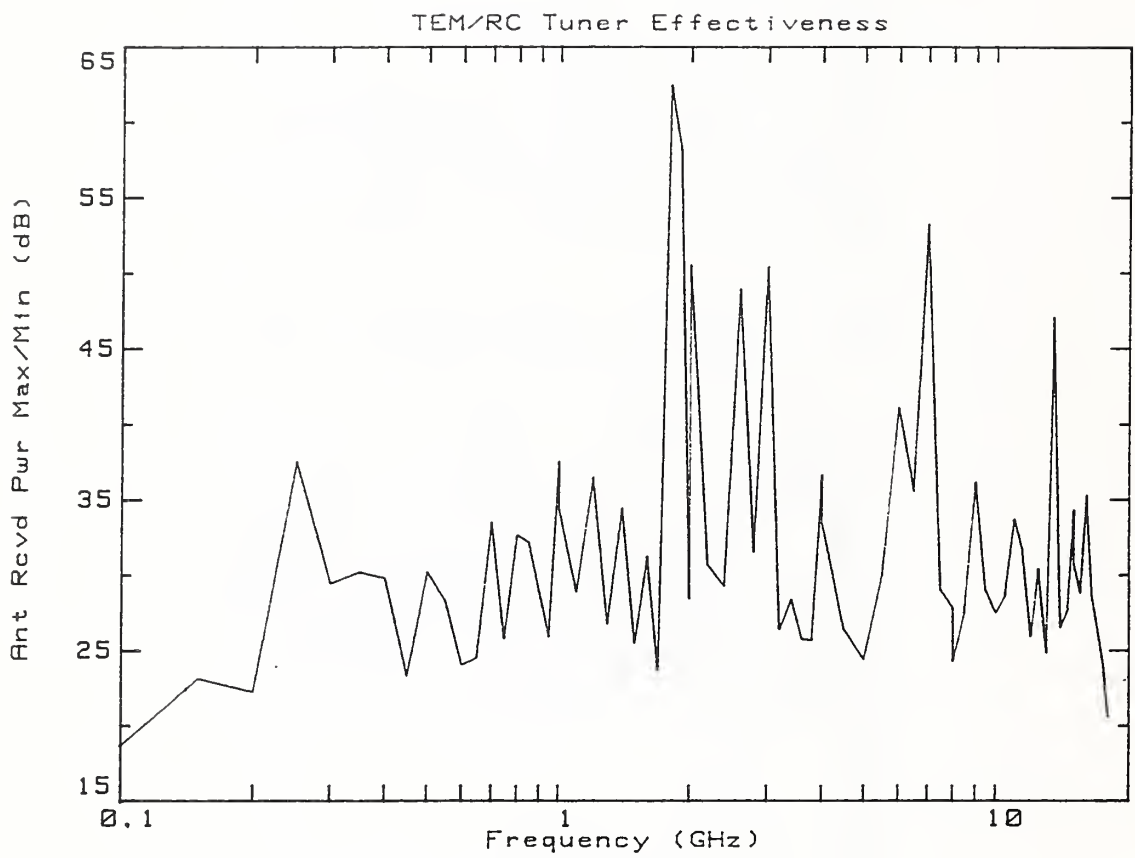


Figure 4.8 Measured tuner effectiveness in the RL TEM/reverberating chamber using receiving antenna power measurements. (Same receiving antennas as figure 4.4.)

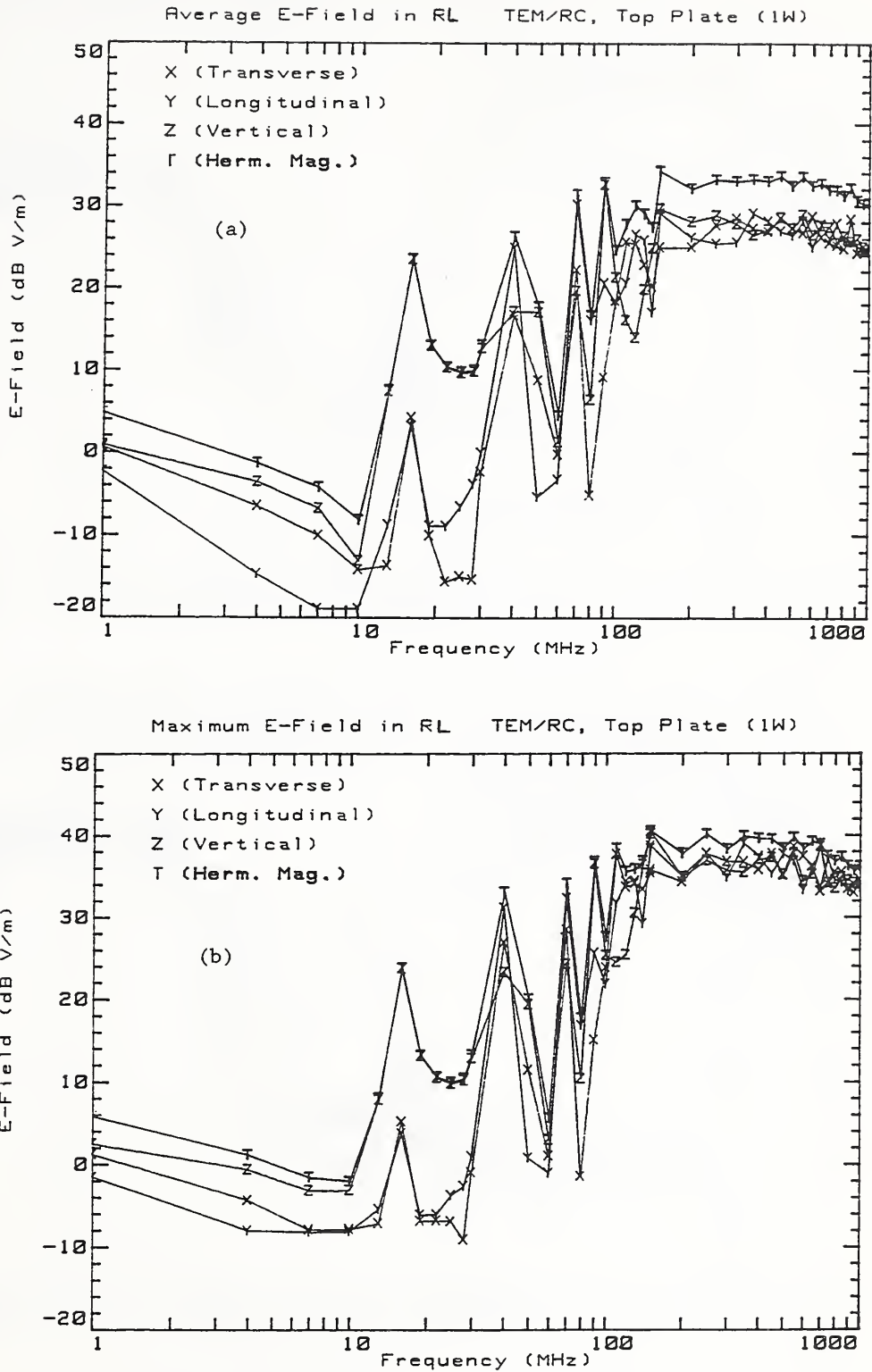


Figure 4.9 E-field components measured at the center of the RL TEM/reverberating chamber using a NIST isotropic (5 cm dipole) probe (position #2 in figure 4.14) with chamber excited by top plate: (a) average, (b) maximum. Net input power is 1 W.

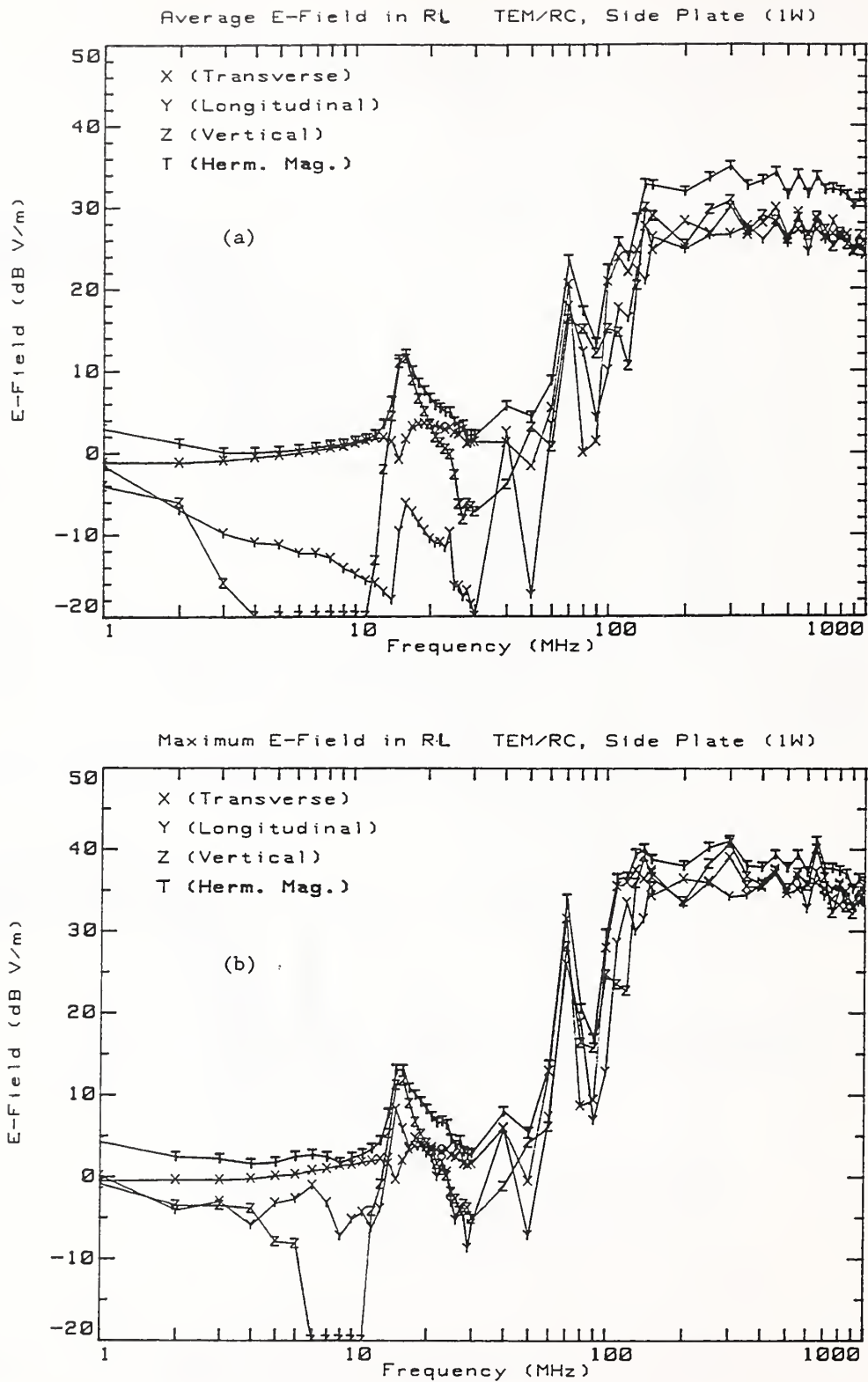


Figure 4. 10 E-field components measured at the center of the RL TEM/reverberating chamber using NIST isotropic (5 cm dipole) probe (position #2 in figure 4.14) with chamber excited b side plate: (a) average, (b) maximum. Net input power is 1 W.

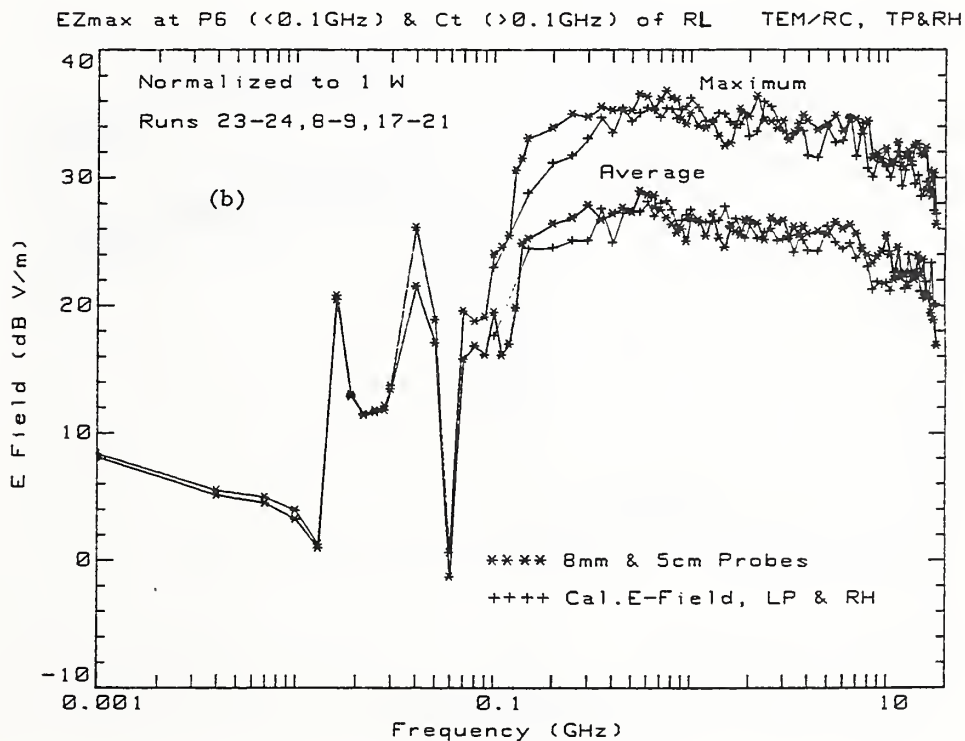
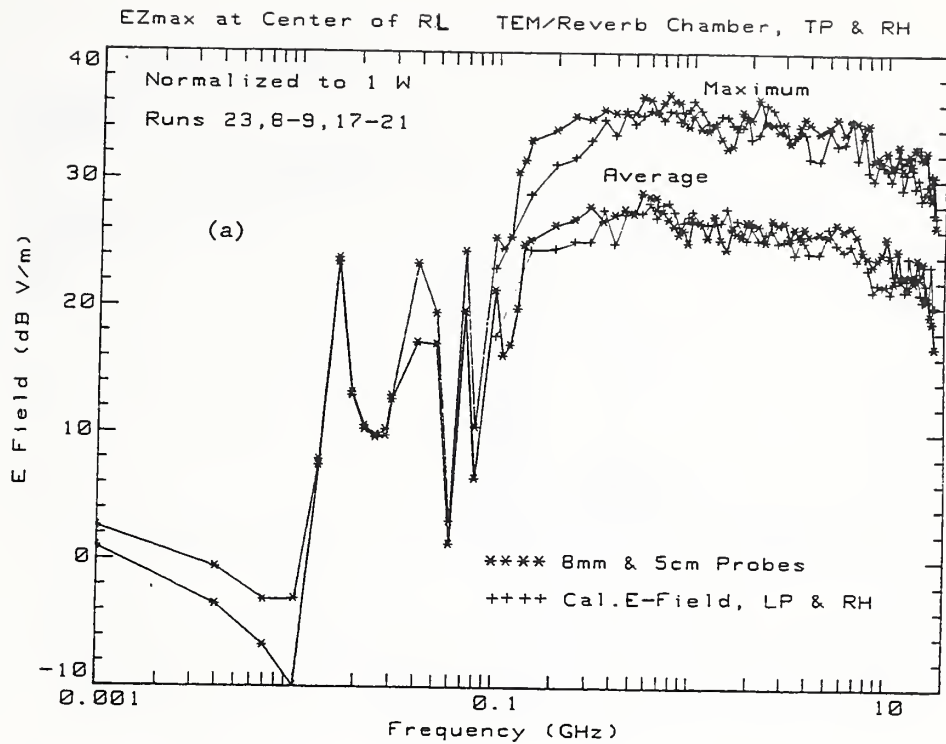


Figure 4.11 Maximum and average vertical component of E-field measured at (a) center and (b) position 6 (figure 4.14) in RL TEM/reverberating chamber using NIST 5 cm and 0.8 cm dipole probes and log periodic (0.1 - 1.0 GHz) and broadband horn (1.0 - 18 GHz) antennas. Chamber excited by 1 W input to top plate (0.001 - 1 GHz) and broadband horn (1 - 18 GHz).

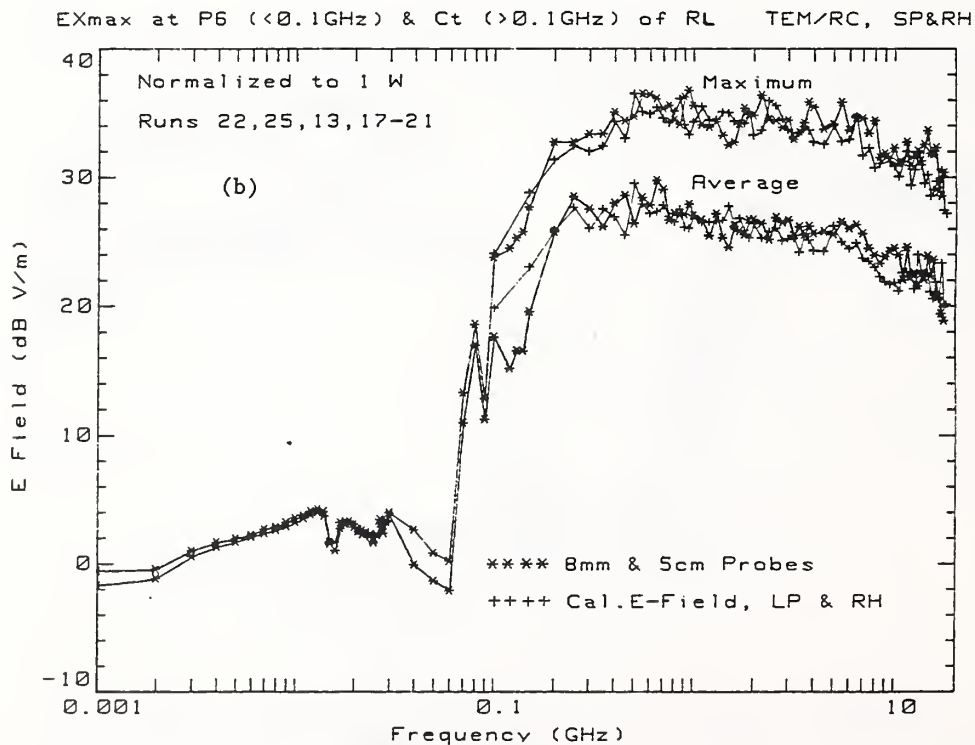
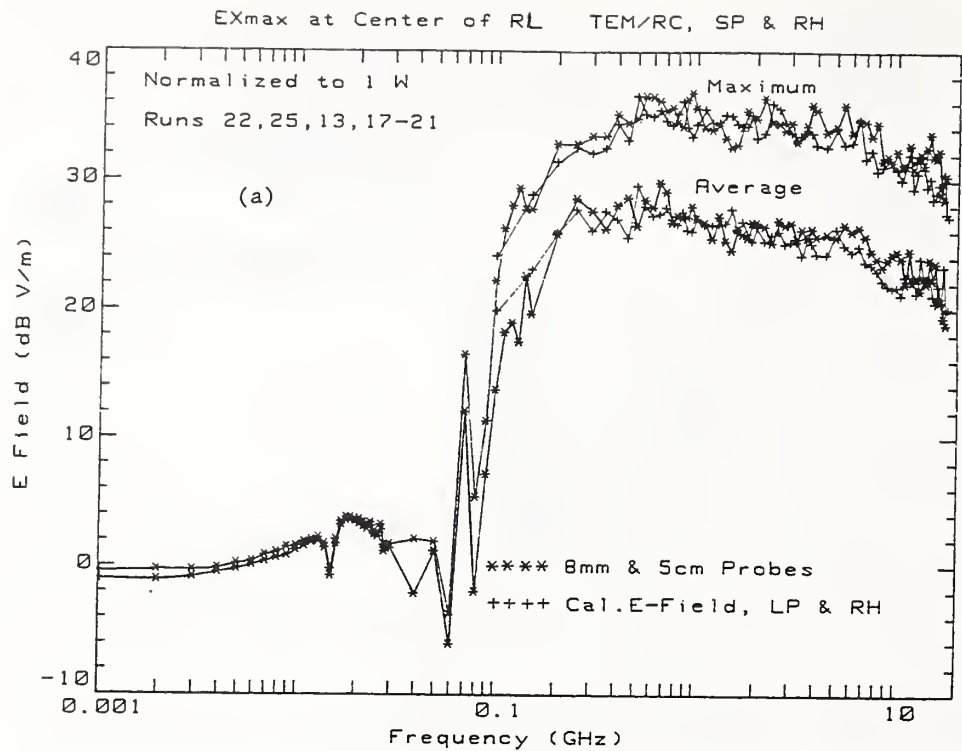


Figure 4.12 Maximum and average horizontal component of E-field measured at (a) center and (b) position 6 (figure 4.14) in RL TEM/reverberating chamber using NIST 5 cm and 0.8 cm dipole probes, and log periodic (0.1 - 1 GHz) and broadband horn (1.0 - 18 GHz) antennas. Chamber excited by 1 W input to side plate (0.001 - 1 GHz) and broadband horn (1 - 18 GHz).

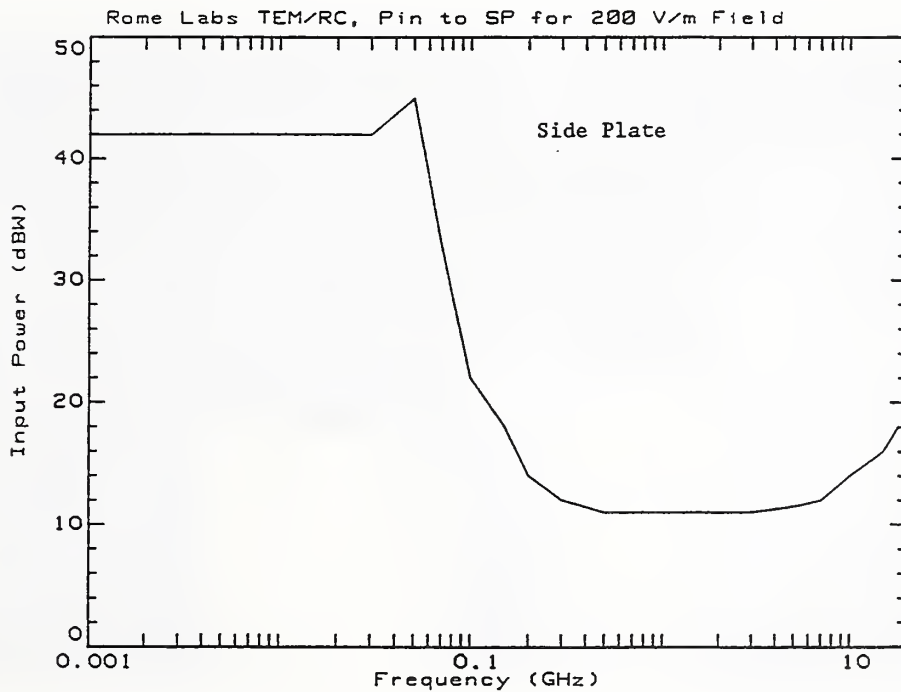
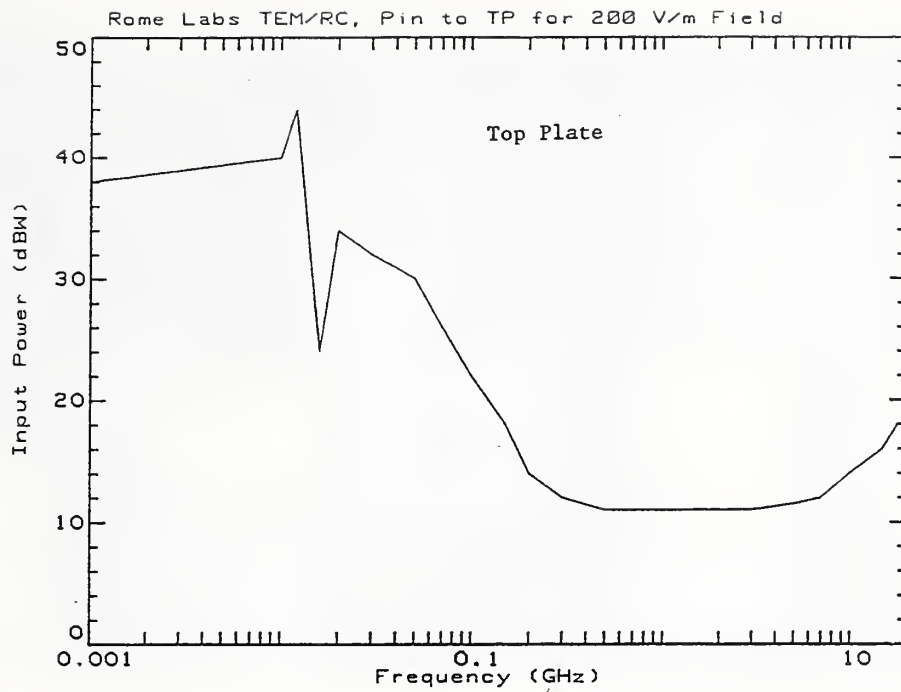
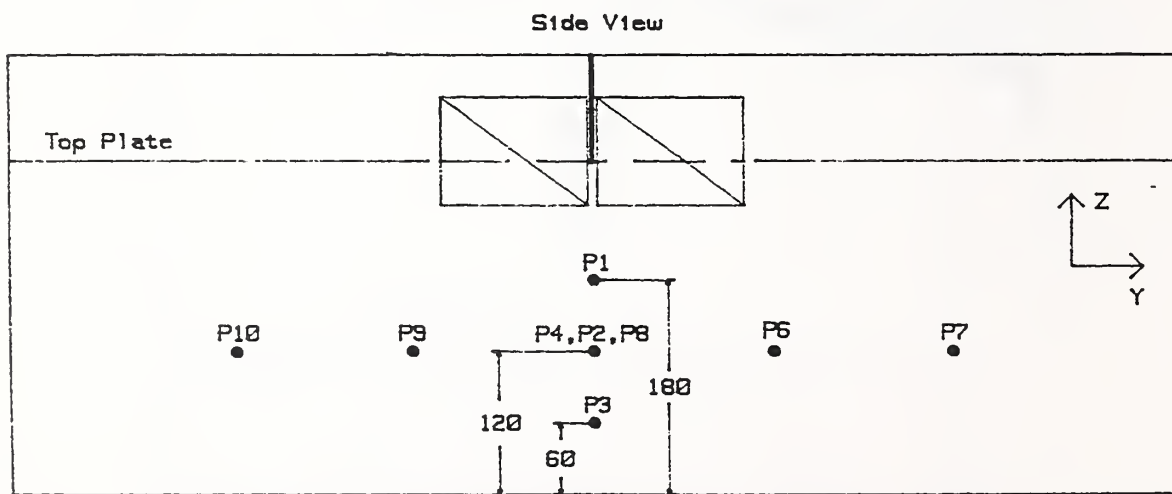
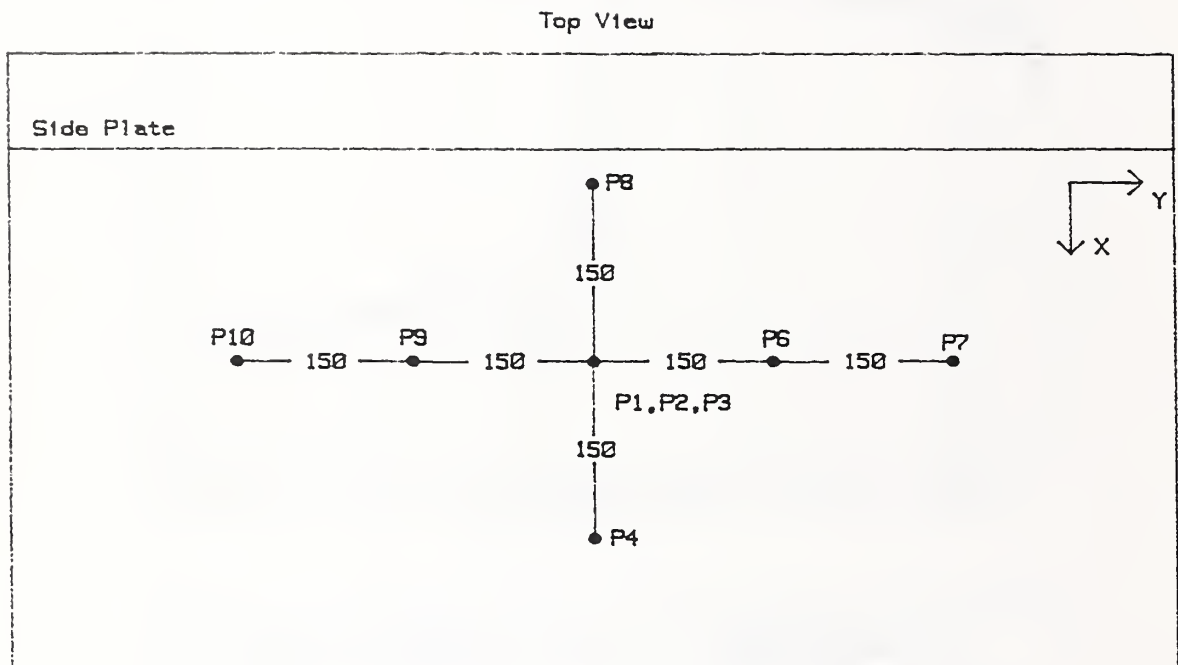


Figure 4.13 Input power required to generate a 200 V/m maximum E-field at the center of the RL TEM/reverberating chamber using: (a) top plate (Vert. Pol.) and (b) side plate (Hor. Pol.). (0.001 - 1 GHz) and broadband horn antenna (1 - 18 GHz).



Units: cm

Figure 4.14 Cross-sectional sketch of the RL TEM/reverberating chamber showing placement of calibrated isotropic probes for measuring spatial E-field uniformity.

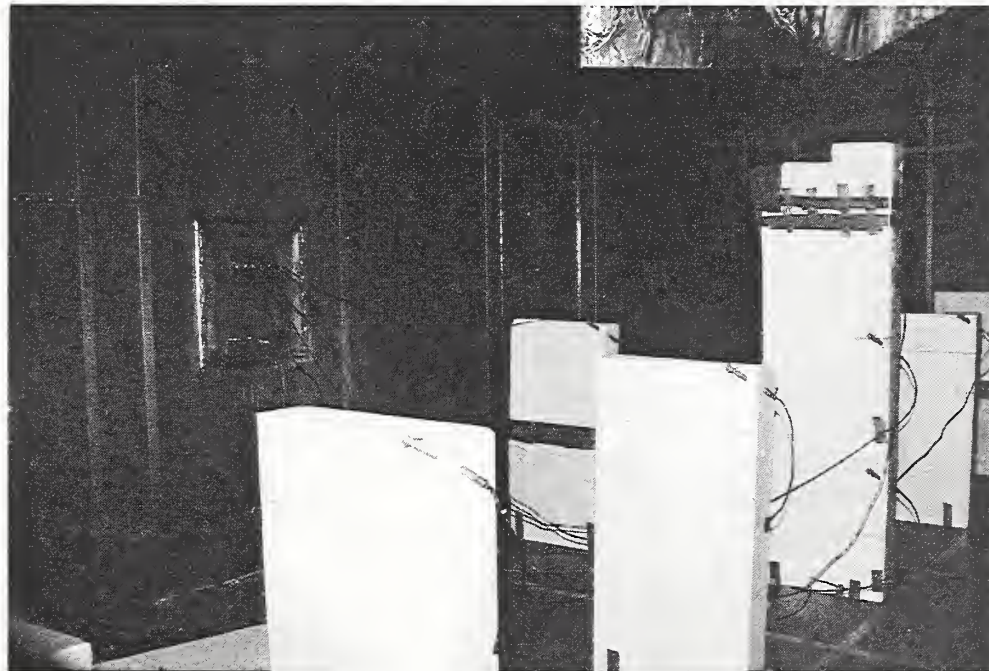
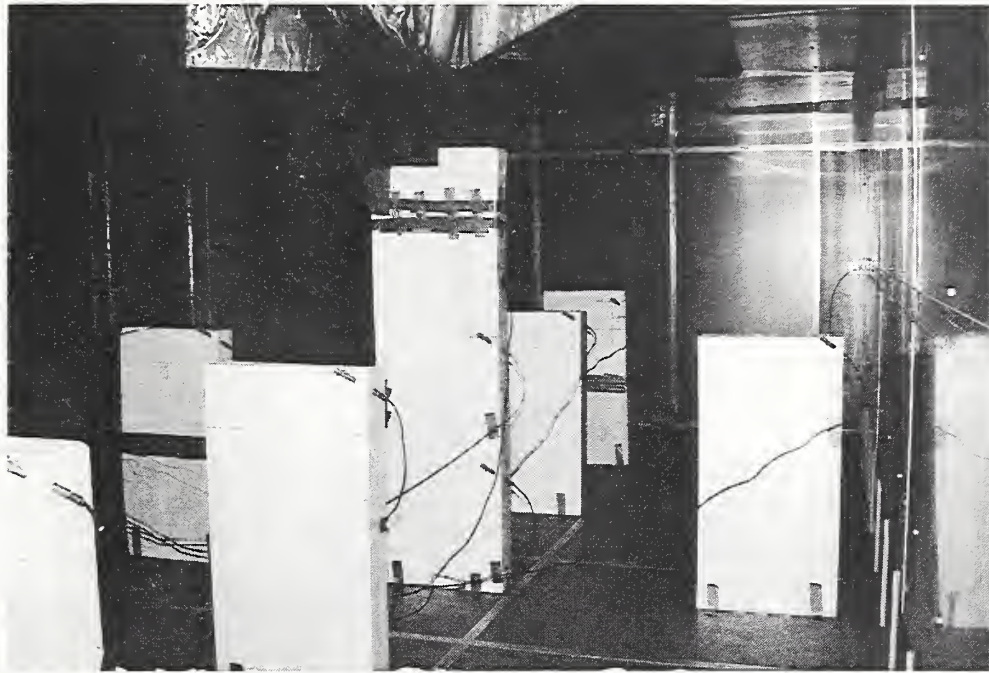


Figure 4.15 Photographs of interior of RL TEM/reverberating chamber showing placement of NIST isotropic probes for evaluation of spatial distribution of E-field.

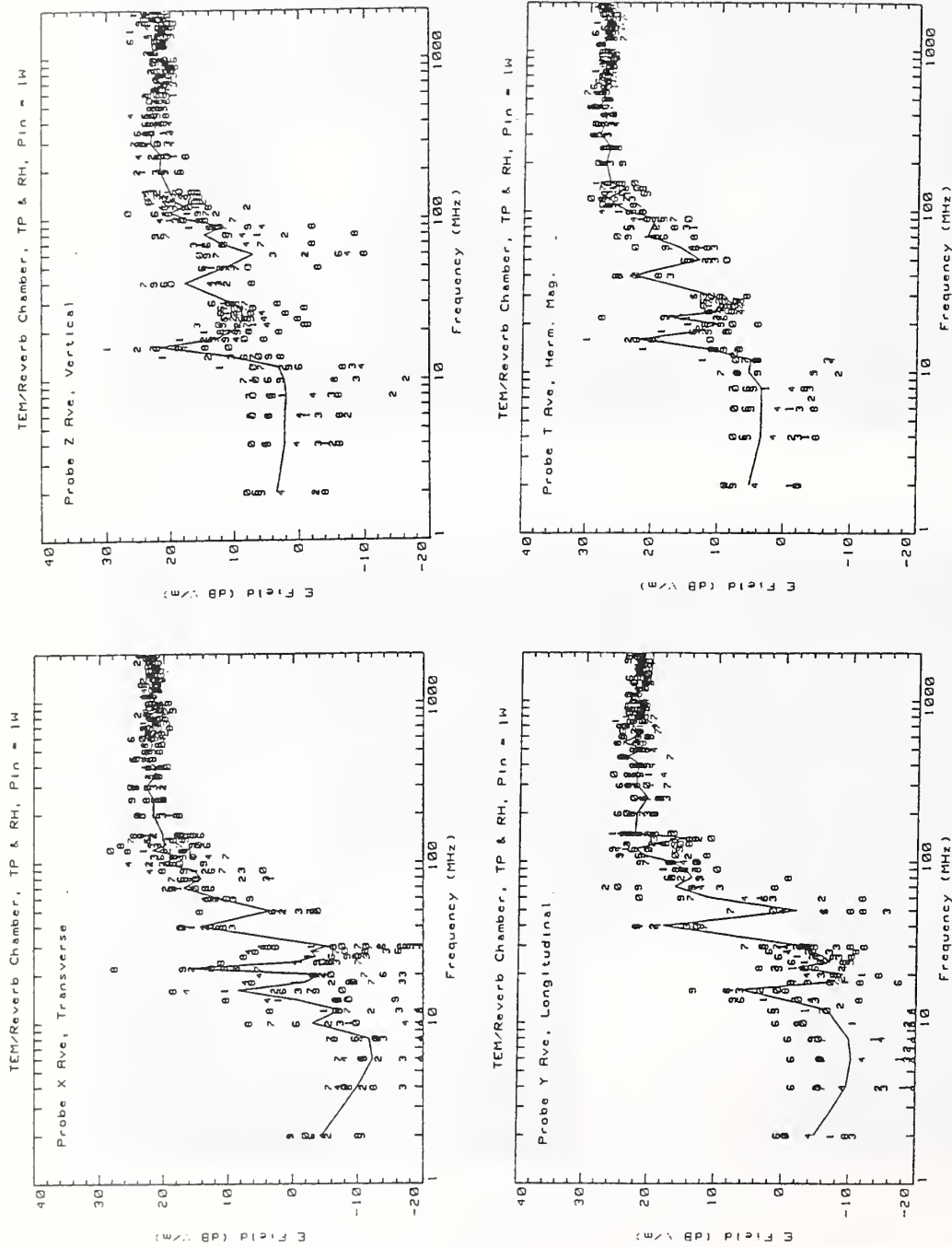


Figure 4.16(a) Spatial distribution of the E-field components in the RL TEM/reverberating chamber measured with nine NIST isotropic probes (5 cm dipoles) for 1 W net input power to the top plate and horn transmitting antenna: average and maximum values. Average of the average components shown as solid curve. Average values of components, top plate, and ridged horn antenna.

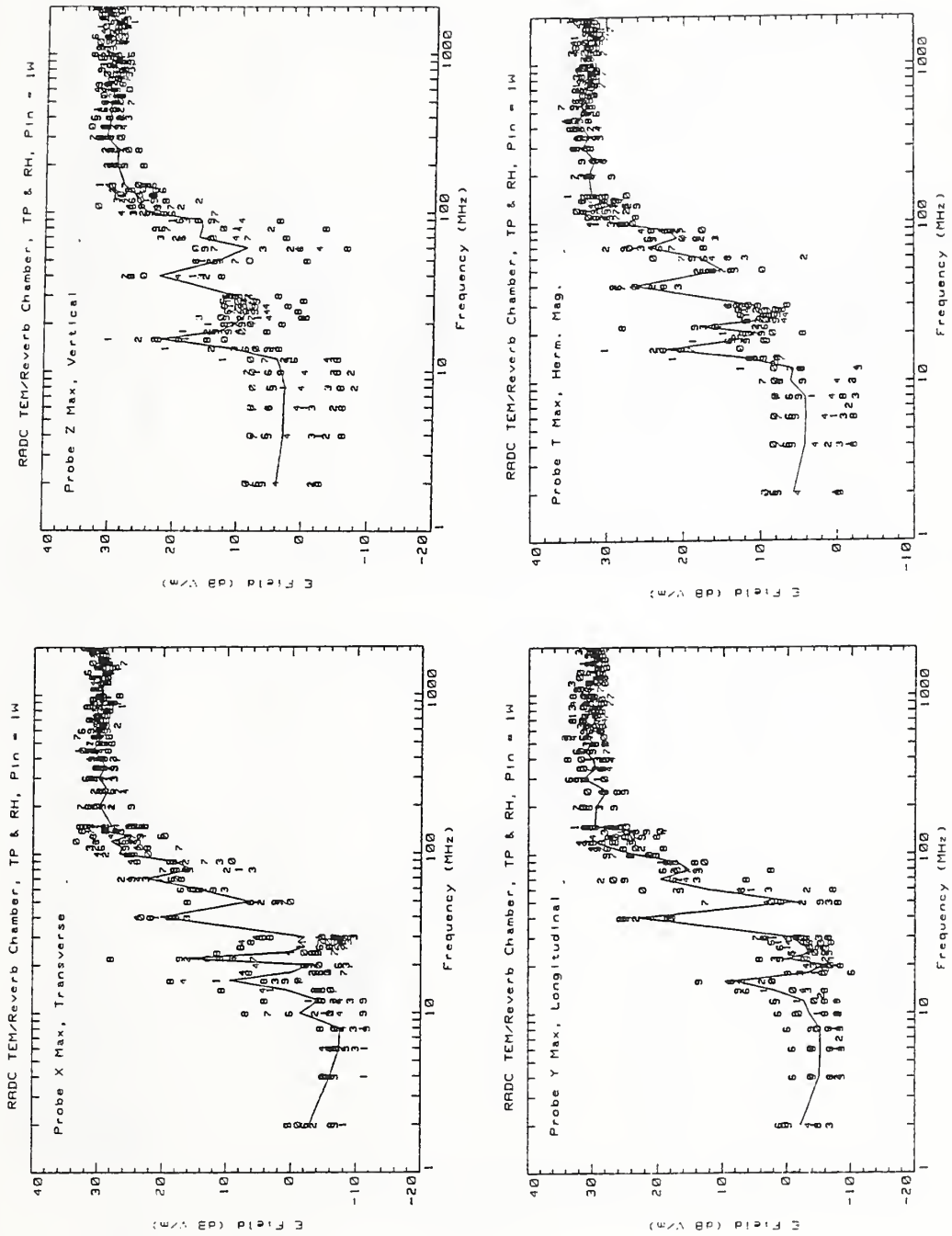


Figure 4.16(b) Spatial distribution of the E-field components in the RL TEM/reverberating chamber measured with nine NIST isotropic probes (5 cm dipoles) for 1 W net input power to the top plate and horn transmitting antenna: average and maximum values. Average of the maximum components shown as solid curve. Maximum values of components, top plate, and ridged horn antenna.

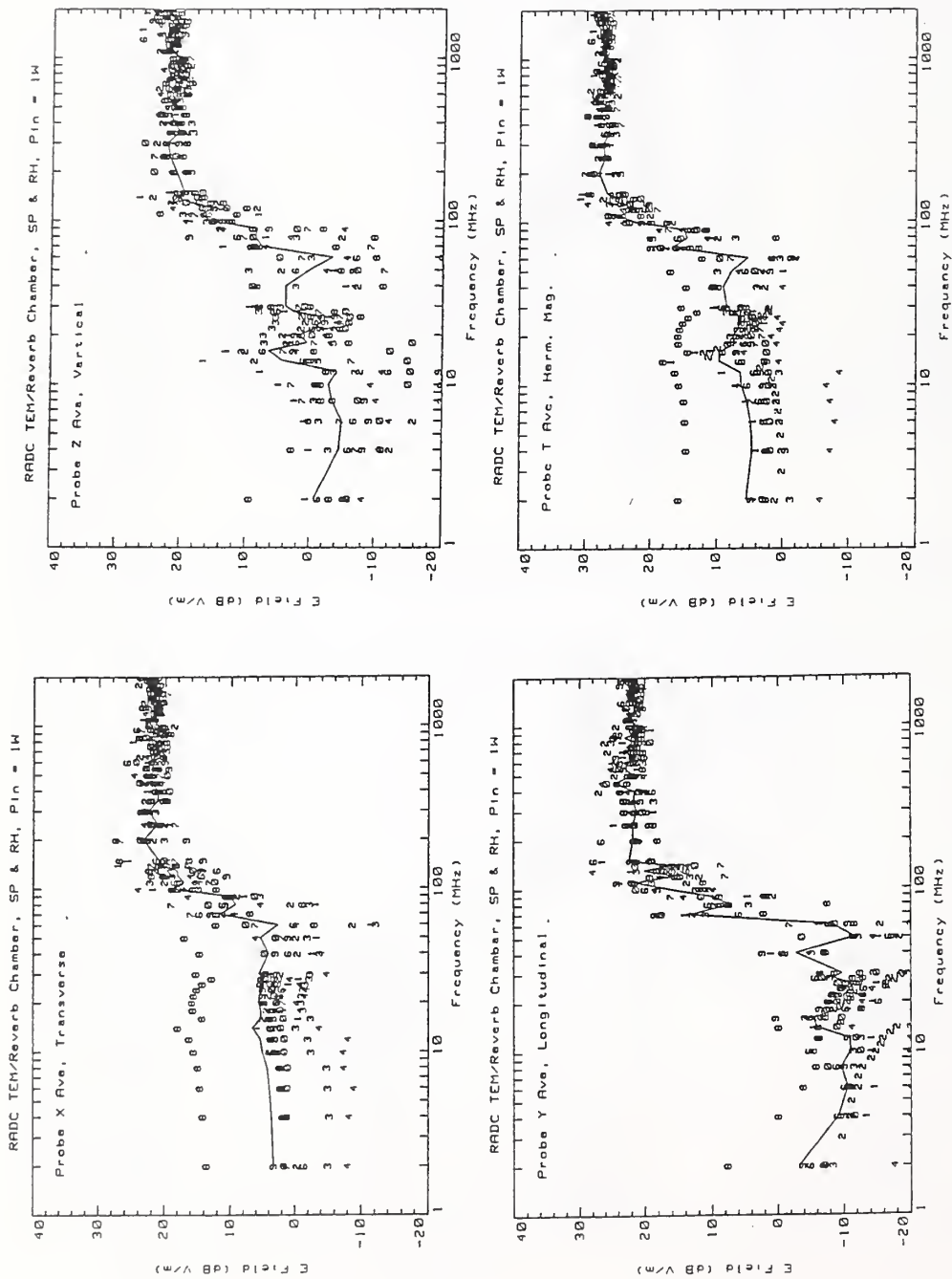


Figure 4.17(a) Spatial distribution of the E-field components in the RL TEM/reverberating chamber measured with nine NIST isotropic probes (5 cm dipoles) for 1 W net input power to the side plate and horn transmitting antenna: average and maximum values. Average of the average components shown as solid curve. Average values of components, side plate, and ridged horn antenna.

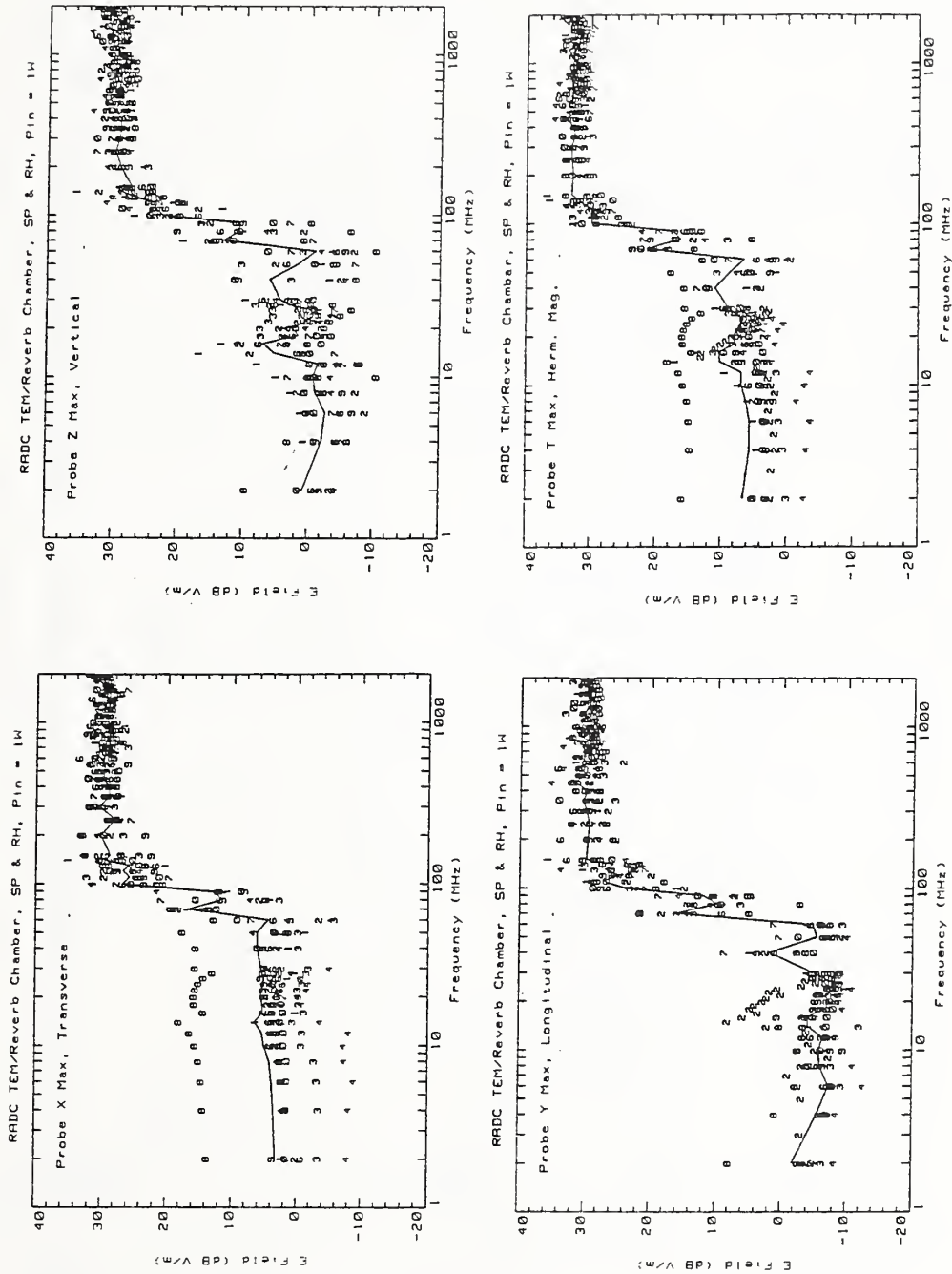


Figure 4.17(b) Spatial distribution of the E-field components in the RL TEM/reverberating chamber measured with nine NIST isotropic probes (5 cm dipoles) for 1 W net input power to the side plate and horn transmitting antenna: average and maximum values. Average of the maximum components shown as solid curve. Maximum values of components, side plate, and ridged horn antenna.

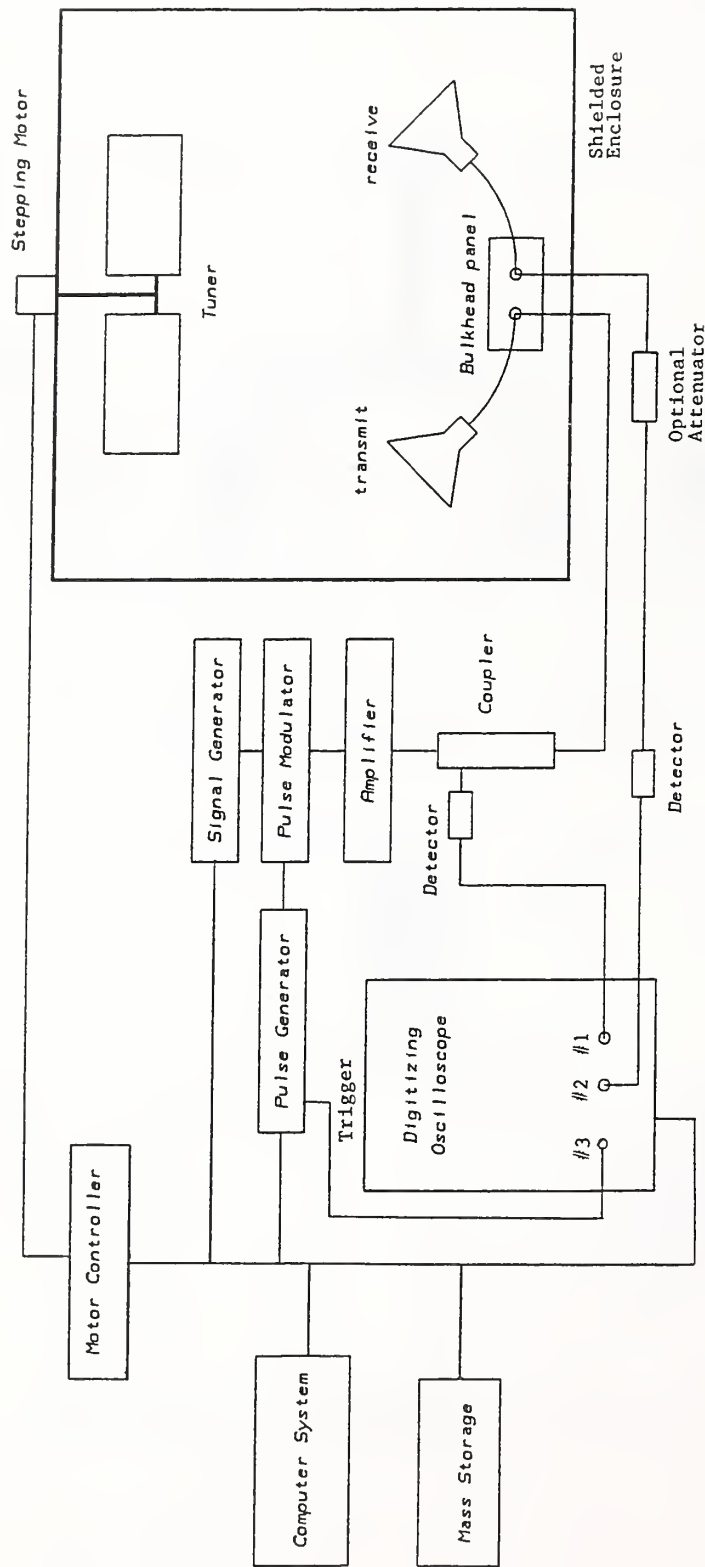


Figure 5.1 Block diagram of instrumentation used in pulsed rf evaluation of the RL TEM/reverberating chamber.

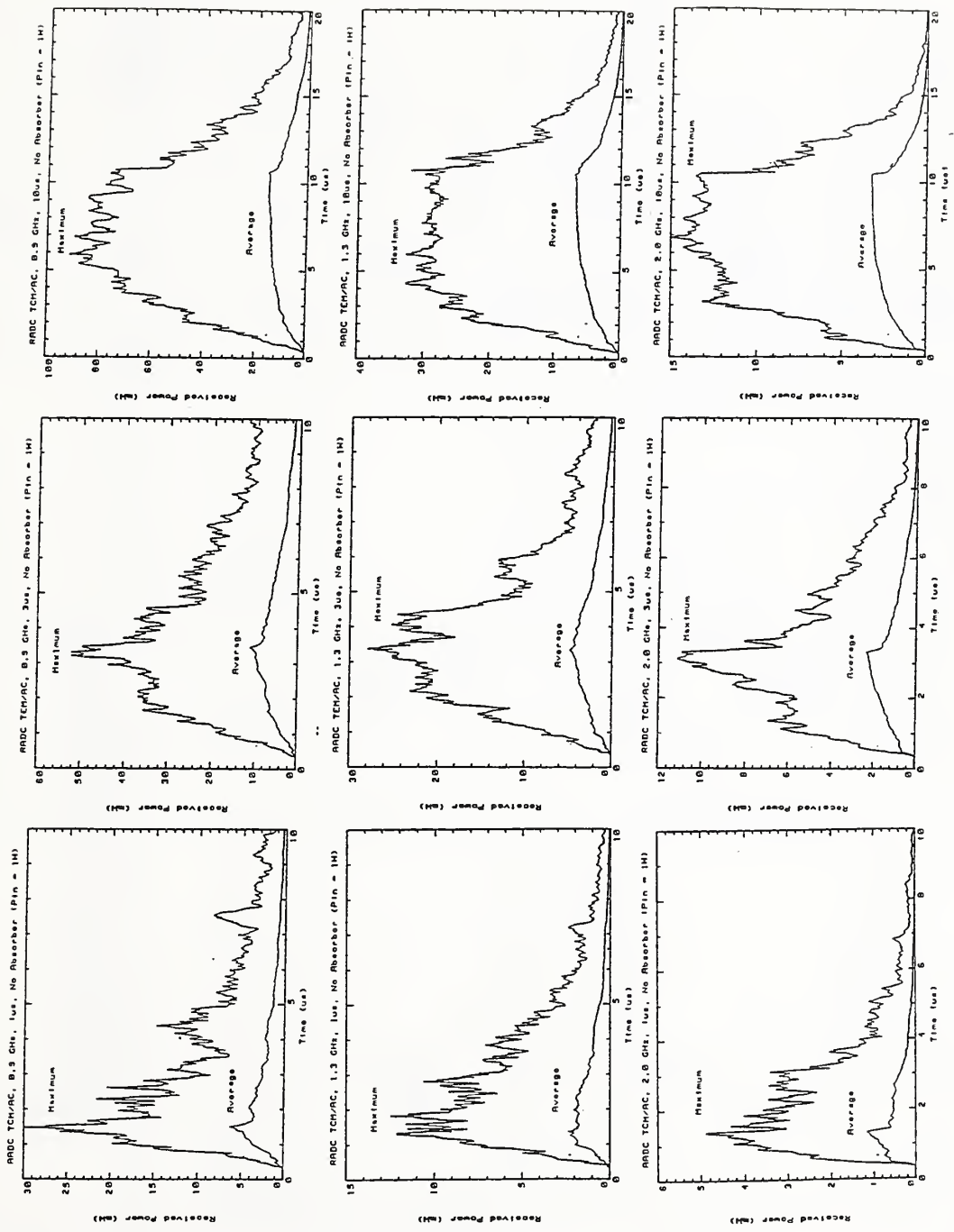


Figure 5.2(a) Maximum and average values of received rf pulse waveforms inside the RL TEM/reverberating chamber determined by mode-tuned approach. Chamber empty (no absorber). Measurements were taken at nine selected frequencies and three pulse widths.

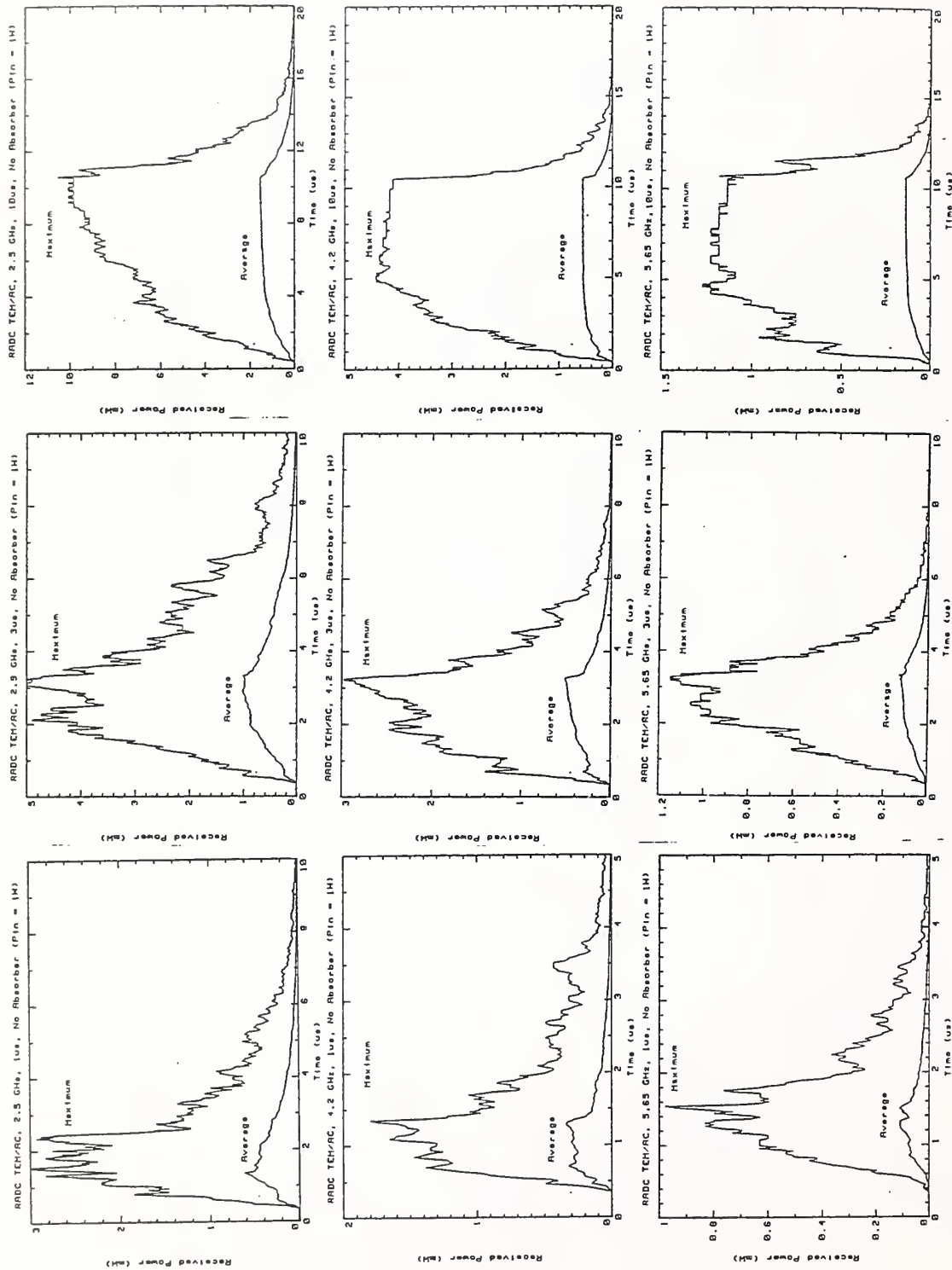


Figure 5.2(b) Maximum and average values of received rf pulse waveforms inside the RL TEM/reverberating chamber determined by mode-tuned approach. Chamber empty (no absorber). Measurements were taken at nine selected frequencies and three pulse widths.

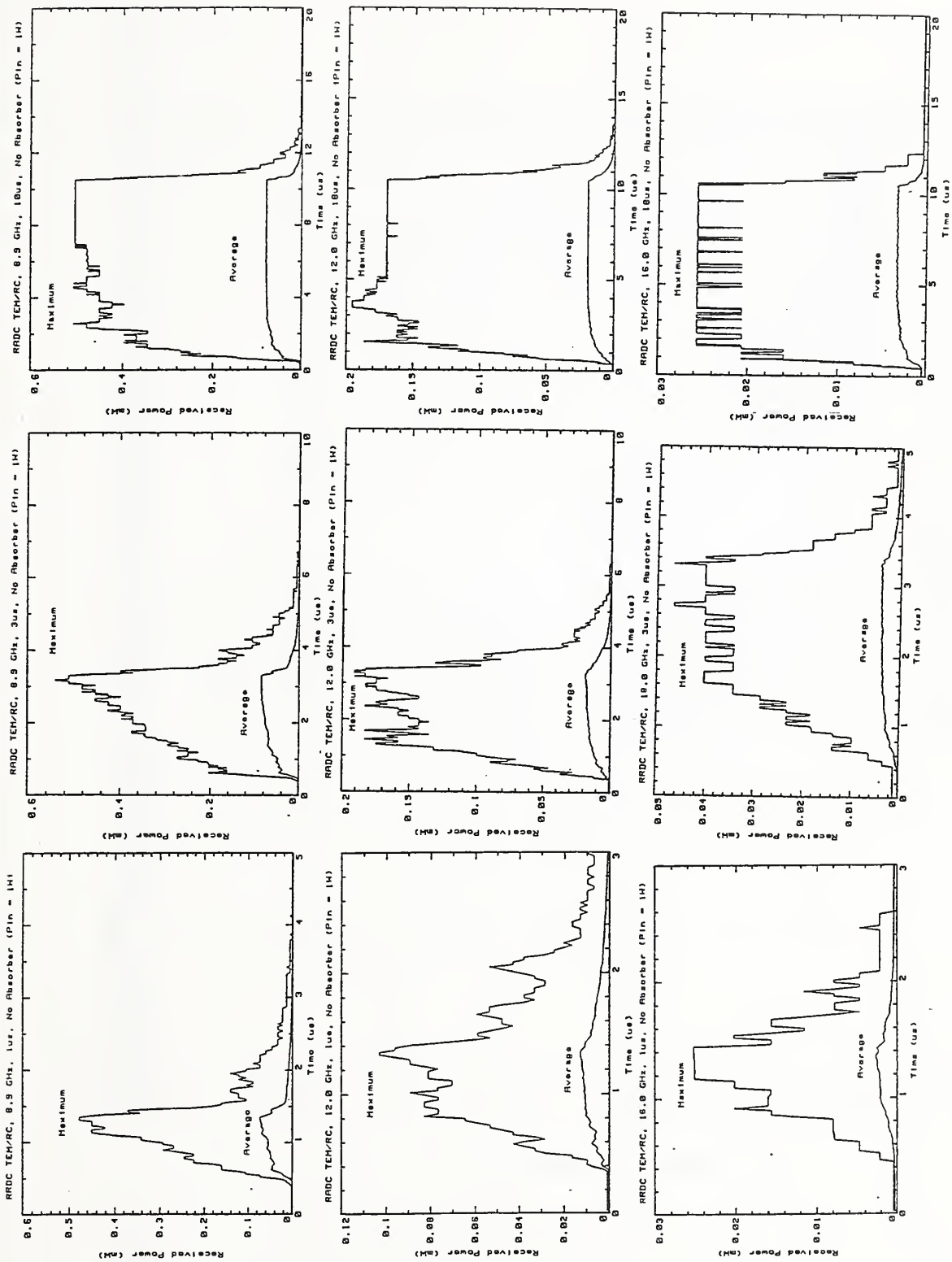


Figure 5.2(c) Maximum and average values of received rf pulse waveforms inside the RL TEM/reverberating chamber determined by mode-tuned approach. Chamber empty (no absorber). Measurements were taken at nine selected frequencies and three pulse widths.

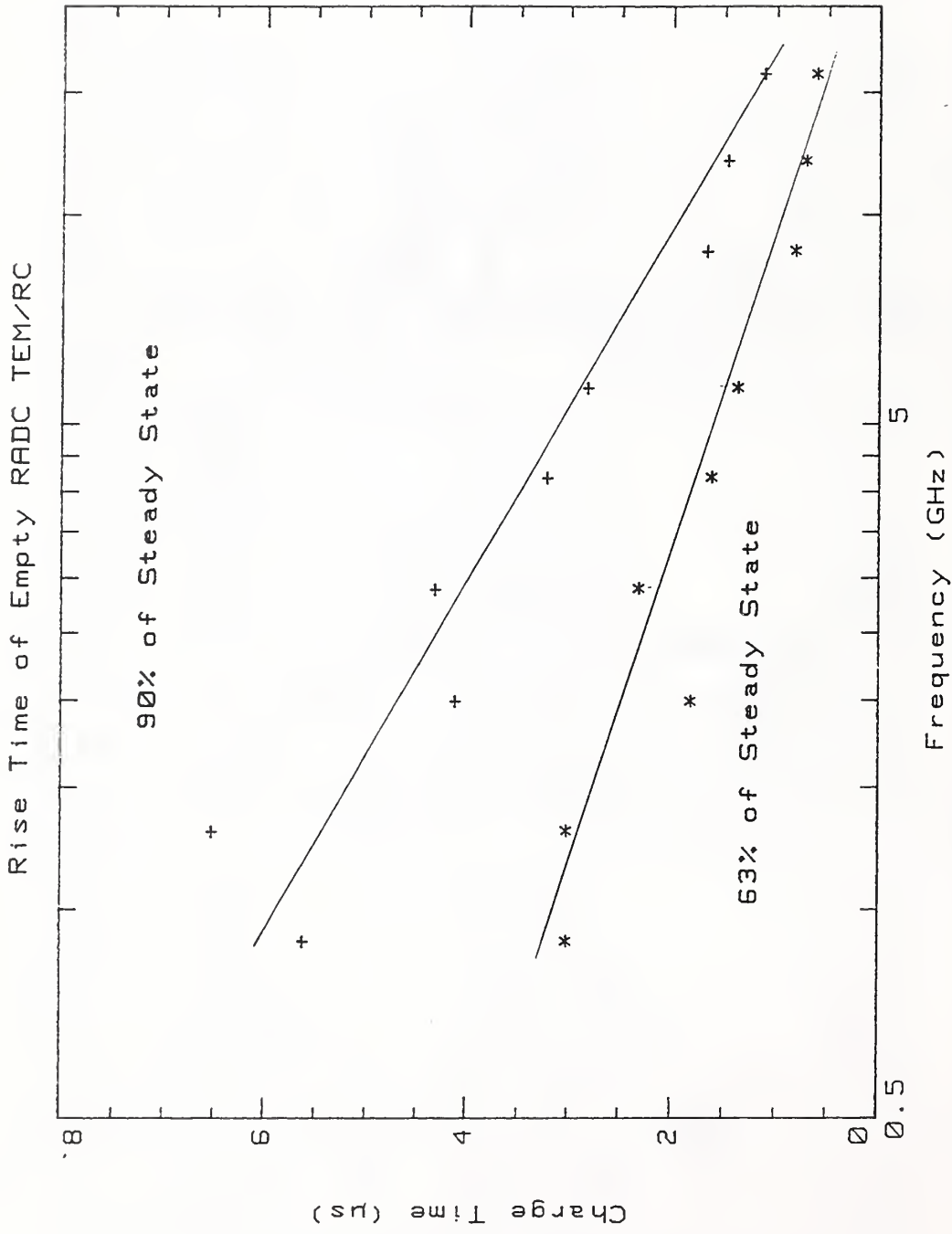


Figure 5.3 Time required for rf signal transmitted into the RL TEM/reverberating chamber to rise 63% and 90% of steady-state amplitude.

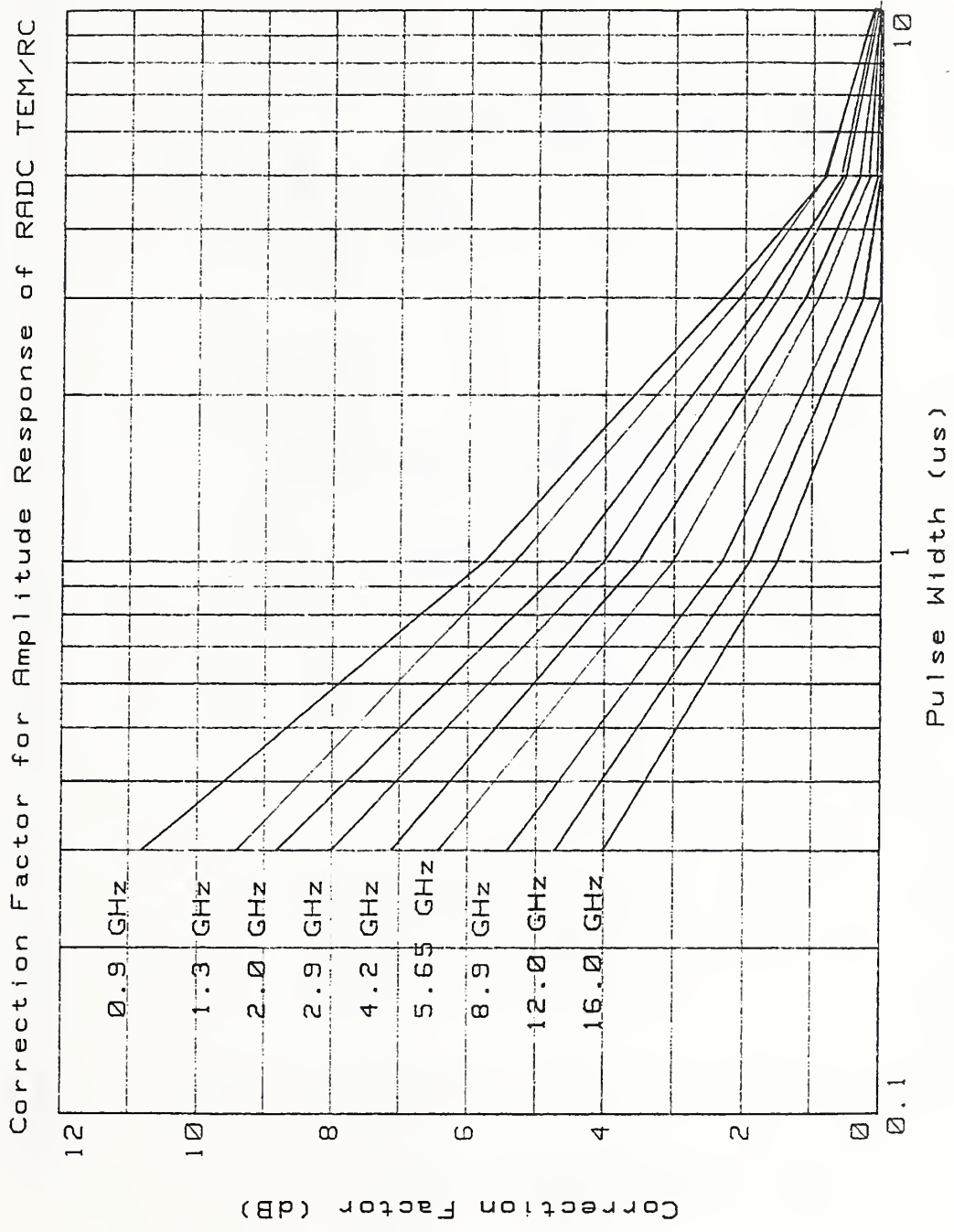


Figure 5.4 Estimated correction factors for amplitude response of rf test pulses in the RL TEM/reverberating chamber at selected frequencies as a function of input pulse width.

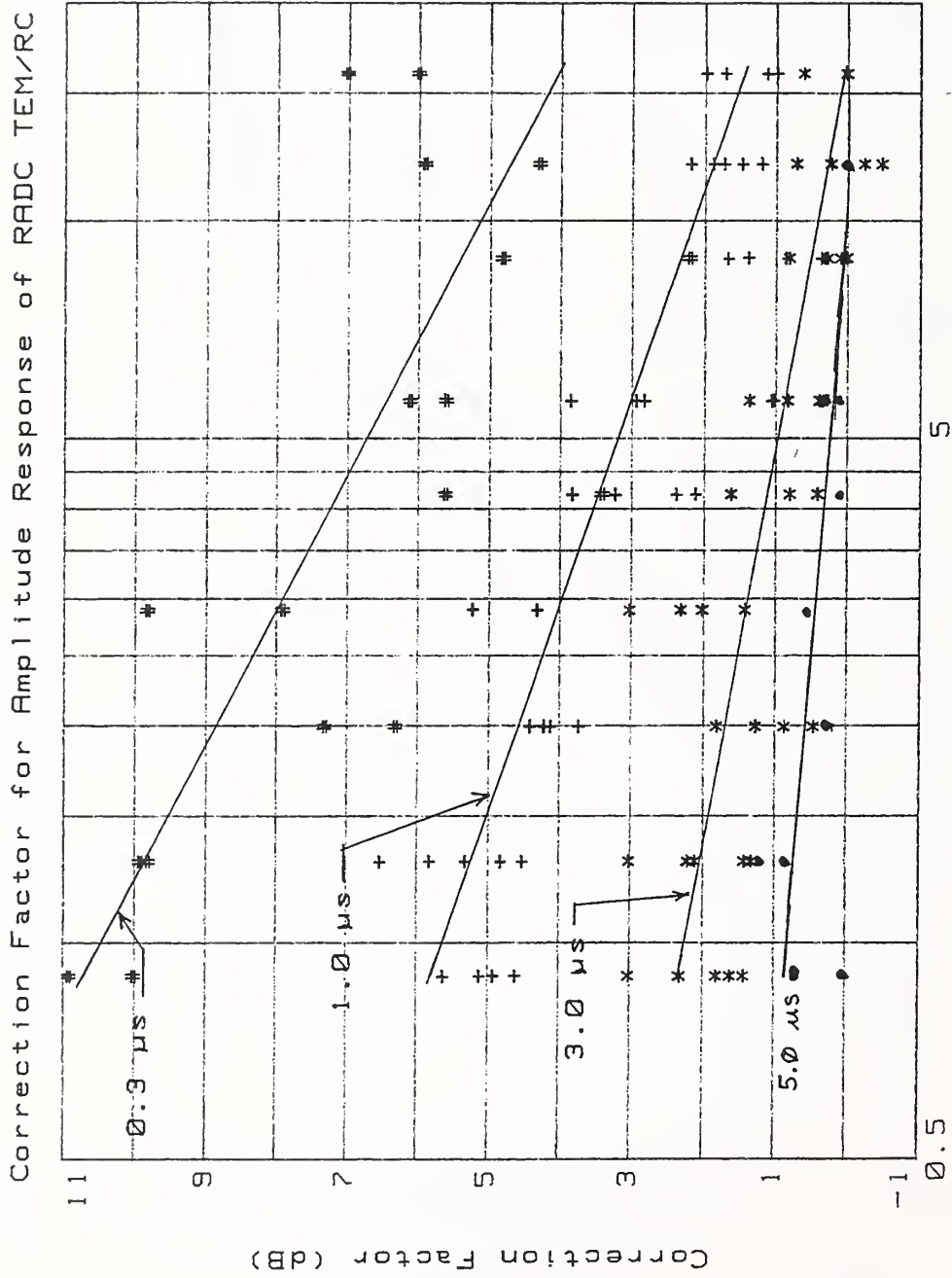


Figure 5.5 Estimated correction factors for amplitude response of rf test pulses in the RL TEM/reverberating chamber at selected input pulse widths as a function of frequencies.

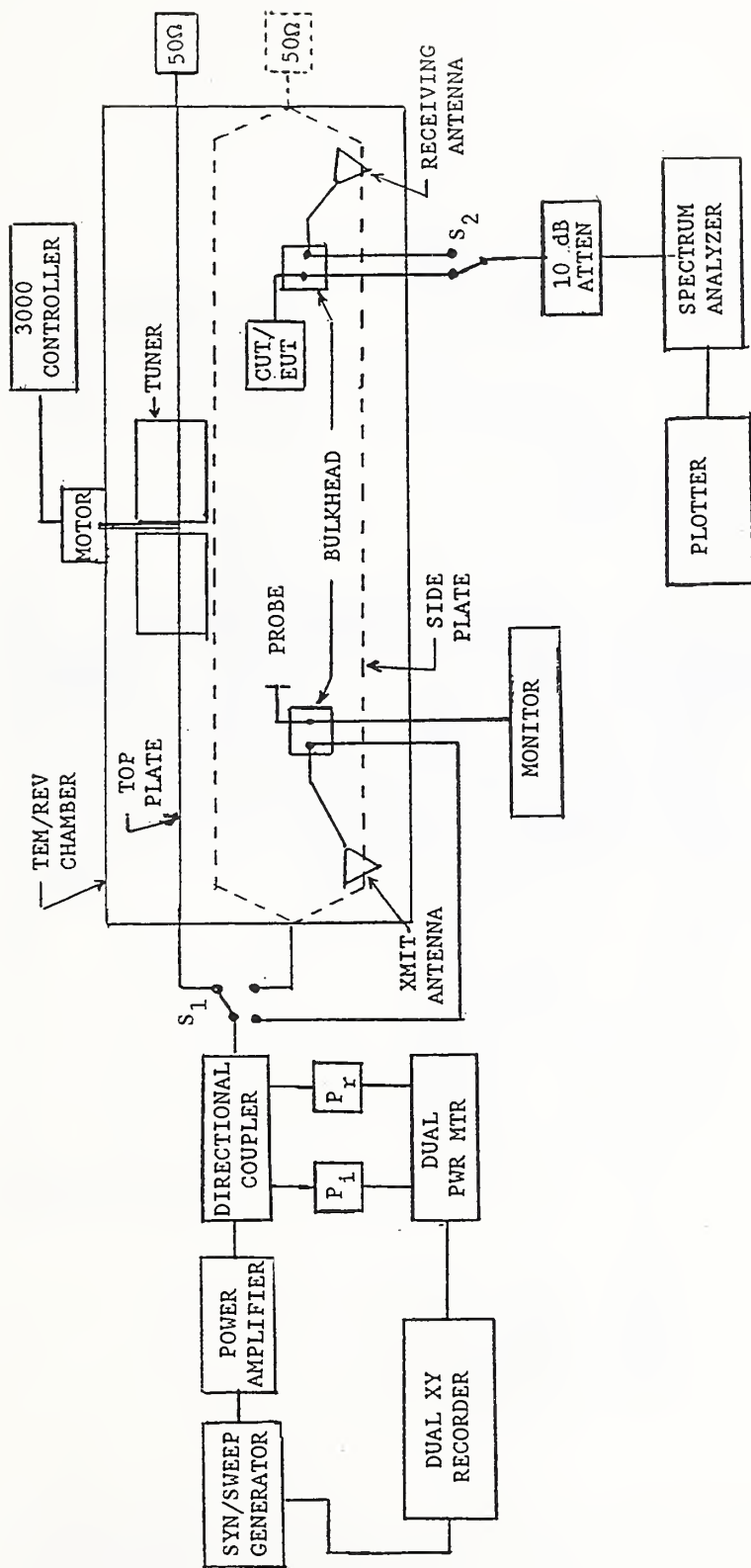


Figure 6.1 Block diagram of swept frequency EM radiated immunity and shielding effectiveness measurement system using TEM/reverberating chamber.

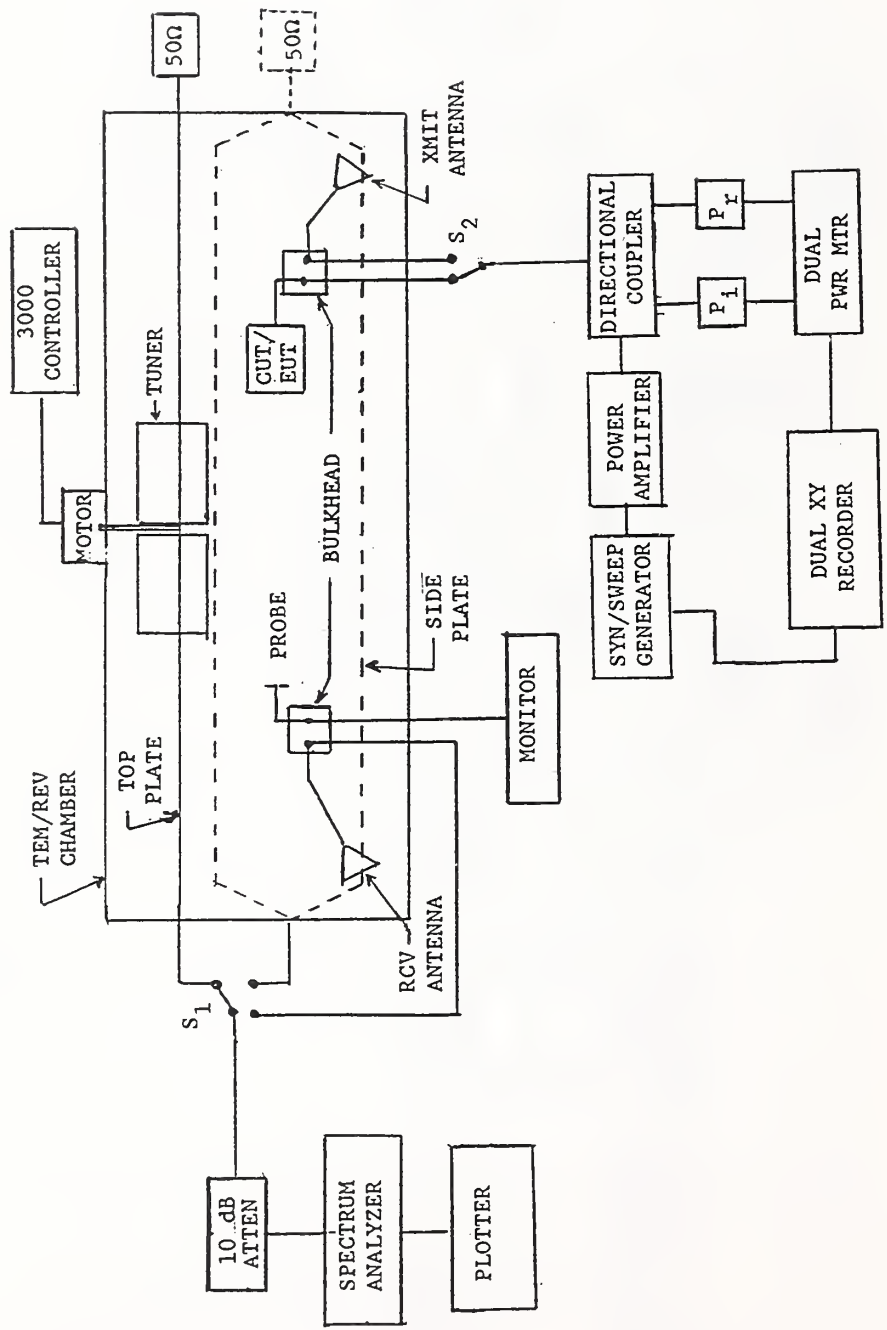


Figure 6.2 Block diagram of swept frequency EM radiated emissions and shielding effectiveness system using TEM/reverberating chamber.

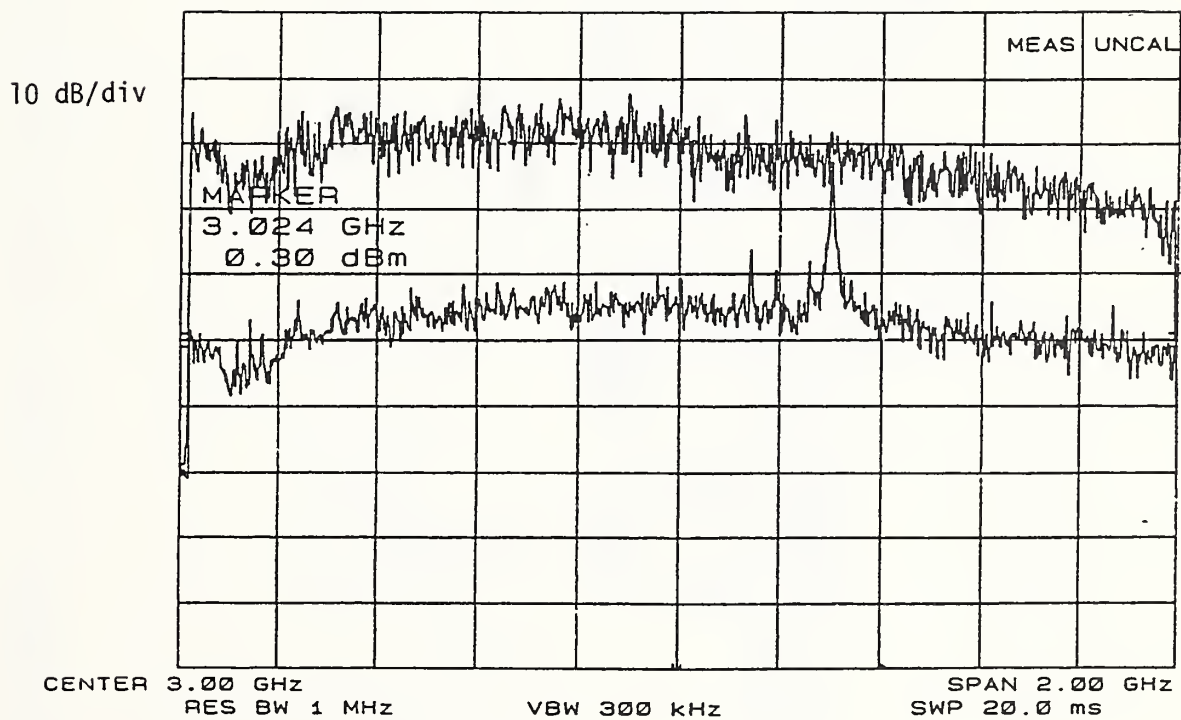


Figure 6.3 Measured SE data of 3 cm x 6 cm TEM cell with 15 mm diameter circular aperture using TEM/reverberating chamber and swept frequency measurement system. (a) reference antenna (no shielding), (b) TEM cell with aperture.

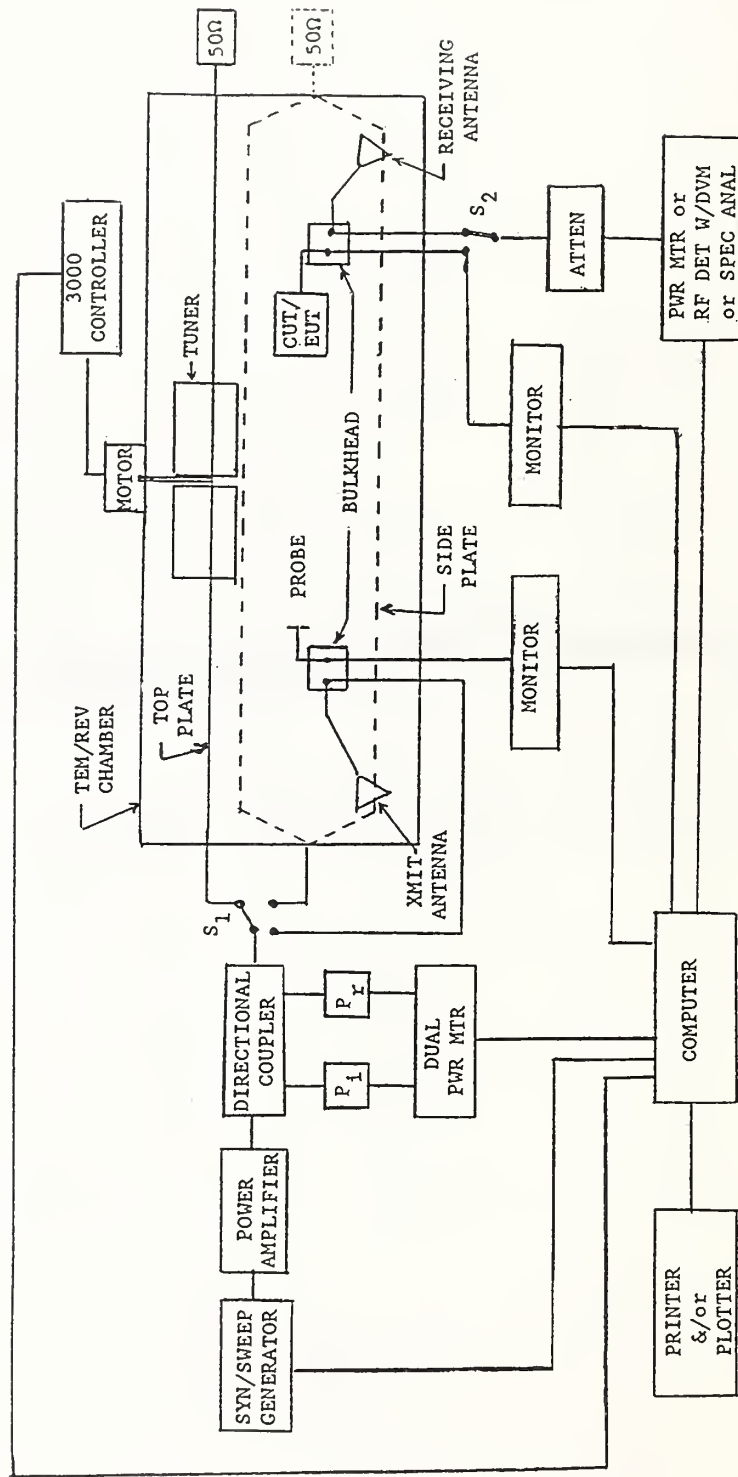


Figure 6.4 Block diagram of automated susceptibility measurement system using the TEM/reverberating chamber in the TEM mode of operation.



